Università degli Studi del Piemonte Orientale

"Amedeo Avogadro"

Dipartimento di Scienze del Farmaco

Dottorato di Ricerca in Biotecnologie Farmaceutiche ed Alimentari

XXVII ciclo a.a. 2011-2014

DESIGN AND CHARACTERIZATION OF Ln(III)-CHELATES AS CONTRAST AGENTS FOR CLINICAL DIAGNOSTIC TECHNIQUES

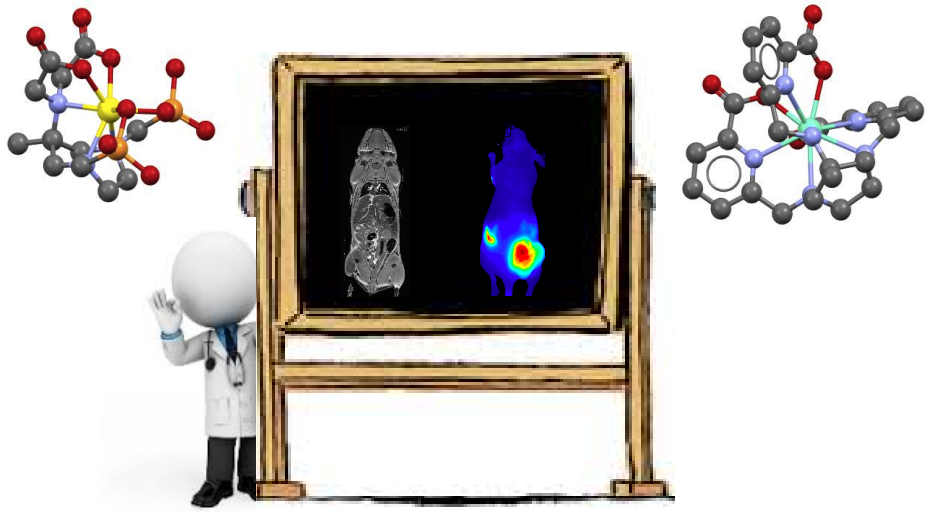

Claudia Guanci

Università degli Studi del Piemonte Orientale
"Amedeo Avogadro"

Dipartimento di Scienze del Farmaco

Dottorato di Ricerca in Biotecnologie Farmaceutiche ed Alimentari
XXVII ciclo a.a. 2011-2014

DESIGN AND CHARACTERIZATION OF Ln(III)-CHELATES AS CONTRAST AGENTS FOR CLINICAL DIAGNOSTIC TECHNIQUES

Claudia Guanci

Supervised by Prof. Giovanni B. Giovenzana
Dr. Luciano Lattuada – Bracco Imaging s.p.a.-

PhD program co-ordinator Prof. Menico Rizzi

Claudia Guanci was the recipient of a Ph. D. fellowship by Bracco Imaging S.p.A., Colleretto Giacosa (To), Italy, deeply acknowledged.

To Giacomo, my force, my breath, my life

To Mum and Dad, my smile

Contents

Introduction

Clinical images are produced through a variety of processes relying on physical phenomena applied to human body, detecting tissues damages in strikingly different ways: submission of the body to photons of all energies (X-rays, gamma-rays, ultraviolet, visible, infrared, microwaves, radiofrequencies), weak electric and magnetic fields or ultrasound waves provides important anatomical and physiological information, differing substantially in their ability to penetrate in and interact with the body. Indeed, in the past three decades the use of non-invasive imaging techniques for disease diagnosis has been a tremendous growth, becoming an indispensable component in the clinical practice. Afterwards, imaging systems are in widespread clinical use: Computed Tomography (CT), Magnetic Resonance Imaging (MRI), Positron Emission Tomography (PET), Single Photon Emission Tomography (SPECT) and Ultrasound (US) are the most common imaging modalities used today. Only recently Optical Imaging (OI), witnessed significant advancements, showing an emerging clinical utility (**Figure 1**)[1].

Figure 1: summary of modalities used for molecular imaging in preclinical/ clinical diagnosis.

A crucial role in the technology for imaging was the advent of contrast agents (CAs): a contrast agent is a molecular media used to improve the spatial and temporal resolution of the common diagnostic technique, affording to higher-contrast images, with consequently advantages for the diagnosis of tissue diseases. For their relevant repercussion on diagnostic improvements, the research in the field of contrast agents (CAs) has received a marked impulse due to the increasing request of better agents to use for the detection of different diseases. In addition to this, recently CAs found a new alternative and well-promising application to the Molecular Imaging: to their initial role as emphasizer of the diagnostic, new potential uses were added by the introduction of targeting vectors, leading to therapy monitoring, drug discovery and development, with the aim to better-understand biochemical events at cellular and sub-cellular level.

Starting from this observations, a brief introduction to the classical imaging modalities, that are CT, MRI, PET, SPECT, US and OI, will be discussed in the next pages, referring to their relative applications, advantages, limitations and emerging technologies. After that, a well-detailed description of different classes of contrast agents for MRI and OI will be described as preface for the discussion of the results obtained during the PhD program, object of this defence.[2]

1. Overview of Classical Imaging Modalities

Imaging modalities can be broadly divided into primarily morphological/anatomical and primarily molecular imaging techniques.

They are usually compared each other evaluating their use, but also the spatial and temporal resolution, the depth of penetration, the sensitivity, the safety profile and the costs of the technique (**Table 1**).

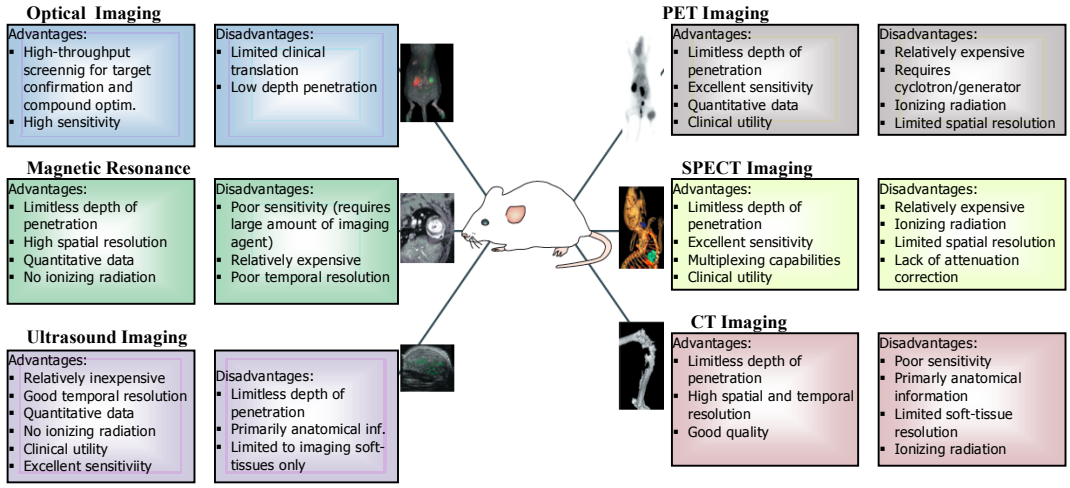

Figure 2: Pros and cons of the techniques used for molecular imaging

Each modality has particular characteristics, advantages and limitations, which are highlighted here. Most imaging modalities are used clinically and can be translated from animals to humans in the drug development process. The different imaging modalities should be generally considered complementary rather than competitive.

Primarily morphological and anatomical imaging technologies include CT, MRI and US: they are characterized by high spatial resolution but share the same limitation of detection diseases until tissue structural changes (for example, growth of a tumour). On the other hand, primary molecular imaging modalities, such as OI, PET, and SPECT (with fluorescent or radiotracer injected at nanomolar blood concentrations), offer the potential to detect molecular and cellular changes of

diseases (for example, before the tumour is large enough to cause structural changes). However, these modalities suffer from their poor spatial resolution with currently available technology (nuclear techniques) or from a low penetration depth (OI) (**Figure 2**).

A detailed description of the various imaging modalities is introduced in the next pages, taking account for *key strengths* and *limitations* of the single technique, introduced in the next table.

Table 1. *Features of available and emerging imaging modalities*

Modality	Temporal Resolution	Spatial resolution	Depth of Penetration	Sensitivity	Safety Profile	Cost
CT	Minutes	50-200 μm (preclinical) 0.5-1 mm (clinical)	Limitless	ND	Ionizing radiation	$$
MRI	Minutes-hours	25-100 μm (preclinical) 0.5-1 mm (clinical)	Limitless	10^{-3} to 10^{-5} M	No ionizing radiation	$$$
PET	Second-minutes	1-2 mm (preclinical) 5-7 mm (clinical)	Limitless	10^{-11} to 10^{-12} M	Ionizing radiation	$$$
SPECT	Minutes	1-2 mm (preclinical) 8-10 mm (clinical)	Limitless	10^{-10} to 10^{-11} M	Ionizing radiation	$$
US	Second-minutes	0.01-0.1 mm for superficial applications 1-2 mm for deeper	mm-cm	Excellent with microbubbles (10^{-12} M)	Good safety profile	$
OI	Second-minutes	2-3 mm	< 1 cm	10^{-9} to 10^{-12} M	Good safety profile, but depends on fluorophore used and mass needed	$

Combining the strengths of morphological/anatomical and molecular imaging modalities allows the detection of pathophysiological changes in an early disease phase at higher structural resolution (for example, PET-CT and PET-MRI technology). These technologies may change the current primary approach of diagnostic imaging into a more disease-oriented approach for both basic research and clinical applications[3].

1.1. Computed Tomography (CT)

CT is a technique that relies on differential level of X-ray attenuation by body tissues to produce images reflecting anatomy.

Unlike traditional X-ray examination, CT employs imaging by sections (tomography) resulting in a three-dimensional anatomic image of the subject being scanned. The X-ray source, linked to rotating detector arrays produces a "fanbeam" spanning the whole subject width. Usually, a large number of detectors are needed to obtain an adequate number of measurements and information: tissues that strongly absorb X-ray (*e.g.*, bones) appear bright while other that absorb poorly (e.g., air) appear dark, creating a high contrast-image displaying detailed morphological information. Often, an iodinated-contrast agent will be used during CT imaging to improve spatial resolution and soft tissue contrast **(Figure 3)**[4].

In clinical, CT has obtained invaluable success in the identification and assignment of tumours, ischemia, brain injury, pulmonary embolism and a vast array of other conditions. Some advantages of CT include fast acquisition time, high spatial resolution (preclinical = 0.05 – 0.2 mm, clinical = 0.5-1.0 mm), cost effectiveness, availability, clinical utility and relative simplicity. One of the main limitations of CT is the high exposure to radiation, which often limits the number of scans that can be performed in the same patient in a given time frame. Addition to this, the low-quality of soft tissue contrast-image entails the use of non-specific iodinated-contrast agents that should be relatively toxic for patient.

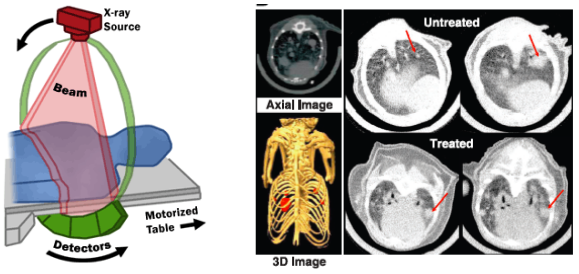

A) Schematic illustration of CT: a suitable contrast agent is administered to the subject. The X-ray source produces a fanbeam, shining the entire subject. X-rays will be differentially attenuated depending on the type of tissues, obtaining a high-contrast image displaying detailed morphological information. B) Small animal CT axial images and 3D representation.

Figure 3: Schematic mechanism of CT

However, advances in X-ray detector sensitivity have been made in the last ten years affording to a significant dose reduction.

1.1 Magnetic Resonance Imaging (MRI)

MRI is a highly versatile imaging technique that uses a powerful magnet and a radiofrequency energy to visualize the internal structure and morphology of soft tissue in the body.

The tecnique is based on the ability of some nuclei to produce a small magnetic field able to interfer with an external magnetic field: this interference originates a detectable signal. In detail, nuclear particles (protons and neutrons) are in constant motion and spin about their axes, giving rise to angular momentum. Atoms with an equal number of protons and neutrons have a net angular momentum of zero, whereas atoms with an unequal number possess a specific spin angular momentum. Moreover, due to their mass, spin, and charge of protons , certain nuclei produce a small vectorial magnetic field, named magnetic moment. The ratio of angular momentum to magnetic moment is known as gyromagnetic ratio and it is unique for each magnetically active nucleus. During an MRI scan, a living subject is placed inside a magnet; when anatomic nuclei are placed in an external magnetic field, they behave like magnetic dipoles which assume either a parallel or anti-parallel alignment to the magnetic field. The MR signal is generated from the small net difference in the number of magnetic dipoles that align parallel versus those that align anti-parallel (named polarization). External magnetic field with 1.5- 3 T are usually employed. The MRI signal is proportional to

1) concentration of nuclei,
2) gyromagnetic ratio,
3) polarization.

Additionally, the MRI signal is dependent on the natural abundance of magnetically active isotope of the element: all ^{1}H nuclei are magnetically active and for this properties ^{1}H is the most common nucleus used in clinical.
Anatomical images are usually performed using the hydrogen nuclei in tissue water, found at a concentration of ~80M in the body. Other nuclei such as ^{31}P, ^{13}C, ^{23}Na, ^{19}F and ^{17}O can be used for imaging, usually achieved through magnetic resonance spectroscopy (MRS).

A MRI scanner is composed of a set of embedded coils: one coil generating the main relatively homogeneous magnetic field, gradient coils that produce variations in the magnetic field in the X, Y, and Z directions that are used to localize the source of the MR signal, and a RF coil generating RF pulses at the Larmor frequency responsible for altering the alignment of the magnetic dipoles by the absorption process. After every RF pulse, the magnetic dipoles are "tipped" from equilibrium and they subsequently undergo into two forms of relaxation back towards equilibrium, spin-lattice (or longitudinal, T_1) relaxation and spin-spin (or trasverse, T_2) relaxation. The contrast between different tissues in MR images is generated from the different relaxation times of each tissue. MRI is of diagnostic value because it can be used to generate two or three-dimensional maps reflecting the spatial distribution of the values of T_1 and T_2 **(Figure 4)**.
Proton relaxation times mainly depend on the degree of binding of the water molecules to nearby biomolecules and the water-biomolecule interactions are sensitive to the histologic characteristic of a tissue and its physiologic status. So a T_1 or T_2-weighted MR image reveals information on both the anatomy and the state of health of tissues: for instance, proton nuclei in fat and hydrocarbon-rich environments have relatively short relaxation times compared with those in aqueous environments.
Agents that are used to create contrast enhancement on T_2-weighted images usually are superparamagnetic iron oxide nanoparticles, which are composed of a core of

iron oxide measuring 3-5 nm, coated with dextran, starch, polymer or citrate. On the other hand, T_1 contrast agents usually consist of chelates of paramagnetic metal ions, most commonly Gd(III), which exhibit a high magnetic moment due to its seven unpaired electrons. The detection threshold of gadolinium chelates locates in the micromolar range, lower than iodinated contrast agents commonly used in CT, which is estimated to be in the range of hundreds of millimolar to molar concentrations. However, many molecular targets of interest are expressed in the low nanomolar range, and therefore the detection sensitivity of routinely used gadolinium chelates is inadequate for molecular MRI; to address these limitations, several new gadolinium constructs have been developed: examples include gadolinium-containing dendrimers[5], micelles[6], liposomes and high-density lipoproteins. These nanoparticles possess both longer intravascular half-lives and higher longitudinal relaxivities (r_1)[7].

MRI has a number of important advantages compared with other imaging modalities, including

1) the use of non-ionizing radiation,

2) unlimited depth of penetration,

3) high spatial resolution (clinical: ~1 mm compared with 5-7 mm for PET, preclinical: micrometer, as opposed to millimeter resolution achievable via optical and radionuclide imaging),

4) unparalleled soft tissue contrast, superior to that attainable with CT,

5) excellent diagnostic potential.

One of the most important limitations of MRI is its extremely poor sensitivity that can lead to relatively long acquisition times and large amounts of imaging agents required to obtain an adequate signal.

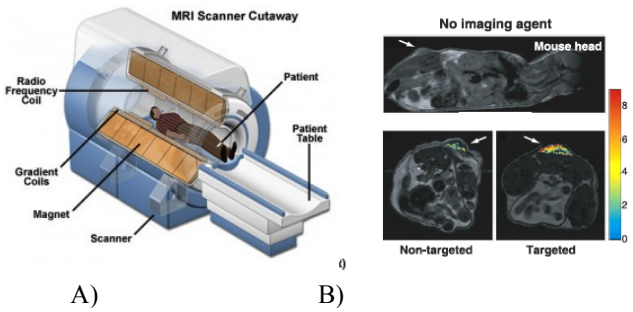

Figure 4: Magnetic resonance imaging (MRI)

A) Schematic illustration of MRI: a living subject is placed inside a magnet; unpaired nuclear spin within the body either align parallel or anti-parallel with the direction of the magnetic field. The MR signal is generated from the very small net difference in the number of parallel versus anti-parallel spins. B) MRI images, evaluating the presence and absence of contrast agents.

1.3 Positron Emission Tomography (PET)

PET is one of the first molecular imaging technologies, that permits the evaluation of biochemical changes and levels of molecular targets within a living subject. To image a certain molecular target using PET, identification and synthesis of a specific and selective radiolabeled imaging agent is needed in the beginning.

The generation of short-lived radionuclides through a cyclotron , such as ^{18}F (β^+, $t_{1/2}$ = 109.8 min), ^{64}Cu (β^+, $t_{1/2}$ = 12.7 h), ^{76}Br (β^+, $t_{1/2}$ = 12.6 h), allows to take advantage of the unique properties of radioactive isotopes to decay via positron emission, otherwise known as β^+ decay. Indeed, nuclei that decay in this manner have an excess of protons, making them unstable: That instability is rectified by transforming a proton into a neutron, a positron and a neutrino.

A nanomolar amount of the chosen radiolabeled agent containing a positron emitting radioisotope is administered to the patient. One positron is emitted from each imaging agent, then they travel short distances and collide soon with electrons in the surrounding tissues, an event known as annihilation, resulting in

the production of two γ-rays, each with energy of 511 keV, travelling at opposite directions. The radioactivity is traced through the body and its distribution determined from scans obtained with a PET camera. PET detectors take the form of a closed ring, or set of rings, surrounding the subject to be imaged, designed to detect the annihilation events. The resulting electrical signals are converted into sinograms that reconstructes the tomographic image reflecting the distribution of the imaging agent in the subject and providing information on biochemical events **(Figure 5**).

Isotopes of Zr, Y, In, Ga, and Cu have been investigated as radionuclide labels for biomolecules since they have the potential to combine their favourable decay characteristics with biological one of the targeting molecule to become useful radiopharmaceutical: ^{60}Cu (β^+, $t_{1/2}$ = 0.4 h), ^{61}Cu (β^+, $t_{1/2}$ = 3.3 h), ^{62}Cu (β^+, $t_{1/2}$ = 0.16 h), ^{64}Cu (β^+, $t_{1/2}$ = 12.7 h), ^{66}Ga (β^+, $t_{1/2}$ = 9.5 h), ^{67}Ga (β^+, $t_{1/2}$ = 78.3 h), and ^{68}Ga (β^+, $t_{1/2}$ = 67.71 min) find application in PET[8].

Recently radioisotopes of gallium(III) find large interest in PET and SPECT technology: due to this potential application, the coordination chemistry of Ga(III) to several different polyaminocarboxylic ligands has been investigated leading to the development of new and improved chelating agents[9].

Clinical PET is mainly used to image cancer through the use of ^{18}F-labeled imaging agent[10]. In addition to its clinical utility, PET has a wide range of application in the basic research and preclinical studies. For example, PET can be used to investigate basic physiological and molecular mechanisms of human diseases through the use of appropriate radiolabeled imaging agents[11].

Since biochemical changes generally occur before anatomical ones in disease, PET have a clear diagnostic advantage over classical CT and MRI. The key strengths of PET include excellent sensitivity (10^{-11}-10^{-12}M), requiring very small amounts of imaging agents (nanogram to milligram range) and limitless depth of penetration. The limited spatial resolution, the high-cost of the technique, the use of ionizing radiation and the need for a cyclotron are the key limitations of PET.

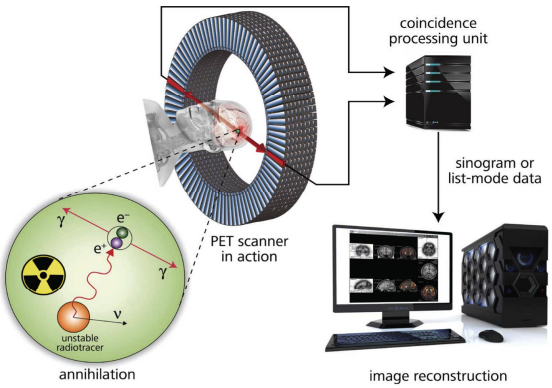

Figure 5: The basic principles of PET

Imaging agents containing a positron emitting radioisotope are administered to the patient. Positron are emitted from each imaging agent only once; these positrons travel short distances and collide with electrons in the surrounding tissue (annihilation) resulting in the production of two gamma rays, each with energy of 511 keV, travelling at the opposite directions to one another. Following the detection, the resulting electrical signal are converted into sinograms to reconstruct the tomographic image.

1.4 Single Photon Emission Computed Tomography (SPECT)

SPECT is similar to PET, but the radioisotopes used for SPECT emit only a single high-energy (γ) photon: for this property, it requires the use of a contrast agent labelled with a γ-emitting radionuclide that is detected by a SPECT detector and elaborated giving an image of the radiotracer localization.

Generally, a SPECT contrast agent is administered to the subject and the gamma rays are detected via a rotating gamma camera; the detected γ–rays are then reconstructed into a tomographic image providing information on the location of the imaging agent in the subject (**Figure 6).**

^{67}Ga (γ, $t_{1/2}$ = 78.3 h) and ^{111}In (γ, $t_{1/2}$ = 67.9 h) complexes find application as contrast agent in single photon emission computed tomography[12].

According to the diversity of nuclides used in SPECT, a completely unique set-up is required to collect and reconstruct the data. Comparing to PET, the sensitivity of SPECT is several orders of magnitude lower than PET due to a different collimator used to detect the γ–rays, is less expensive and more widely available than PET, and it show a lower spatial resolution (8-10 mm, compared with 5-7 mm for PET).
Like PET, SPECT has a clear diagnostic advantage over anatomical techniques as CT and MRI and it remains the most commonly used nuclear medicine modality in the clinic. Key disadvantage of SPECT are the lack of anatomical reference frame, and the safety profile: due to the use of ionizing radiation, each subject can be submitted to a limited number of scans *per* year. Unlike MRI and OI, both PET and SPECT only require small mass amounts of imaging agent (nanogram to milligram range).
Currently both PET and SPECT are being used either clinically or as research tool, to image a vast range of biological processes and disease states.

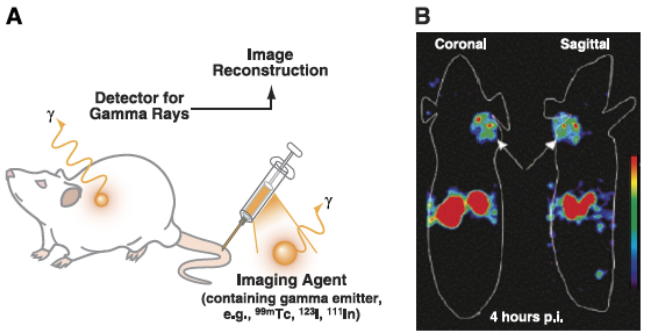

Figure 6: Single photon emission computed tomography (SPECT) principles

A) Schematic illustration of SPECT: an imaging agent contaning a γ–emitting radioisotope is administered to the subject and gamma rays are detected via a gamma camera rotating around the subject. The detected signals re then reconstructed into a tomographic image. B) SPECT images, highlight detailed morphological/anatomical information.

1.5 Ultrasound Imaging (US)

Medical US is an imaging tool that exploits the properties and behavior of high-frequency sound waves as they travel through biological tissues, finding application in diagnostic imaging and therapeutic tool[13].

During an US scan, a transducer sends sound waves and receives it back: in details, the transducer convert an electrical signal to US-waves, the US-waves enter the body, and some of them are reflected back to the transducer where they are detected and converted into electrical signals, subsequently processed by a computer and displayed as an image. Contrast agents, in the form of gas-filled microbubbles typically coated with lipids or biopolymers are used for enhancing the reflection signal-to-noise ratio for blood[14] **(Figure 7**).

Resolution of US improves significantly with higher frequencies, but limiting the depth of penetration: this effect is due to the fact that high-frequencies sound waves possess shorter wavelengths, meaning they are more likely to interact with matter and slow down, thus reducing their travelling distance[15].

The technique is cheap, it does not required the use of ionizing radiation and achieves excellent sensitivity with microbubbles and good temporal resolution. On the other hand, it shows limited depth of penetration, limited imaging applications (only for soft tissues) and it provides primarily anatomical information.

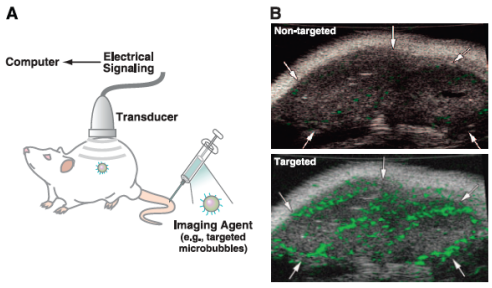

A) Schematic illustration of US: after administration of a targeted US imaging agent (microbubbles), high-frequency sound waves are transmitted into the subject. The sound wave reflections produced due to travelling through the subject are recorded, converted into electrical signals, analyzed affording to an image representative of the subject's internal structure. B) US images demonstrating the significant advantage of using microbubbles contrast agents.

Figure 7: Small animal ultrasound (US)

1.6 Optical Imaging (OI)

The visualization of cells and tissues using light has long been one of the most informative approach in basic research and medical diagnostic imaging. Optical techniques, unlike other imaging modalities, include multiple methods of imaging. The acquired images depends on the wavelength applied, the instrumental mode of detection, and whether or not intrinsic optical signatures or exogenously imaging agents are being explored as the constrast source. Generally, light interaction with tissues may involve the processes of absorption, photon scattering and the generation of fluorescence emission. All these phenomena have been exploited to differentiate tissue components. Depending on the light wavelength used, different penetration can be achieved.

In recent years, fluorescence microscopy and imaging have received particular attention. This is due to the increasing availability of fluorescent proteins, dyes and probes[16] that enable the non-invasive study of a large number of cellular processes. On the other hand, there was an increasing list of fluorescent imaging techniques that offer microscopic resolutions, or methods that operate at resolution beyond the diffraction limit and offer single-molecule sensitivity, yielding unprecedented insights into biology.

Along the developments in live cells fluorescent microscopy, a number of non-invasive macroscopic optical imaging modalities have emerged: two examples are fluorescence and bioluminescence imaging.

Optical Fluorescence Imaging is associated with the administration of an engineered fluorescent imaging agent such as fluorophores, fluorescent proteins, and QDots[17]; after the administration of the fluorescent imaging agent, an appropriate excitation wavelength is used to illuminate the subject; this leads to excitation of the fluorophore and subsequent emission of light.

The light emitted is detected via a CCD camera, collected, analyzed and finally converted into a tomographic image detailing the location of emitted light from the subject.

Optical imaging techniques, like fluorescence and bioluminescence imaging, are important tools for mapping specific molecular events in mice and for tracking cells, *e.g.*: metastatic cells. These techniques are cheap, fast and require no radioisotopes. Structural and functional imaging with high resolution has become more and more important in the drug development process.

2. Gd-based-MRI Contrast Agents: State of Art

Since the introduction of Magnetic Resonance Imaging (MRI) as diagnostic technique for the determination of diseases, the development of new contrast agents (CAs) has become of wide interest. Currently, about 35% of MRI scans make use of CAs and this percentage should further increase with the avaibility of more specific and sensitive agents. MRI-CAs are complexes of paramagnetic metal ions with cyclic and acyclic polyaminocarboxylic ligands, as the commercially available Gd-DTPA and Gd-DOTA (**Table 2**). The paramagnetic metal ions most extensively used in MRI are either transition metals or lanthanides: indeed, Gd(III) is preferred due to its high paramagnetism (7 unpaired electrons) and relaxation properties and it is the most investigated.[18]

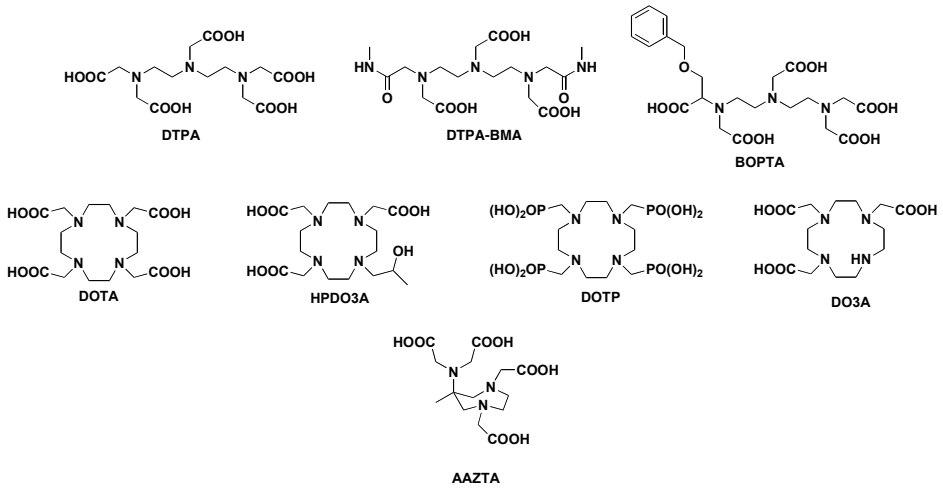

Figure 8: Common chelating agents for lanthanide(III) ions

Acyclic and cyclic chelating agents are reported: most of them are octadentate ligands, able to host only one water molecule in the inner-sphere. For this reason they generally show discrete relaxivity (4-5 $mM^{-1}s^{-1}$). On the other hand, DO3A and AAZTA are heptadentate ligands with two water molecules in the inner sphere coordination. Some of Gd-L represented are clinically available (Gd-DTPA, Gd-DTPA-BMA, Gd-DOTA, Gd-HP-DO3A, Gd-BOPTA).

Due to the toxicity of free Gd(III) ion and its high coordination number, acyclic and cyclic polyaminocarboxylic chelating agents are used to wrap around the metal centre affording to very stable and inert complexes which should coordinate at least one molecule of water. In **Figure 8** common cyclic and acyclic chelating agents are reported as example.

Table 2. *Clinically relevant Gd-based-MRI-CAs*

Chemical name	Generic name	Brand name	Company
$[Gd(DTPA)(H_2O)]^{2-}$	Gadopentetate dimeglumine	Magnevist	Schering
$[Gd(DOTA)(H_2O)]$	Gadoterate meglumine	Dotarem	Guerbet
$[Gd(DTPA\text{-}BMA)(H_2O)]$	Gadodiamide	Omniscan	Nycomed-Amersham
$[Gd(HP\text{-}DO3A)(H_2O)]$	Gadoteridol	ProHance	Bracco
$[Gd(DO3A\text{-}butrol)(H_2O)]$	Gadobutrol	Gadovist	Schering
$[Gd(BOPTA)(H_2O)]^{2-}$	Gadobenate dimeglumine	MultiHance	Bracco
$[Gd(EOB\text{-}DTPA)(H_2O)]^{2}$	Gadoxetic acid disodium	Eovist	Schering
$[Gd(DTPA\text{-}BMEA)(H_2O)]$	Gadoversetamide	OptiMARK	Mallinckrodt

2.1. Properties of a good MRI-CAs

An efficient CAs for MRI is characterized by:

- *suitable relaxometric properties (high relaxivity, r_1)*;
- *thermodynamic stability and kinetic inertness;*
- *high water solubility;*
- *low toxicity.*

2.1.1 *Relaxometric Properties*[19]**.** Signal intensity in Gd-based MRI is largely related to the local value of the longitudinal relaxation rate of water protons, $1/T_1$: indeed, signal tends to increase with increasing $1/T_1$ and

consequently, a pulse sequence that emphasize this parameter is referred as T_1-weighted scan.

The longitudinal relaxation rate is matematically defined as the sum of diamagnetic and paramagnetic relaxation rate: the linear dependece of paramagnetic relaxation rate on the concentration of paramagnetic species permit to determine the relaxivity (r_1) as $mM^{-1}s^{-1}$ from the following equations:

$$(1/T_1)_{obs} = (1/T_1)_D + (1/T_1)_P \quad (1)$$

$$(1/T_1)_P = r_1*[Gd(III)] \quad (2)$$

$$(1/T_1)_{obs} = (1/T_1)_D + r_1*[Gd(III)] \quad (3)$$

$$r_1 = [(1/T_1)_{obs} - (1/T_1)_D]/ [Gd(III)] \quad (4)$$

Relaxivity (r_1) is defined as the enhancement in relaxation rate of water protons of inner and outer sphere per mM of concentration at the field of 0.5 T and 298 K: the inner-sphere contribution is mainly related to the number of water molecule direcly coordinate to the metal centre (q) (**Figure 9)**, the distance between the water proton and the unpaired electron spin (r), the lifetime of the solvent molecule in the complex (τ_m), the electronic relaxation time (τ_S), the molecular reorientational time (τ_R) and the correlation time (τ_v).

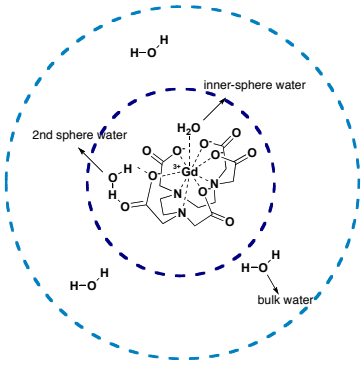

Figure 9: water molecules of inner and outer sphere coordinated to a Gd-complex

$$(1/T_1)_P = (1/T_1)_{inner\text{-}sphere} + (1/T_1)_{outer\text{-}sphere} \qquad (5)$$

$(1/T_1)_{inner\text{-}sphere} \propto q,\ 1/\tau_m,\ 1/r^6,\ 1/\tau_r,\ 1/\tau_v,$ and $1/\tau_s$

The second hydration sphere contribution, originating from water molecules interactions with the complex not directly bound to the metal centre, significantly partecipates to the relaxivity (5-15%) in complexes containing phosphonic or phosphinic ligands[20].

The number of water molecule directly coordinated to the metal centre is closely related to the denticity of the chelating agents: octadentate ligands as DTPA and DOTA, employed as chelating agents for Gd, permit the inclusion of no more than one water molecule in the first coordination sphere (q = 1) affording to complexes with relatively low relaxivity; the decrease of denticity of the ligand corresponds to an increase of q and, consequently, marked relaxivity properties. On the other hand, the simple shift from octadentate to heptadentate ligand affects the thermodynamic stability, leading to toxic effects related to the release of free Gd(III) in the blood.

The distance between the water proton and the umpaired electron spin, r, is a difficult parameter to measure and to control, but of relevant importance: For example, because of the $1/r^6$ dependence, a decrease of about 0.2 Å would result in a 50% increase in relaxivity.

Rotation of the paramagnetic molecule is another critical variable, even if tunable: indeed, enancing the rigidity of the complex, relaxivity can be optimized; starting from these observations, supramolecular adducts of MRI-CAs with human serum albumin (HSA)[21], low-density lipoproteins and high-density lipoproteins (HDL), characterized by

reduced mobility, were prepared, showing surprising and well-promising relaxivity values well higher than 20 $mM^{-1}s^{-1}$.[22]

Table 3. *Correlation time τ_i, molecular reorientational time τ_r, electronic relaxation τ_s, distance Gd-H hydration number and relaxivity for a selection of Gd(III) complexes at 25°C*

Ligand	τ_V (ps)	τ_r (ps)	τ_S (ps)	R (Å)	q	r_1
DTPA	25	58	72	3.13	1	3.8
DTPA-BMA	25	66	81	3.13	1	4.39
DOTA	11	77	473	3.13	1	4.2
DO3A	14	66	129	3.15	2	4.8[b]
HP-DO3A	-	-	-	-	1	3.7[b]
DOTP	12.7	73	90.7	-	3[c (ss)]	3.5
AAZTA	31	74	-	-	2	7.1
BOPTA	26	88	76	2.96	1	5.2

[b] Relaxivity value determined at 40°C; [c] q = q' correspond to the water molecules in the second-sphere; indeed for DOTP q = 0.

2.1.2 *Thermodynamic and kinetic properties.* Thermodynamic stability and kinetic inertness are important properties for a Gd-CAs because they are related to the release of free Gd(III) ion in *in vivo* applications through dissociation or transmetallation mechanism with Ca^{2+}, Mg^{2+}, Zn^{2+}, Cu^{2+} presented in human blood causing toxicity at low doses (10-20 μmol/Kg). Indeed, recent reports outlined the development of pathologies related to the slow dissociation of Gd(III) complex from the complexes with acyclic ligands (nephrogenic systemic fibrosis / nephrogenic fibrosing dermopathy or NFS/NFD) in patients with renal failure[23].

Stability constants, defined by Equations (6) and (7), are reported for different Gd-MRI-CAs in **Table 4**.

$$Gd + L = Gd\text{-}L \quad (6)$$

$$K_{GdL} = [GdL]/[Gd][L] \quad (7)$$

Table 4. *Stability Constants for GdL*

GdL	Denticity	$LogK_{GdL}$ ()
DTPA	8	22.46
DTPA-BMA	8	16.85
DOTA	8	25.3
DO3A	7	21.1
HP-DO3A	8	23.8
DOTP	8	28.8
AAZTA	7	20.24
BOPTA	8	22.59

Stability constants for heptadentate ligands are generally some orders of magnitude lower than octadentate complexes due to the reduced denticity. Reduction of the ligand denticity in order to enhance *q* must take care of the possible detrimental effect on the stability.

2.1.3 *Solubility and Toxicity.* High solubility and low toxicity are not less important parameters to be considered for a Gd-based MRI-CAs; high water solubility permits to prepare highly concentrated solutions of contrast agents to inject, while low toxicity is generally related to its thermodynamic stability and the kinetic inertness. Low molecular weight chelates are widely known to be among the safest drugs ever introduced due to their efficient excretion from the body. This minimizes the exposure to the drug and reduces the chance that slow uptake processes might internalize the agents in cells. As opposed to the free excreted small molecules, macromolecular conjugates tend to spend more times in the body and which, associated with the less complete

elimination, increase the odds of cellular uptake, leading to the release of potentially toxic byproducts, including free gadolinium ions itself.

2.2 Classification of Chelating Agents

Chelating agents for Gd(III) ions could be classified into different classes: ionic/ non-ionic and acyclic/cyclic contrast agents; the second classification is of greater interest because it is closely related to the thermodynamic and kinetic properties (**Figure 10)**.

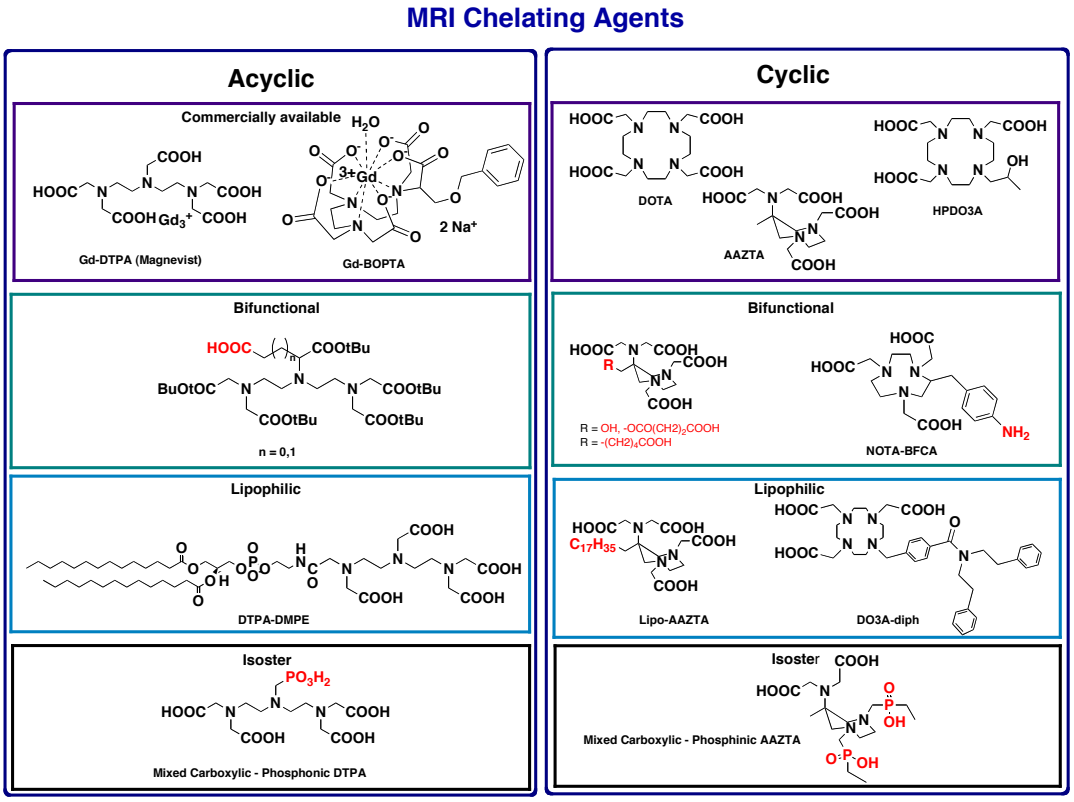

Figure 10: Schematic classification of chelating agents for Gd(III) ions.

Common examples of each class of chelating agents are reported: they are divided into cyclic/acyclic; their ability to enhance the contrast effect can be modulate reducing the denticity, adding water molecule of inner or outer sphere (q), limitating the mobility, or substituting the coordinating group.

2.2.1 *Acyclic chelating agents:* DTPA was one of the first chelating agents employed in clinical diagnostics with Gd-DTPA, also known as Magnevist. It is defined as linear or acyclic octadentate ligand which coordinates Gd(III) permitting the coordination of only one molecule of water in the inner coordination sphere. The linear structure entails low values of stability constant, while the high denticity is responsible of the relatively low values of relaxivity. Several octadentate ligands based to the DTPA scaffold were synthesized, substituting acetate moiety with different amides (DTPA-BMA) obtaining Gd-DTPA-bisamides complexes with relaxivity properties similar to DTPA.

2.2.2 *Cyclic chelating agents*: macrocyclic ligands as DOTA are preferable to the DTPA-like open-chain ones, as the latter show lower thermodynamic stability and kinetic inertness. During the last decades, the research in the field of cyclic chelating agents for lanthanides were widely explored: in this framework DO3A and its derivates as HP-DO3A were investigated leading to interesting results and clinically employed derivatives. Recently a new cyclic heptadentate ligand with efficient chelating properties was synthesized, *i.e.*: AAZTA: comparing with DOTA and DTPA, an efficient size-match with lanthanide ions, the satisfactory thermodynamic and kinetic inertness and relaxometric properties of its Gd(III) complex make it a suitable choice as a cyclic chelating agent for Gd-based MRI-CAs[24].

2.2.3 *BFCAs*: bifunctional chelating agents were introduced with the aim to link the functionality of contrast agent to a targeting vector to accurately orient the diagnosis of tissue disease and therapy[25]: The most common BFCAs derive from cyclic and acyclic polyaminopolycarboxylic acids similar to DTPA, DOTA and AAZTA, on which a suitable versatile and

reactive functional group is added, better without altering the chelating properties of the coordination cage. Due to its easy formation and chemical stability, amide bond is one of the preferred choices for the preparation of coniugates containing metal complexes. Bifuctional DTPA-like ligands containing carboxylic, amino or phosphonic groups as functional groups were prepared and they have found several applications in the different diagnostic imaging techniques relying on contrast agents based on chelated metal ions.

2.2.3 *Lipophilic Chelating Agents*: the introduction of a lipophilic alkyl chain on the skeleton of the common contrast agents supports the self-assembly into micelles that exhibit enhanced values of r_1. In addition to this, lipophilic CAs can further form supramolecular adducts with HSA, LDL and HDL with significative increments in the relaxivity due to the reduced and lower mobility of the systems: example of lipophylic MRI-CAs are Gd-DTPA-DMPE and Gd-AAZTA-C17 with potential applications for *in vivo* imaging of tumours and cardiovascular diseases. The importance of this aspect is highlighted if related to the current safety requirenments: indeed, by increasing the efficacy of Gd-chelated it may be possible to reduce the dose and minimize the potential toxicity associated with Gd probes exhibiting prolonged circulation times.

2.2.4 *Phosphonic and Phosphinic Chelating Agents*: as mentioned above, the second hydration sphere, originating from interactions of the complex with water molecules not directly bound to the metal centre, can significantly contribute to the relaxivity particularly in complexes containing phosphonic or phosphinic ligands as P-DTPA, DOTP[26]: indeed, the bulkier phosphonic group may hinder the access of water molecules in the inner sphere, while the ability to form strong H-bonds

promotes the formation of a well-structured hydrated second sphere with consequently increase in relaxation efficiency. Starting from that observations, substitution of carboxylic groups with phosphonic ones was extensively investigated: indeed, the tetrahedral deprotonated form $-PO_3^{2-}$ ion occurring at physiological pH values offers multiple coordination modes, while the residual anionic charge after complexation provide a better solubility in water. Recently it was demonstrated that phosphonate-containing analogues of the commercially used Gd-DOTA and Gd-DTPA show faster water exchange than the original systems. Even though complete substitution of carboxylic with phosphonate groups affords to too much hindrance which leads to chelate systems unable to coordinate water molecules in the inner-sphere (*q =0),* partial substitution seem to guarantee better results: indeed, the hindrance of only one phosphonate group on the coordination cage usually does not cause a reduction of the number of molecules water bond with the metal centre. Alternative monophosphinic and monophosphonic complexes as Gd-DO3AP^{BP} and Gd-PC2AP with q≥ 1 were developed and they show higher relaxivity values[27,28], respectively 7.4 mM-^{1}s^{-1} and 8.3 mM-^{1}s^{-1} (**Figure 11**).

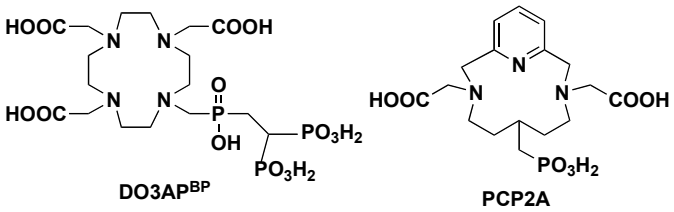

Figure 11: examples of mono phosphonic/phosphinic chelating agents.

In the same context a mixed carboxylate-phosphinate AAZTA-like ligand, named AAZ2A2P, was recently reported with relaxivity value of

6.1 $mM^{-1}s^{-1}$ (20 MHz, 298K), slightly lower than Gd-AAZTA (q = 2, r_1 = 7.2 $mM^{-1}s^{-1}$), suggesting the presence of only one water molecule coordinated to the paramagnetic metal centre (q=1)[29].

Conclusions

The relaxivity of a contrast agent is the measure of an MRI-CA efficacy to produce image-contrast. There is continuosly the desire to increase the longitudinal relaxivity of Gd-based contrast agents since the r_1 values of currently available commercial agents fall too short of what is theoretically possible. The octadentate coordination guarantees the formation of very stable complex but limited to the coordination of only one molecule of water in the inner sphere. Better results are obtained for octadentate cyclic chelating agents as Gd-DOTA and Gd-DO3A: indeed, they show r_1 values of 4.3 and 4.6 $s^{-1}mM^{-1}$ respectively, while relaxivity of Gd-DTPA is 3.8 $s^{-1}mM^{-1}$.

Reducing the denticity of the chelating agent interesting results were achieved with AAZTA, an heptadentate cyclic ligands which the reduced denticity is the explanation of relaxivity like 7.1 $s^{-1}mM^{-1}$, tipical value for MRI-CAs with q = 2.

An alternative strategies to obtain this effect is the delivery of a high number of imaging reporters at the site of interest by conjugating several Gd-chelates to macromolecules or nanoparticles linked to a targenting vector, obtaining multimeric/dendrimeric MRI-CAs.

Finally, another parameter that could be modified to improve the longitudinal relaxivity of a contrast agent is the molecular reorientational time (τ_R) that is related to mobility of the Gd-complex: indeed, the introduction of an alkyl chain limits the unrestrained movement of the contrast agent affording to surprising results, especially when they could form supramolecular adducts with HSA, LDL, and HDL.

In conclusion, the research in the field of MRI-diagnosis have reached great results during the last decade, affording to important results for clinical and also therapeutical applications; in spite of that, improvements are still needed to optimize the relaxometric properties and to reduce the toxicity risks.

3. Luminescent probes for Optical Imaging

The unique spectroscopic and magnetic properties of lanthanide ions allow the use of their complexes in a wide range of medical and biochemical applications. If the high magnetic moment and the slow electronic relaxation of gadolinium make it ideal for the design of magnetic resonance imaging relaxation agents, the long-lived luminescence of Eu(III) and Tb(III) complexes has been exploited in the development of sensor and time-resolved fluorescence imaging. The ligand design is crucial for the effective use of the lanthanide in such biochemical application and it has incited a large number of coordination chemistry studies.

Optical Imaging is a high–resolution, sensitive and semi-quantitative technique of diagnosis developed in the last 30 years, contemporary with MRI. As MRI, Optical Imaging uses non-ionizing radiation and the signal or contrast could be modulated in response to biological events. The technique requires low concentration of contrast agent to produce high contrast images and cellular/subcellular resolution[30].

Lanthanide-based luminescent probes are particularly attractive for OI due to their long luminescent lifetime that offers a several advantage for the time-gated detection in biological samples.

3.1 Architecture of luminescent probes for OI

Lanthanides show intrinsic luminescence originating from *f-f* electron transitions in the 4*f* shell with lifetime in the milli to microsecond range. The 4*f* orbitals do not participate in chemical bonding, so the emission wavelengths are minimally perturbed by the surronding matrix and ligand field showing an emission spectra that preserves the same fingerprint of the corresponding free Ln(III) salts.

Despite that, lanthanides have low molar absorbivity requiring intense light sources to populate the excited states by direct excitation. Complexation with an appropriate chelate able to transfer energy to the metal centre would be a valid alternative to increase the population of excited state (**Figure 12)**.

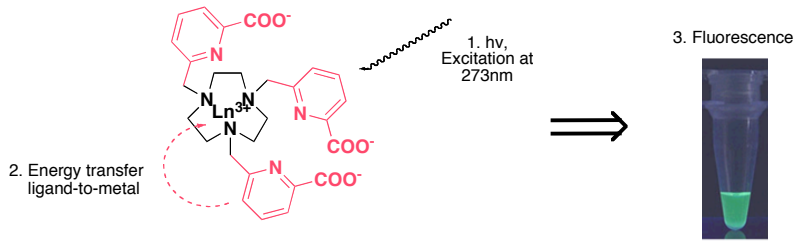

Figure 12: Fluorescence mechanism through energy trasfer activation.

Ln(III)-complex is initially at the groud state S_0; excitation of picolinic group with λ_{exc} = 273 nm affords to excited state S_1; Picolinic groups transfer energy to the metal centre that relax emitting fluorescence.

The architecture[31] of emissive lanthanide complexes consists of a metal centre surrounded by a chelate equipped with a sentitizer, named antenna. The chelate prevents the release of free Ln(III) into the biological system and protects the metal centre from the solvent coordination, avoiding the quenching and maximizing the quantum yield: chelates with high coordination numbers are requested for luminescent probes (n >8). In addition to this, also rigidity of the coordination cage can minimize the energy loss through X-H vibrations.

Europium and terbium complexes are the most favourable probes for Optical Imaging because they have high emission intensity in the visible region spectra, longer luminescent lifetime than most of the common organic fluorophores and low sensitivity to quenching by singlet oxygen and by vibrational transfer to X-H (X = C, N,O).

The antenna effect consists in the harvest of energy through high molar absorption to the singlet excited state. After undergoing ISC to the triplet state, the antenna transfers energy to the excited state of Ln(III) (^5D_j) that relax to the ground state (^7F_j) emitting luminescence.

For a satisfactory antenna effect the following photophysical properties are required[32] (**Figure 13)**:

- high molar absorbivity for $S_0 \rightarrow S_1$;

- excitation wavelength > 340 nm (but generally they are limited to excitations < 420nm);
- the ISC for $S_1 \rightarrow T_1$ transition must be favoured over antenna fluorescence and non radioactive relaxation $S_1 \rightarrow S_0$;

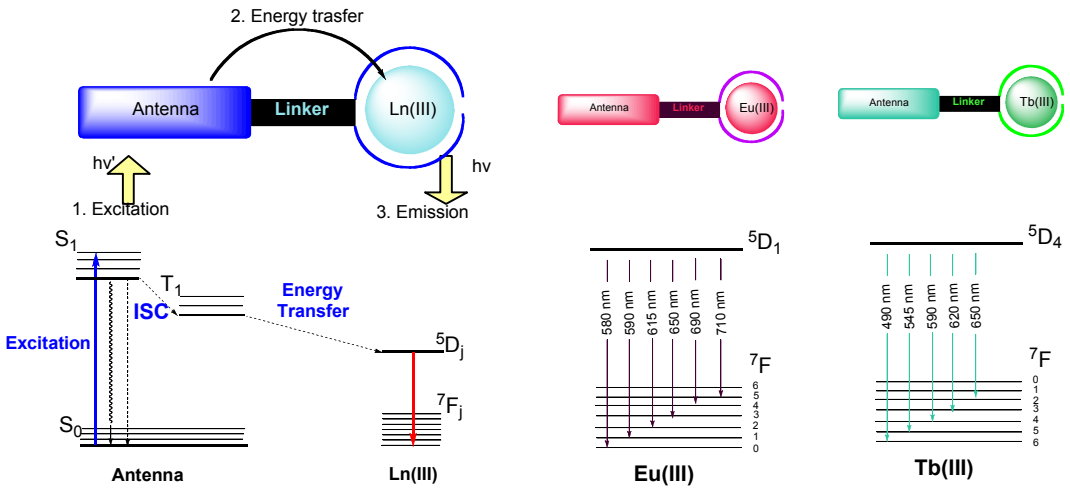

Figure 13: Fluorescence mechanism in detail

The antenna harvest energy through high molar absorption to the singlet excited state. After undergoing intersystem crossing to the triplet state, the antenna transfers energy to the excite ^5D_j state of the lanthanide. The radiative transition of electrons from excited ^5D_j to the ^7F_j states results in luminescent emission from the lanthanide ion.

Picolinic moyety was routinely introduced as antenna in the basic scaffold of typical chelating agents as DOTA and NOTA, promoting the energy transfer to the metal centre, affording to interesting luminescent probes for OI[33,34].

3.2 Photophysical properties

The photophysical properties of lanthanides (sharp emission, long luminescence lifetime allowing to discriminate between the background fluorescence of

biological material and the target signal) make their complexes very attractive for the application as luminescent labels in time-resolved imaging and in biomedical assays. The preparation of lanthanide complexes, that are stable and highly emissive in water environment, requires the design of polydentate ligands that contain suitable sensitizer of the lanthanide emission, capable to prevent nonradiative deactivation.

3.2.1 *Absorption and emission spectra of Eu and Tb-complexes*. The absorption spectra of typical Eu- and Tb-chelates recorded in water generally show band with maxima in the UV region, assigned to $\pi \rightarrow \pi^*$ and $n \rightarrow \pi^*$ transitions centred on the (het)arene antenna moiety. The excitation spectra recorded upon metal-centred emission are very similar to the corresponding absorption spectra, indicating that the coordinated picolinate moiety provides an efficient energy transfer to the Eu(III) and Tb(III) ions. The corresponding emission spectra of ~10^{-5}M solutions of Eu- and Tb-complexes, obtained under excitation through the ligand bands usually display the $^5D_0 \rightarrow {}^7F_j$ (Eu(III), j = 0-4) and $^5D_4 \rightarrow {}^7F_j$ (Tb(III), j = 6-0) transitions typical of Ln(III) ions. Specifically, Eu-complexes are characterized by five bands in the range of 570-730 nm with the main band attributed to the $^5D_0 \rightarrow {}^7F_2$ transition appearing in the 600-630 nm range. Tb-complexes are characterized by seven bands in the range of 450-700 nm with the maximum around 540-550 nm attributed to the $^5D_4 \rightarrow {}^7F_5$ transition (**Figure 14).**

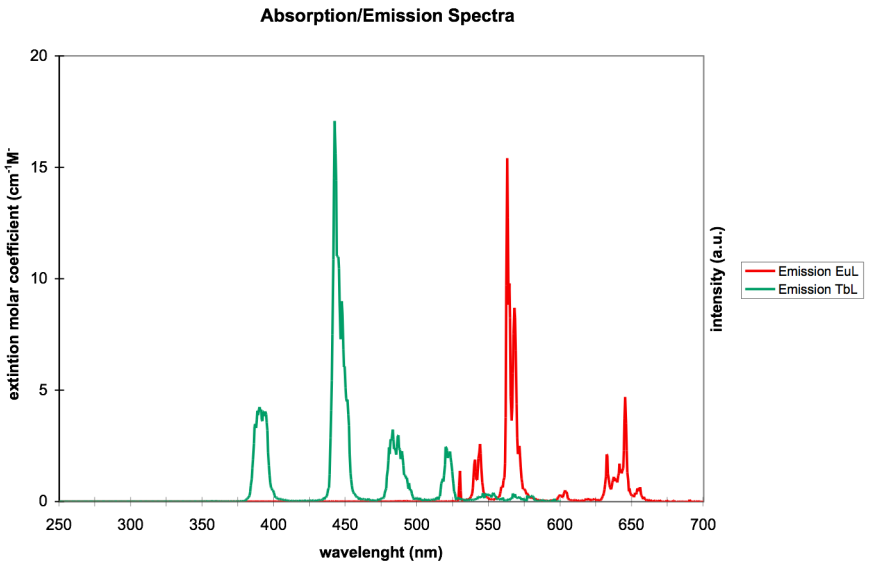

Figure 14: Emission spectra of luminescent Eu- and Tb-complexes

The emission spectra of ~10^{-5}M solutions of Eu- (red) and Tb-complexes (green), embodying picolinate groups as coordinating/antenna residues. Excitation through the ligand band at 273 nm are reported: Eu-L is characterized by five bands in the range of 570-730 nm with the main band attributed to the $^5D_0 \rightarrow {}^7F_2$ transition appearing in the 600-630 nm range with a maximum at 615 nm. Tb-L is characterized by seven bands in the range of 450-700 nm with the maximum at 545 nm attributed to the $^5D_4 \rightarrow {}^7F_5$ transition.

3.2.2 *Luminescent lifetime.* Determination of luminescence lifetimes (τ) in H_2O and D_2O allows an accurate estimation of the number of coordinated water molecules present in solution (q) by using the equation of Beeby and co-workers[35]

$$q = A*[(1/\tau_{H2O})-(1/\tau_{D2O})-B]$$

For europium complex A= 1.2 ms and B = 0.25 ms^{-1}, while for terbium complex A = 5 ms and B =0.06 ms^{-1} ;

For a luminescent probe q = 0 is desiderable because it strongly reduces the quenching effect due to the O-H vibrational oscillators.

3.2.3 *Quantum yield*. An efficient ligand-to-metal energy transfer is suggested by the close matching of the excitation and emission spectra: indeed, quantum yield (ϕ_{Ln-L}) is an indicative index related to the efficient energy transfer and emission fluorescence in spite of radiationless deactivation mechanisms.

3.3 Chelating agents for OI

For biological imaging, lanthanides are typically chelated with multidentate ligands to attenuate the toxicity of free lanthanide ions. In luminescent applications, chelation has an additional role of protecting the metal center from solvent coordination. Indeed, coordination of water molecules shorten the excited-state lifetimes of the Ln(III) ions through nonradiative vibrational energy transfer to the high-frequency O-H oscillator. Thus, the number of water molecule directly coordinated to the matal centre, *q*, highly influences lanthanide emission. Chelate minimize *q* via coordinative saturation or steric hindrance, thereby attenuating solvent quenching and maximizing the ϕ_{Ln} term.

For use as cellular probes, the chelate must form a complex that firmly saturates the Ln(III) coordination sphere over a wide pH range and resists hydrolysis. Given the hard-acid nature of lanthanide ions, hard bases, such as carboxylate ligands, amides and pyridines, are typically implemented as ligands. Macrocycles, such as NOTA and DOTA, and open nona-or octadentate chelates equipped with sterically bulky arms are commonly used for luminescent applications.

Increasing the rigidity of the chelate itself can further minimize energy loss through other X-H (X = C, N, O) vibrations of the chelate.

The majority of luminescent lanthanide probes exhibit the antenna covalently bound to the chelate through a linker or spacer, termed “pendant” antenna. It is

often derived from existing organic chromophores with well-defined fluorescence profiles that are appropriate for sensitization energy requirements. The photophysical properties of Eu(III) and Tb(III) sensitizers, such as azaxanthone, phenanthridine and tetracycline, have been extensively studied in the context of lanthanide probes for time-resolved luminescent bioassays and are being applied to cellular imaging applications (**Figure 15)**.

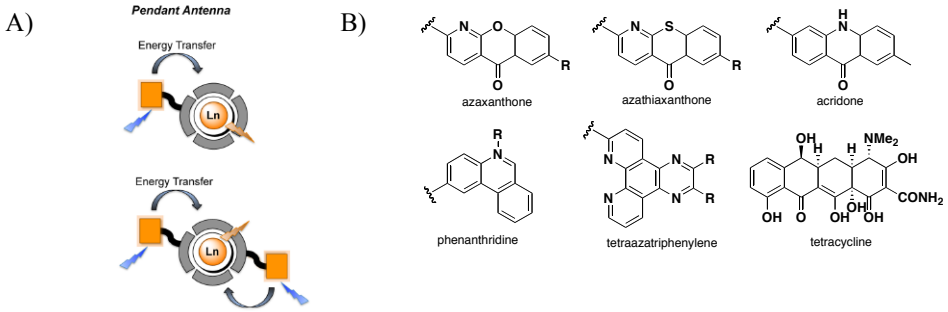

Figure 15: Pendant antennae used to sensitize lanthanide complexes.

A) Schematic of lanthanide chelates that utilize pendant antennae; the pendant antenna is attached to the chelate, as DOTA or DTPA, with a linker, and multiple pendant antennae can be incorporated. B) Examples of common sensitizers used as pendant antennae, deriving from organic fluorophores on the basis of favorable photophysiscal properties for sensitization.

Improving sensitization efficiency of pendant antennae has focused on increasing the energy gap $T_{1(antenna)} \rightarrow {}^5D_{j(Ln)}$ either decreasing linker length or using antennae that can directly coordinate to the metal center. An alternative way consists in the increasing the number of pendant antennae attached to a single chelate: regarding that, high luminescent Eu(III) and Tb(III) probes incorporating pendant picolinic antennae into 1,4,7-triazacyclononane and cyclen derivate were synthesized: generally, the fully coordination of europium and terbium ions with nona-coordinating ligands as TPATCN and TPMPTCN affords to stable complex with $q = 0$, that means no molecules of water coordinated in the first coordination sphere of the metal in solutions: the lanthanide ion results fully saturated with the three endocyclic *N*-atoms, the three *N*-atoms of the pyridine and the three *O*-atoms of

carboxylic or phosphonic groups. As consequence, they show high quantum yield, promoting these as well-promising luminescent probes.

The reduction of the ligand denticity affords to complexes with drastically reduced luminescent properties.

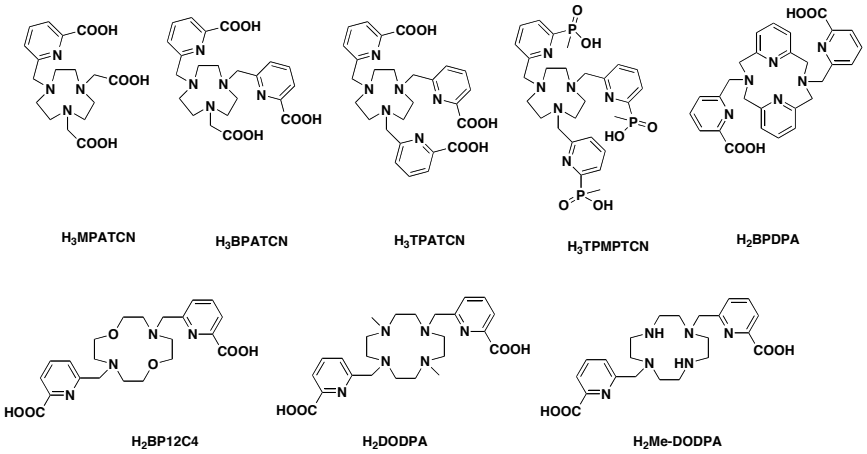

Figure 16: Picolinate ligands based on 1,4,7-triazacyclononane and cyclen with interesting luminescent properties.

Table 5. *Photophysical properties of such Ln(III)-L complex*

Ligand	λ_{abs} (nm)/ ε ($cm^{-1}M^{-1}$)	τ_{H2O} (ms)	τ_{D2O} (ms)	q	ϕ (%)
Eu(MPATCN)	273 nm, -	0.394	1.58	2	-
Eu(BPATCN)	273 nm, 9050 $cm^{-1}M^{-1}$	0.542	1.67	1	5
Eu(TPATCN)	274 nm, 14400 $cm^{-1}M^{-1}$	1.08	1.47	0	9
Eu(TPMPTCN)	272 nm, 8400 $cm^{-1}M^{-1}$	1.56	1.60	0	7
Eu(BPDPA)$^{+1}$	264 nm, -	0.66	1.70	0.7	1.3
Eu(DODPA)$^{+1}$	272 nm, -	0.26	0.39	1.1	-
Eu(Me-DODPA)$^{+1}$	272 nm, -	0.91	1.27	0.0	-
Tb(MPATCN)	273 nm, -	1.23	2.54	2	-
Tb(BPATCN)	273 nm, 9100 $cm^{-1}M^{-1}$	1.49	2.46	1	43
Tb(TPATCN)	274 nm, 15800 $cm^{-1}M^{-1}$	2.00	2.14	0	60
Tb(TPMPTCN)	272 nm, 7500 $cm^{-1}M^{-1}$	2.59	2.98	0	60
Tb(BPDPA)$^{+1}$	263 nm, -	1.16	1.53	0.7	16
Tb(DODPA)$^{+1}$	272 nm	1.18	1.51	0.6	-
Tb(Me-DODPA)$^{+1}$	272 nm	2.39	2.68	0	-

Comparing highly-coordinated chelates in **Table 5**, the lifetimes are longer than less coordinated complexes due to the absence of O-H oscillators in their coordination sphere.

Higher absorbing antennae with efficient ISC should be achieved with *d-f* bimetallic complexes where *d*-metal complexes can serve as sensitizing pendant antennae.

Finally, the use of chromophores that simultaneously serve as protective multidentate chelates, termed has chelating antennae, can sensitize Ln(III) luminescence: example of chelating agents are simple aromatic compounds such as pyridines and isophtalamides; Recently a chelating antennae based on 2-hydroxyisophtalamide (IAM) was used to sensitize Tb(III); initial evaluations of the sensitization efficiency of IAM binding units observed remarkably quantum yield leading to the development of octadentate ligands comprising a series of connected IAM units: while favourable properties of the free IAM unit, such as high molar absorptivity and quantum yield (ε = 26800 $M^{-1}cm^{-1}$; ϕ = 59%) were retained, the first generation of octadentate IAM derivatives was not water-soluble.

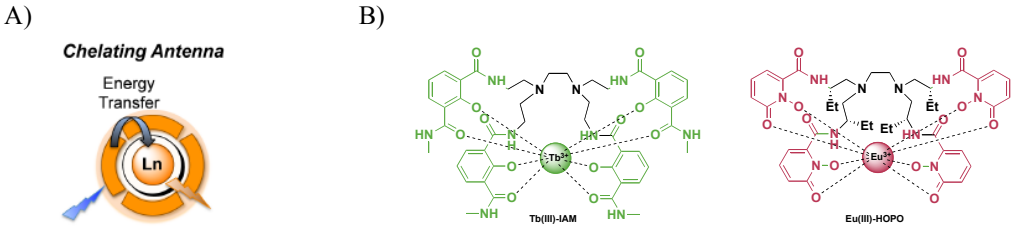

Figure 17: Chelating antennae used to sesitize lanthanide complexes.

a) Schematic of a chelating antennae that serves a dual function as both the protective lanthanide and sensitizing antenna. B) Examples of recently reported lanthanide complexes with chelating antennae as IAM and 1,2-HOPO.

For this reasons, substitution of the methylamide with methoxyethyl was attempted to improve the solubility, retaining excellent photophysical properties. Addition to this, 1-hydroxypyridine-2-one (1,2-HOPO) derived ligands were tested for Eu(III)

sensitization: they are more stable than the IAM ligands, but they are incapable of sensitizing Tb(III) due to their energies being too close to the excited state of Tb(III), displaying lower quantum yield as consequence (**Figure 17).**

Conclusions

While stringent requirements on stability, solubility, and photophysical properties have limited advances of chelating agents/antenna systems in intracellular applications The examples highlighted above can be useful for the future design. Such properties are highly attractive for the remarkable sesitization efficiencies.

References

1. J.K. Willmann, N. Bruggen, L. M. Dinkelborg, A. A. Gambhir (2008) *Nat. Rev. Drug Disc.* **7**, 591-607.

2. M.L.James, S.S. Gambhir (2012) *Physiol. Rev.* **92**, 897-965.

3. S. Lee, X. Chen (2009) *Mol. Imaging* **8(2)**, 87-100.

4. T.F. Massoud, S.S. Gambhir (2003), *Genes & Dev.* **17**, 545-580.

5. G.Gugliotta, M.Botta, L.Tei (2010) *Org. Biomol. Chem*, **8**, 4569-4574.

6. E. Gianolio, G.B. Giovenzana, A. Ciampa, D. Imperio, S. Aime (2008), *ChemMedChem* **3**, 60-62.

7. S. Crich, S. Lanzardo, D. Alberti, S. Belfiore, D. Ciampa, G.B. Giovenzana, C. Lovazzano, R. Pagliarin S. Aime (2007) *Neoplasia* **9(12)**, 1046-1056

8. T.J. Wadas, E.H. Wong, G.R. Weisman, C.J. Anderson (2010) *Chem. Rev* **110**, 2858-2902.

9. B.P. Waldron, D. Parker, C. Burchardt, D. S. Yufit, M. Zimny, F. Roesch (2013) *Chem. Commun.* **49**, 579-581.

10. W.Krause -Contrast Agent II: Optical, Ultrasound and Radiopharmaceutilca Imaging (2002)- *Topics in Current Chemistry* **222**, p.291

11. M. F. Phelps (2000) *J. Nucl. Med,* **41**, 661-681.

12. Z. Baranyai, F. Uggeri, A. Maiocchi, G.B. Giovenzana, C. Cavallotti, A. Takacs, I. Toth, J. Bànyai, A. Bényei, E. Brücher, S. Aime (2013) *Eur. J. Inorg. Chem*, 147-162

13. R. Gessner, P.A. Dayton (2010) *Mol. Imaging* **9**, 117-127.

14. M.F. Kircher, S.R. Willmann (2012) *Radiology* **263**, 633-643.

15. A.B. Wolbarst, W.R. Hendee (2006) *Radiology* **238**, 16-39.

16. D. Santra, D. Dutta, G.A. Walter, B.M. Moudyil (2005) *Technology in Cancer Research and Treatment* **4(6)**, 593-602.

17. X. Michalet, F.F. Pianud, L.A. Bentolila, J.M. Tsay, S. Doose, J.J. Li, G. Sundaresan, A.M. Wu, S.S. Gambhir, S. Weiss (2005) *Science* **307(5079)**, 538-544K.Licha, C. Olbrich (2005) *Adv. Drug Disc. Rev.* **57**, 1087-1108.

18. P. Caravan, J. J. Ellison, T.J. McMurry, R.B. Lauffer (1999) *Chem. Rev.* **99**, 2293-2352.

19. L. M. Manus, R.C.. Strauch, A. H. Hung, A. L. Eckermann, T. J. Meade (2012), *Anal. Chem*. **84**, 6278-6287.

20. G.A. Pereira, L. Balli, A. D. Sherry, J. A. Peters, C.F.G.C. Geraldes (2009) Helv. *Chim Acta* **92**, 2532-2551.

21. S. Aime, D. Longo, I. Longo, I. Menegotto, E. Gianolio, G.B. Giovenzana (2007), *Chem. Eur J.* **13**, 5785-5797.

22. S. Aime, K.C.Briley-Saebo, S. Geninatti-Crich, d. O. Cormode, A. Barazza, W. J. M. Mulder, W. Chen, E. A. Fisher, Z. A. Fayad, G.B. Giovenzana (2009), *J.Phys. Chem. B* **113**, 6283-6289.

23. Z. Baranyai, F. Uggeri, G.B. Giovenzana, A. Bényei, E. Brucher, S. Aime (2009) *Chem. Eur. J.* **15**, 1696-1705.

24. S. Aime, L. Calabi, C. Cavallotti, E. Gianolio, G.B. Giovenzana, P.Losi, A. Maiocchi, G. Palmisano, M. Sisti (2004), *Inorg. Chem* **43**, 7588-7590.

25. Lattuada, L.; Barge, A.; Cravotto, G.; Giovenzana, G.B.; Tei (2010) L. *Chem. Soc. Rev.* **40**, 3019-3049.

26. Z. Kotkovà, G.A. Pereira, K. Djanasvli, J. Kotek, J. Rudorsky, P. Hermann, L. Vander Elst, R. N. Muller, C.F.G.C. Geraldes, I. Lukes, J.A. Peters (2009) *Eur. J. Inorg. Chem*, 119-136.

27. S. Aime, M. Botta, L.Frullano, S. Geninatti, G.B. Giovenzana, R. Pagliarin, G. Palmisano, F. Riccardi Sirtori, M. Sisti (2000) *J. Med. Chem.* **43**, 4017-4024.

28. T. Vitha, V. Kubicek, J. Kotek, P. Hermann, L. Vander Elst, R.N. Muller, I. Lukes, J. Peters (2009) *Dalton Trans*, 3204-3214.

29. A. Ermelindo, G. Gambino, L. Tei (2013), *Tetrahedron Letters* **54**, 6378-6380.

30. A. Nonat, C. Gateau, P.H. Fries, M, Mazzanti (2006), *Chem. Eur. J.* **12**, 7133-7150.

31. J.C.G. Bunzli (2010) *Chem. Rev.* **110**, 2729-2755.

32. M.C. Heffern, L.M. Matosziuk, T.J. Meade (2014), *Chem. Rev.* **114**, 4496-4539.

33. J.W.Walton, R. Carr, N. Evans, A.M. Funk, A. M. Kenwright, D. Parker, D.S. Yufit, M. Botta, S. de Pinto, K. Wong. (2012) *Inorg. Chem.* **51**, 8042-8056.

34. A.R.Rodriguez, D.E. Gomez, A. de Blas, T.R. Blas, M. Fekete, M. Botta, R. Tripier, C.P. Iglesias (2012) *Inorg. Chem* **51**, 2509-2521.

35. A. Beeby, I.M. Clarkson, R.S. Dickins, S. Faulkner, D. Parker, L. Roule, A.S. de Sousa, J.A. Gareth Qilliams, M.Woods (1999) *J. Chem Soc., Perkin Trans* **2** 493-504.

Outline of the thesis

During the last decades the research in the field of contrast agents (CAs) for MRI, PET, SPECT and OI has received a marked impulse due to the increasing interest to obtain innovative contrast agents to use for the well-detailed detection of tissue diseases. All these techniques offer the possibility to investigate various pathologies, each of them bearing peculiar advantages and drawbacks.

According to the tradition of this group of research, our attention was mainly focused on the development of new chelating agents for Gd-based-MRI-CAs.

Magnetic Resonance Imaging (MRI) is a diagnostic and research tool poised to overcome a number of challenges facing molecular imaging. The technique permits to obtain high resolution images of the internal structure of organisms. In comparison to other medical imaging techniques, MRI utilizes no ionizing radiation allowing several measurements to be obtained without radioactive risk for the organism.

MRI-CAs are employed to enhance the contrast of hystologically dinstinct tissues; they are stable complexes of paramagnetic metal ions (transition metals and lanthanides) with cyclic and acyclic polyaminocarboxylic ligands, such as Gd-DTPA and Gd-DOTA: indeed, DTPA and DOTA show a common polyaminocarboxylic structure able to coordinate a metal ion with eight coordination sites. Gd(III) is the most used paramagnetic ion, until recent concerns about its toxicity boosted the search for less harmful substitutes such as Mn(II). Lanthanides are metal ions with an usual number of coordination 9 and for this reason they generally set up mono or dihydrate-complexes (q = molecules of water of inner sphere = 1, 2) in aqueous solution with these polyaminocarboxylate ligands.

Relaxivity (r_{1p}) is the key parameter indicating the ability of paramagnetic complexes to increase the nuclear magnetic relaxation rate of vicinal protons, increasing the contrast in the diagnostic image. The ideal MRI-CA is characterized by the following properties:

- high thermodynamic stability and kinetic inertness to avoid the release of free metal ions, toxic for the organisms;
- high relaxivity, to increase the contrast in the diagnostic images; the relaxivity is enhanced by increasing *q* or the molecular size of the paramagnetic system or the coordinated water exchange rate;
- high water solubility and low toxicity.

Efforts directed towards improvements of MRI contrast agents rely on different strategies involving structural variations of the ligand; according to this, substitution of carboxylate groups with different acidic functionalities was extensively investigated, leading to the preparation of several derivative embodying more or less classical isosteres such as phosphonic acid, phosphinic acid, acylsulphonamide and tetrazole. Among them, the substitution of carboxylic groups with a mixed combination of carboxylic and phosphonic coordinating group on the basic structure of common bifunctional DTPA ligand was explored: indeed, phosphonic group may enhances the coordination properties due to its tetrahedral deprotonated form $–PO_3^{2-}$, while the residual anionic charge after complexation provide a better solubility in water.

Substitution of carboxylic groups with phosphonic ones was also investigated for the alternative polyaminocarboxylic chelating agent AAZTA structure: indeed, the potential improvements in terms of relaxometric and coordinating properties stimulated our interest towards the synthesis of mixed carboxylic-phosphonic species. Three new mono and diphosphonic AAZTA-like ligands were synthesized and investigated: they were obtained in few steps with satisfactory yields; unfortunately the performance of phosphonic AAZTA-chelating agents were not as expected, pointing out that in this istance the substitution of a carboxylic group

with one or two phosphonic moiety causes a reduction in relaxivity and an increase of τ_M due to a reduction of hydration degree.

Alternatively, AAZTA was purposed now as platform for the synthesis of chelating agents for Eu(III) and Tb(III)-based-luminescent probes to applied in Optical Imaging.

Optical Imaging is a high–resolution, sensitive and semi-quantitative technique of diagnosis: it uses non-ionizing radiation and low concentration of contrast agent to produce high contrast images and cellular/subcellular resolution, possibly in response to biological events.

Lanthanide-based luminescent probes are particularly attractive due to their long luminescent lifetimes, especially useful for time-gated detection techniques. Despite that, lanthanides have low molar absorbivity requiring intense light sources for their direct excitation. Complexation with an appropriate chelate able to transfer energy to the metal centre is a practical alternative to increase the population of excited states.

This project was developed in collaboration with the group of research of Prof. Loïc Charbonniere and the *Laboratoire de Ingégniere Moléculaire Appliquée à L'Analyse* (CNR of Strasbourg - France). The seven-membered ring of 6-amino-6-methylperhydro-1,4-diazepine (AMPED), was deemed useful as a platform for the synthesis of a new chelating agent for the luminescent Eu(III) and Tb(III) ions: the stability of the complexes formed by ligands sharing this triamine may be combined with the enhanced rigidity of the resulting chelating system, the latter property potentially improving the luminescence in terms of quantum yield and lifetime.

Alkylation of AMPED with a picolinic derivative as chromophore affords to a new interesting antenna-chelate system able to wrap around the metal centre in a rigid and stable cage surprising luminescent properties.

Nowadays, the development of new CAs for diagnostic applications is a fervent field of research: the functionalisation of the chelating agent affording to more specific CAs, the thermodynamic stability and the kinetic inertness of lanthanides complexes, the improvements of relaxometric and luminescent properties and the limited toxicity of them, are only some of the main goals planned. During this PhD an interesting contribute has been added in the field of CAs for MRI, PET, SPECT and OI, affording to novel chelating agents for lanthanides(III) ions with satisfactory results.

Synthesis of bifunctional chelating agents based on mono and diphosphonic derivatives of diethylenetriaminepentaacetic acid

Giovanni B. Giovenzana[a,]*, Claudia Guanci[a], Silvia Demattio[b], Luciano Lattuada[b,]*, Veronica Vincenzi[b]

Published in Tetrahedron **2014** Vol. *70(32)*, 4809-4813.

Abstract

Bifunctional chelating agents (BFCAs) are small molecules containing a chelating unit, able to strongly coordinate a metal ion, and a reactive functional group, devised to form a stable covalent bond with another molecule. BFCAs are widely employed since their conjugation to a suitable biomolecule (*e.g.* a peptide or an antibody) allows the synthesis of diagnostic or therapeutic agents that specifically target diseased tissue with metals or radiometals. For this reason, BFCAs find application in diagnostic imaging, molecular imaging and radiotherapy of cancer. The synthesis of new BFCAs based on a diethylenetriaminepentaacetic acid (DTPA) structure in which one or two carboxylic groups are replaced with phosphonic units is described. The phosphonic group, aside from being a classical isostere of the carboxylic acid in coordination chemistry, allows to modulate the physico-chemical properties of the ligands and of the corresponding complexes.

Introduction

The use of metal or radiometal complexes in medicine as therapeutic or diagnostic agents is an area of growing interest.[1-3] For diagnostic purposes, gadolinium complexes are employed as contrast agents in magnetic resonance imaging (MRI)[4-6] while complexes of ^{111}In or ^{68}Ga, for example, find application in

single photon emission computed tomography (SPECT) or positron emission tomography (PET), respectively.[7-10] For therapy, and in particular in the treatment of some kind of tumors and metastases, complexes of β or α emitters, such as ^{90}Y, ^{177}Lu or ^{225}Ac, are usually studied and administered to patients.[7-12]

All these metal ions need to be strongly coordinated with a suitable ligand to guarantee a safe administration *in vivo* and prevent an undesirable deposition of toxic metal ions in tissues or organs different from the desired target. Polyaminopolycarboxylic derivatives, such as diethylene-triaminepentaacetic acid **1a** (DTPA) or 1,4,7,10-tetraazacyclododecane-1,4,7,10-tetraacetic acid **2** (DOTA) (Fig. 1), are the ligands of choice and are widely employed because they provide very stable complexes with a wide variety of metal ions.[13]

The metal complex is usually covalently bound to a targeting vector (*e.g.* peptides[14-16] or monoclonal antibodies[17,18]) that allows a specific delivery to particular type of cells by a recognition process. The easiest way of linking a vector to a metal complex is by direct conjugation to a bifunctional chelating agent (BFCA) followed by deprotection of eventual protective groups and final complexation of the metal ion of choice.[19-21]

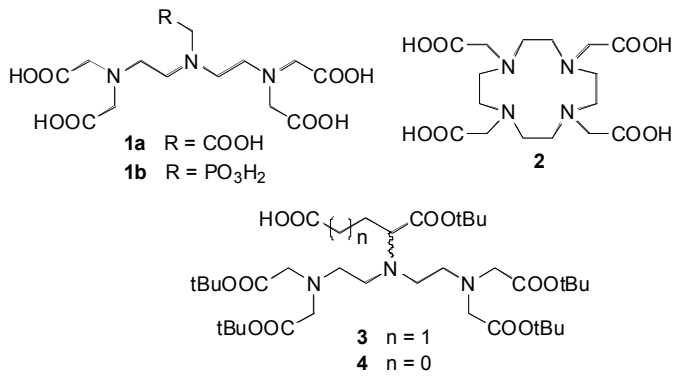

Fig. 1

Among the huge number of polyaminopolycarboxylic bifunctional chelating agents reported in literature,[22] BFCA **3**[23] and **4**[24] (Fig. 1) found a broad spectrum of

applications. For example, BFCA **3** has been conjugated to bile acids,[25,26] oxytocin,[27] aminoacids,[28] CCK8 peptides,[29] RGD (Arg-Gly-Asp) peptidomimetics,[30,31] while BFCA **4** has been exploited in the synthesis of a potential MRI contrast agent,[32] linked to a tamoxifen derivative,[33] and conjugated to a cyclic peptide for fibrin targeting.[34]

Efforts directed towards improvements of MRI contrast agents rely on different strategies involving structural variations of the ligand; among them the substitution of carboxylic groups with different acidic functionalities was extensively investigated, leading to the preparation of several derivatives, embodying more or less classical isosteres such as phosphonic acid,[35,36] phosphinic acid,[37] acylsulphonamide[38] and tetrazole.[39]

The phosphonic acid is particulary appealing as its size and acidic properties closely resemble the behaviour of carboxylic groups.[40] Its tetrahedral deprotonated form ($-PO_3^{2-}$) occurring at physiological pH values offers multiple coordination modes, and residual anionic charges after complexation provide a beneficial effect on the solubility of the corresponding chelate, due to the establishment of an extended hydrogen bond network leading to improved solvation. Several examples of polydentate ligands embodying one[41] or more[42,43] phosphonic groups were reported for different purposes ranging from water corrosion inhibitors to diagnostic and therapeutic applications.

Phosphonic derivatives of the octadentate ligand DTPA (diethylenetriaminepentaacetic acid) are already known: the per-phosphonated derivative (DTPMP)[44] is commercially available (Dequest® 2060), while the monophosphonic DTPA-analog **1b**[45] is reported to form thermodynamically very stable metal complexes, with stability constants comparable with the parent DTPA ligand.[46]

Despite the growing interest in phosphonic derivatives of polyaminocarboxylic ligands, it is surprising to observe only a few examples of bifunctional derivatives. A perphosphonic derivative (DOTP) of the macrocyclic ligand DOTA was decorated with different appendages, among them a *p*-aminophenyl residue amenable to use for conjugation purposes.[47] Moreover, two different cyclohexane-1,2-diamine tetraphosphonic ligands bearing ready-to-use isothiocyanate groups were designed for application in ^{153}Sm-based radioimmunotherapy.[48] To the best of our knowledge, the only BFCA with carboxylic and phosphonic moieties reported so far, is a triethylenetetraaminehexaacetic acid (TTHA) analog.[49]

We describe here the synthesis of two novel BFCA based on the DTPA structure but having one (Scheme 1, compound **11**) or two (Scheme 2, compound **18**) phosphonic group replacing the corresponding carboxylic moieties.

Results and discussion

The synthesis of the phosphonic derivatives **3** and **4** was realized adapting the original protocol of Rapoport,[50] widely applied for the easy assembly of DTPA derivatives and implying the double *N*-alkylation of a primary amine (representing the "central" nitrogen atom of DTPA) with two molar equivalents of a *N*-(β-bromoethyl)iminodiacetate ester (representing the "left" and "right" wings of the DTPA).

The synthesis of monophosphonic BFCA **11** is shown in Scheme 1. Benzylamine was bisalkylated with bromoderivative **5**[50] in acetonitrile and in the presence of micronized K_2CO_3 as base. Compound **6** was then hydrogenated to give in good yield the symmetrical diethylenetriaminetetraacetic acid tetra-*t*-butyl ester **7**[51], with the central secondary amine available for further functionalization. Reaction of **7** with the aldehyde-ester **8**[52] and tri-*t*-butylphosphite **9**[53] in refluxing acetonitrile produced the monophosphonic derivative **10**. Selective deprotection of the

carboxylic ester located on the side chain by hydrogenolysis afforded the protected BFCA **11**.

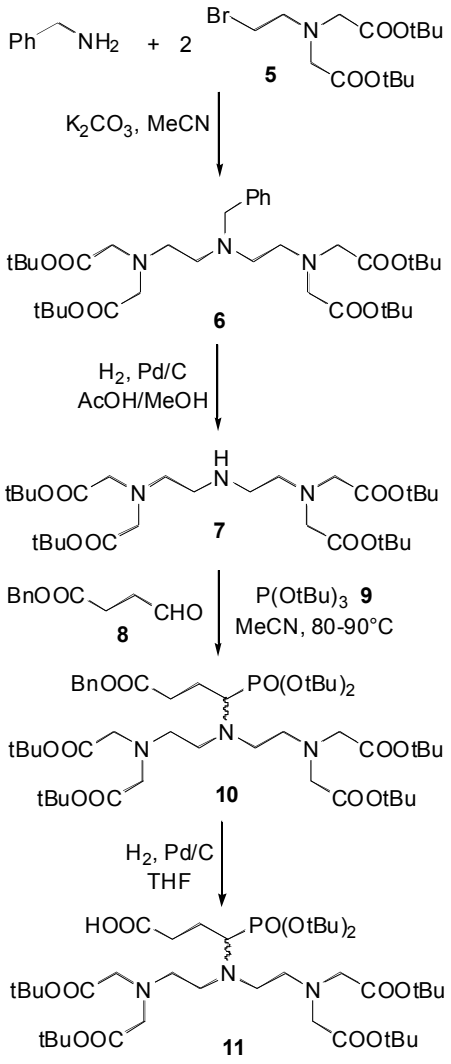

Scheme 1. Synthesis of BFCA 11

The synthesis of diphosphonic BFCA **18** relied on a similar strategy, necessarily implying the modification of the *N*-(β-bromoethyl)iminodiacetate ester alkylating agent to include a (protected) phosphonate group. The novel bromoderivative **14**

(Scheme 2) was synthesized by phosphonomethylation of *N*-(2-hydroxyethyl)glycine 1,1-dimethylethyl ester **12**[54] with paraformaldehyde and tri-*t*-butylphosphite **9**[53] to give the aminoalcohol **13**. Mesylation of the primary alcohol with the combination methanesulfonyl chloride/triethylamine in THF and a prompt treatment with lithium bromide generated the desired "mixed" alkylating agent **14**.

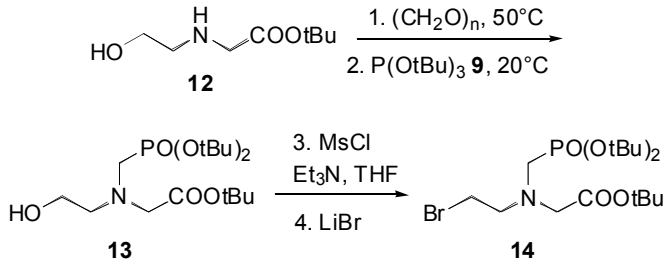

Scheme 2. Synthesis of bromoderivative 14

The assembly of the BFCA **18** continues with the bis-alkylation of the nitrogen atom of a suitable protected aminoacid. Esterification of aspartic acid 4-phenylmethyl ester **15** into its *t*-butyl ester derivative **16** was easily performed in *t*-BuOAc with perchloric acid, as reported by Taschner.[55] Treatment of **16** with 2 molar equivalents of the bromoderivative **14** in a buffered system gave compound **17**. As for the previous example, selective hydrogenation of the benzyl ester located on the side chain released the corresponding free carboxylic acid completing the synthesis of the diphosphonic BFCA **18** (Scheme 3).

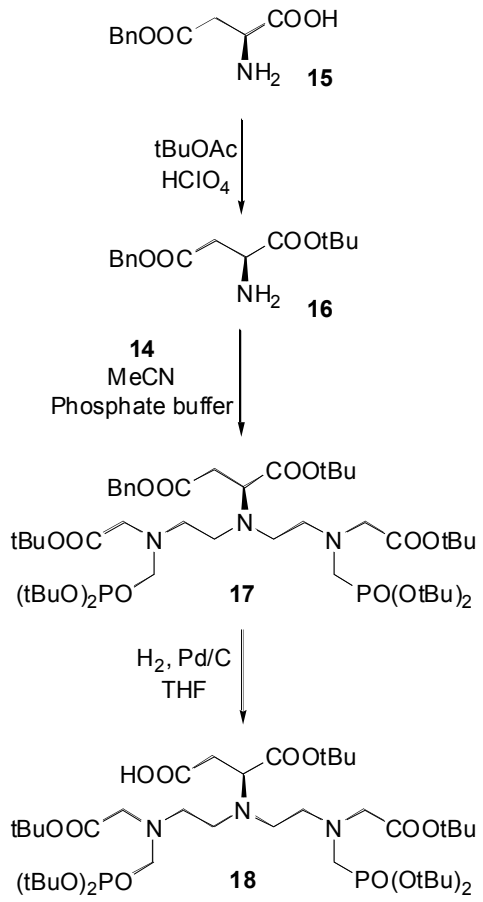

Scheme 3. Synthesis of BFCA 18

Conclusions

The preparation of two original bifunctional chelating agents formally based on mono and diphosphonic derivatives of diethylenetriaminepentaacetic acid, was designed and realized. For the first time, DTPA ligands with a mixed combination of carboxylic and phosphonic coordinating group are endowed with an additional

remote carboxylic group, devised for direct conjugation to biomolecules or to be coupled to terminal amino groups or lysine ε-amine during solid phase synthesis.[56] The availability of a multigram synthesis of these BFCA will pave the way to the preparation of several conjugated derivative of the corresponding metal complexes, exploiting the potential of these mixed ligands in their diagnostic and therapeutic applications.

Experimental section

1. General

Reagent-grade chemicals and solvents were obtained from commercial sources and directly used without further purification. *N*-(2-Bromoethyl)-*N*-[2-(1,1-dimethylethoxy)-2-oxoethyl]glycine 1,1-dimethylethyl ester **5**,[50] 4-oxobutanoic acid phenylmethyl ester **8**,[52] tri-*t*-butylphosphite **9**[53] and *N*-(2-hydroxyethyl)glycine 1,1-dimethylethyl ester **12**[54] were synthesized as reported in literature. TLC was performed on Merck silica gel 60 TLC plates F254 and visualized by using UV or 1% $KMnO_4$ in 1 M NaOH. Column chromatography was performed by using silica gel 60 (70-230 mesh) while flash chromatography was carried out on silica gel 60 (230-400 mesh). The ^{1}H, ^{13}C and ^{31}P spectra were recorded on a Bruker Avance 400 instrument and using $CDCl_3$ as solvent. Mass spectra were recorded with a ThermoFinnigan TSQ700 triple-quadrupole instrument equipped with an electrospray ionization source. Analytical HPLC was performed on a Merck KGaA apparatus with the following method: stationary phase: Lichrosorb RP-Select B 5 μm, 250 x 4 mm column packed by Merck KGaA; mobile phase: eluent A = 0.01 M KH_2PO_4 and 0.017 M H_3PO_4 in H_2O, eluent B = MeCN, gradient elution: t = 0 min (5% B), t = 45 min (80% B); T = 45°C; flow rate: 1 mL min^{-1}; UV detection: 210 nm.

*2. N,N'-[[(Phenylmethyl)imino]di-2,1-ethanediyl]bis[N-[2-(1,1-dimethylethoxy)-2-oxoethyl]glycine bis(1,1-dimethylethyl) ester (**6**)*

Micronized K_2CO_3 (13.82 g; 100 mmol) was added to a solution of benzylamine (5.46 mL; 50 mmol) and *N*-(2-bromoethyl)-*N*-[2-(1,1-dimethylethoxy)-2-oxoethyl]glycine 1,1-dimethylethyl ester **5**[50] (37.2 g; 100 mmol) in MeCN (100 mL). The mixture was stirred at room temperature and in a nitrogen atmosphere. After 72 h the mixture was filtered and the solvent evaporated. The residue was dissolved in CH_2Cl_2 (150 mL) and the solution was washed with water (3 x 100 mL). The organic phase was dried (Na_2SO_4) and evaporated. The residue was purified by column chromatography (EtOAc/petroleum ether, 1:1) to give **6** (28.0 g; 86%) as a yellow oil. Found: C, 64.4; H, 9.1; N, 6.4. $C_{35}H_{59}N_3O_8$ requires C, 64.69; H, 9.15; N, 6.47%; HPLC R_t=28 min, 97% (area %); ^{1}H NMR ($CDCl_3$, 400 MHz, 298K): δ 7.32-7.20 (5H, m, Ph), 3.63 (2H, s, C*H*$_2$Ph), 3.41 (8H, s, C*H*$_2$COOtBu), 2.86-2.82 (4H, m, NC*H*$_2$), 2.64-2.60 (4H, m, NC*H*$_2$), 1.46 (36H, s, tBu); ^{13}C NMR ($CDCl_3$, 100.6 MHz, 298K): δ 171.1 (CO), 140.0 (C), 129.2 (CH), 128.5 (CH), 127.2 (CH), 81.1 (C), 59.5 (CH_2), 56.5 (CH_2), 53.2 (CH_2), 52.4 (CH_2), 28.6 (CH_3); ν_{max} (KBr): 3086, 3063, 2978, 2933, 1741, 1603, 1455, 1393, 1255, 1219, 1152, 738, 700; ESI/MS *m/z* calcd for: $[C_{35}H_{59}N_3O_8+H]^+$ 650.87, found: 650.65.

*3. N,N'-(Iminodi-2,1-ethanediyl)bis[N-[2-(1,1-dimethylethoxy)-2-oxoethyl]glycine bis(1,1-dimethylethyl) ester (**7**)*

5% Palladium on charcoal (2.85 g) was added to a solution of **6** (28.49 g; 43.8 mmol) in AcOH (10 mL; 175.4 mmol) and MeOH (1250 mL) and the mixture was stirred under hydrogen atmosphere at room temperature. After 2.5 h the catalyst was filtered and the solvent was evaporated. The residue was dissolved in CH_2Cl_2 (150 mL) and the solution was washed with saturated solution of $NaHCO_3$ (3 x 100 mL) then with water (2 x 100 mL). The organic phase was dried (Na_2SO_4) and evaporated to give **7** (23.48 g; 96%) as a yellow oil. Found: C, 59.8; H, 9.4; N, 7.4.

$C_{28}H_{53}N_3O_8$ requires C, 60.08; H, 9.54; N,7.51; R_f=0.24 (MeOH/EtOAc, 1:4); ^{1}H NMR ($CDCl_3$, 400 MHz, 298K): δ 3.35 (8H, s, CH_2COOtBu), 2.79 (4H, t, *J*=6.3 Hz, NCH_2), 2.61 (4H, t, *J*=6.3 Hz, NCH_2), 1.37 (36H, s, tBu); ^{13}C NMR ($CDCl_3$, 100.6 MHz, 298K): δ 171.2 (CO), 81.1 (C), 56.7 (CH_2), 54.7 (CH_2), 48.4 (CH_2), 28.4 (CH_3); ν_{max} (KBr): 3313, 2978, 2933, 1736, 1457, 1393, 1368, 1254, 1220, 1151; ESI/MS *m/z* calcd for: $[C_{28}H_{53}N_3O_8+H]^+$ 560.75, found: 560.63.

*4. 9-[1-[Bis(1,1-dimethylethoxy)phosphinyl]-4-oxo-4-(phenyl methoxy)butyl]-6,12-bis[2-(1,1-dimethylethoxy)-2-oxoethyl]-2,2-dimethyl-4-oxo-3-oxa-6,9,12-triazatetradecan-14-oic acid, 1,1-dimethylethyl ester (**10**)*

A solution of 4-oxobutanoic acid phenylmethyl ester **8** (7.7 g; 40 mmol)[52] in MeCN (50 mL) was added dropwise in 30 min to a solution of **7** (20.15 g; 36 mmol) in MeCN (200 mL) at 80 °C. The reaction mixture was stirred for further 30 min and then cooled to room temperature. A solution of tri-*t*-butylphosphite **9** (14.62 g; 40 mmol) was added dropwise over 20 min, then the mixture was stirred at room temperature for 4 days. After evaporation of the solvent, the residue was purified by flash chromatography (EtOAc/petroleum ether, 3:7→1:1) to give **10** (12.08 g, 36%) as a yellow oil. Found: C, 60.7; H, 8.9; N, 4.4; P, 3.1. $C_{47}H_{82}N_3O_{13}P$ requires C, 60.82; H, 8.91; N, 4.53; P, 3.34; R_f=0.45 (EtOAc/*n*-hexane, 1:1); HPLC R_t=34.5 min, 98% (area %); ^{1}H NMR ($CDCl_3$, 400 MHz, 298K): δ 7.35-7.28 (5H, m, Ph), 5.10 (2H, s, CH_2Ph), 3.39 (8H, s, CH_2COOtBu), 2.94-2.86 (5H, m, NCH_2 and C*H*), 2.74-2.69 (4H, m, NCH_2), 2.56 (2H, t, *J*=7.2 Hz, CH_2COOBn), 1.95 (1H, m, CH_2), 1.79 (1H, m, CH_2), 1.49 (18H, s, POtBu), 1.42 (36H, s, COOtBu); ^{13}C NMR ($CDCl_3$, 100.6 MHz, 298K): δ 174.0 (CO), 170.9 (CO), 136.6 (C), 128.8 (CH), 128.6 (CH), 128.4 (CH), 82.9 (d, J_{CP}=12.1 Hz, C), 82.2 (d, J_{CP}=9.3 Hz, C), 81.0 (C), 66.3 (CH_2), 60.8 (d, J_{CP}=138.8 Hz, CH,), 56.0 (CH_2), 54.2 (CH_2), 50.6 (CH_2), 31.3 (d, J_{CP}=12.4 Hz, CH_3), 31.0 (d, J_{CP}=3.4 Hz, C) 30.9 (d, J_{CP}=3.3 Hz, CH_3,), 28.6 (CH_3), 24.3 (d, J_{CP}=6.5 Hz, CH_2); ^{31}P NMR($CDCl_3$, 162 MHz, 298K): δ 19.9(s); ν_{max} (KBr): 3066, 2979, 2934, 2874,

1738, 1457, 1393, 1369, 1257, 1155, 978, 752, 698; ESI/MS *m/z* calcd for: $[C_{47}H_{82}N_3O_{13}P+Na]^+$ 951.14, found: 951.25.

*5. 9-[1-[Bis(1,1-dimethylethoxy)phosphinyl]-3-carboxypropyl]-6,12-bis[2-(1,1-dimethyl ethoxy)-2-oxoethyl]-2,2-dimethyl-4-oxo-3-oxa-6,9,12-triazatetradecan-14-oic acid, 14-(1,1-dimethylethyl) ester (**11**)*

5% Palladium on charcoal (3.6 g) was added to a solution of **10** (12 g; 13 mmol) in THF (75 mL) and the mixture was stirred under hydrogen atmosphere at room temperature. After 18 h the catalyst was filtered and the solution was evaporated to give **11** (10.2 g; 94%) as a viscous yellow oil. Found: C, 57.4; H, 9.1; N, 5.1; P, 3.7. $C_{40}H_{76}N_3O_{13}P$ requires C, 57.33; H, 9.14; N, 5.01; P, 3.70; R_f=0.41 (EtOAc/*n*-hexane, 4:1); ^{1}H NMR ($CDCl_3$, 400 MHz, 298K): δ 3.42 (8H, s, CH_2COOtBu), 3.27 (1H, bt, C*H*), 3.09-3.00 (4H, m, NCH_2), 2.92-2.83 (4H, m, NCH_2), 2.72-2.65 (2H, m, CH_2COOH), 1.95 (1H, m, CH_2), 1.85 (1H, m, CH_2), 1.51 (9H, s, POtBu), 1.50 (9H, s, POtBu), 1.44 (36H, s, COOtBu); ^{13}C NMR ($CDCl_3$, 100.6 MHz, 298K): δ 176.2 (CO), 170.8 (CO), 83.8 (d, J_{CP}=12.1 Hz,C), 83.1 (d, J_{CP}=9.0 Hz, C), 81.4 (C), 61.5 (d, J_{CP}=141.8 Hz, CH), 55.6 (CH_2), 52.8 (CH_2), 50.3 (CH_2), 34.2 (d, J_{CP}=14.1 Hz , CH_2), 31.0 (d, J_{CP}=4.0 Hz, CH_3), 30.9 (d, J_{CP}=3.0 Hz, CH_3), 28.5 (CH_3), 24.0 (d, J_{CP}=2.0 Hz, CH_2); ^{31}P NMR($CDCl_3$, 162.0 MHz, 298K): δ 17.4 (s); ν_{max} (KBr): 3441 (br), 2978, 2934, 1732, 1457, 1394, 1369, 1256, 1220, 1151, 981; ESI/MS *m/z* calcd for: $[C_{40}H_{76}N_3O_{13}P-H]^-$ 836.50, found: 836.37.

*6. N-[[Bis(1,1-dimethylethoxy)phosphynyl]methyl]-N-(2-hydroxyethyl)glycine 1,1-dimethylethyl ester (**13**)*

A mixture of paraformaldehyde (1.71 g; 57.07 mmol) and *N*-(2-hydroxyethyl)glycine 1,1-dimethylethyl ester **12**[54] (10 g; 57.07 mmol) was stirred at 50 °C. After 16 h CH_2Cl_2 (150 mL) was added, the solution was dried (Na_2SO_4) and the solvent was removed under reduced pressure. Tri-*t*-butylphosphite **9**[52] (14.28 g; 57.07 mmol) was added to the residue and the mixture was stirred

overnight at room temperature, then evaporated *in vacuo*. The residue was purified by flash chromatography (Et_2O/CH_2Cl_2, 45:55) to give **13** (5.21 g; 24%) as a pale yellow oil. R_f=0.19 (Et_2O/CH_2Cl_2, 45:55); ^{1}H NMR ($CDCl_3$, 300.0 MHz, 298K): δ 3.52 (2H, t, *J*=4.9 Hz, C*H*$_2$OH), 3.47 (2H, s, C*H*$_2$COOtBu), 2.95 (2H, d, *J*=8.3 Hz, C*H*$_2$P), 2.84 (2H, t, *J*=4.9 Hz, NC*H*$_2$), 1.45 (18H, s, POtBu), 1.41 (9H, s, COOtBu); ^{13}C NMR ($CDCl_3$, 75.4 MHz, 298K): δ 171.1(CO), 82.7 (d, J_{CP}=9.2 Hz,C), 81.3 (C), 59.9 (CH_2), 58.8 (d, J_{CP}=9.2 Hz , CH_2), 57.2 (d, J_{CP}=3.4 Hz, CH_2), 52.3 (d, J_{CP}=165.7, CH_2), 30.5 (CH_3), 28.2 (CH_3); ^{31}P NMR ($CDCl_3$, 121.4 MHz, 298K): δ 19.4(s); ν_{max} (KBr): 3367 (br), 2973, 2931, 2877, 1732, 1668, 1457, 1387, 1368, 1232, 1155, 1061; ESI/MS *m/z* calcd for: $[C_{17}H_{36}NO_6P+Na]^+$: 404.21; found: 404.30.

*7. N-[[Bis(1,1-dimethylethoxy)phosphynyl]methyl]-N-(2-bromoethyl)glycine-1,1-dimethylethyl ester (**14**)*

Under a nitrogen atmosphere, methanesulfonyl chloride (2.8 mL; 36 mmol) was slowly added to a solution of compound **13** (12.72 g; 33.3 mmol) and triethylamine (6.5 mL; 46.6 mmol) in dried THF (500mL) cooled at -15°C. After 1.5 h lithium bromide (25.0 g; 288 mmol) was added and the slurry was vigorously stirred for 16 h allowing the temperature to rise spontaneously to 20°C. The solvent was evaporated and EtOAc (300 mL), Et_2O (300 mL) and water (200 mL) were added to the residue. The organic phase was separated, washed with water (200 mL), brine (2 x 100 mL) and dried (Na_2SO_4). The solvents were evaporated and the residue was purified by flash chromatography (2-PrOH/Et_2O/*n*-hexane, 0.01:1:1) to give **14** (12.35 g; 83%) as a colourless oil, solidifying upon storage at -18°C. Mp 50-51°C; *R_f=0.*35 (EtOAc/iPr_2O, 1:4); ^{1}H NMR($CDCl_3$, 300 MHz, 298K): δ 3.55 (2H, s, C*H*$_2$COOtBu), 3.41 (2H, t, *J*=7.5 Hz, BrC*H*$_2$), 3.15 (2H, t, *J*=7.5 Hz, NC*H*$_2$), 3.03 (2H, d, *J*=9.6 Hz, C*H*$_2$P), 1.45 (18H, s, POtBu), 1.43 (9H, s, COOtBu); ^{13}C NMR ($CDCl_3$, 75.4 MHz, 298K): δ 171.1 (CO), 82.4 (d, J_{CP}=9.0 Hz, C), 81.3 (C), 58.1 (d, J_{CP}=15.1 Hz,CH_2), 56.7 (CH_2), 54.2 (CH_2), 52.0 (CH_2),

30.6 (d, J_{CP}=4.3 Hz, CH_3), 28.3 (CH_3); ^{31}P NMR ($CDCl_3$, 121.4 MHz, 298K): δ 17.3 (s); ν_{max} (KBr): 2974, 2933, 1735, 1454, 1389, 1370, 1250, 1150, 994, 731; ESI/MS *m/z* calcd for: $[C_{17}H_{35}BrNO_5P+Na]^+$: 466.13; found: 466.00.

*8. L-Aspartic acid 1-(1,1-dimethylethyl) 4-(phenylmethyl) ester (**16**)*

A 70% aqueous solution of $HClO_4$ (0.930 mL; 10.75mmol) was slowly added to a suspension of aspartic acid 4-phenylmethyl ester **15** (2.0 g; 8.95mmol) in *t*-butyl acetate (50 mL). The mixture was then stirred for 36 h at room temperature. The reaction mixture was diluted with H_2O (40 mL) and after separation the aqueous phase was extracted with EtOAc (3 x 15 mL). The combined organic phases were washed with 10% aq. Na_2CO_3 (50 mL) and H_2O (50 mL), then dried (Na_2SO_4). The solvent was evaporated under reduced pressure to give **16** (1.4 g; 56%) as a colourless oil. R_f=0.52 (EtOAc); HPLC R_t=14.4 min, 97% (area %); ^{1}H NMR ($CDCl_3$, 300 MHz, 298K): δ 7.42-7.23 (5H, m, Ph), 5.12 (2H, bs, CH_2Ph), 3.73 (1H, dd, J_1=7.0 Hz, J_2=4.9 Hz, C*H*-N), 2.81 (1H, dd, J_1=16.5 Hz,J_2=4.9 Hz, CH_2), 2.73 (1H, dd, J_1=16.8 Hz, J_2=7.0 Hz, CH_2), 2.68 (2H, bs, NH_2),1.40 (9H, s, tBu); ^{13}C NMR ($CDCl_3$, 75.6 MHz, 298K): δ 173.1 (C), 171.2 (C), 135.7 (C), 128.6 (CH), 128.4 (2xCH), 81.7 (C), 66.6 (CH_2), 51.8 (CH), 39.0 (CH_2), 28.0 (CH_3); $[\alpha]_D^{20}$ +16.0 (*c* 0.57, $CHCl_3$) (lit.[57] +10.9, *c* 0.57, $CHCl_3$); ν_{max} (KBr): 3350, 2974, 2942, 1728, 1736, 1667, 1368, 1360, 1250, 1151, 750, 736, 697; ESI/MS *m/z* calcd for: $[C_{15}H_{21}NO_4+H]^+$: 280.15; found: 280.05.

*9. N,N-Bis[2-[[[2-(1,1-dimethylethoxy)-2-oxoethyl][[bis(1,1-dimethylethoxy)-phosphynyl]methyl]amino]ethyl]]-L-aspartic acid 1-(1,1-dimethylethyl) 4-(phenylmethyl) ester (**17**)*

A mixture of **16** (0.947 g; 3.39 mmol) and **14** (3.32 g; 7.46 mmol) in MeCN (8 mL) and 2M phosphate buffer (pH 8.0, 8.0 mL) was vigorously stirred at room temperature for 24 h.[50] The aqueous layer was separated and replaced with fresh buffer (8 mL) and the mixture was stirred for further 18 h. The organic phase was

separated and the solvent was evaporated. The residue was dissolved in EtOAc (50 mL), washed with water (50 mL), brine (2 x 30 mL) and then dried (Na_2SO_4). The solvent was evaporated and the crude oil was purified by flash chromatography (2-PrOH/Et_2O/petroleum ether, 5:15:75) to give **17** (1.87 g; 55%) as a pale yellow oil. R_f=0.35 (2-PrOH/Et_2O/petroleum ether, 5:15:75); ^{1}H NMR ($CDCl_3$, 400 MHz, 298K): δ 7.36-7.30 (5H, m, Ph), 5.13 (1H, d, *J*=12.3 Hz, CH_2Ph), 5.07 (1H, d, *J*=12.3Hz, CH_2Ph), 3.78 (1H, m, C*H*), 3.54 (4H, s, CH_2COOtBu), 2.98 (4H, d, *J*=9.8 Hz, CH_2P), 2.83 (1H, dd, J_1=15.9 Hz, J_2=8.5 Hz, CH_2COOBn), 2.75-2.67 (8H, m, NCH_2), 2.53 (1H, dd, J_1=15.9 Hz, J_2=6.6 Hz, CH_2COOBn), 1.49 (36H, s, POtBu), 1.45 (18H, s, tBu), 1.44 (9H, s, tBu); ^{13}C NMR ($CDCl_3$, 100.6 MHz, 298K): δ 171.6 (CO), 171.3 (CO), 171.1 (CO), 136.3 (C), 128.9 (CH), 128.7 (CH), 128.5 (CH), 82.4 (d, J_{CP}=10 Hz, C), 81.7 (C), 81.0 (C), 66.6 (CH_2), 61.6 (CH), 56.3 (CH_2), 53.1 (d, J_{CP}=166.0 Hz, CH_2), 51.7 (CH_2), 36.3(CH_2), 30.9 (d, J_{CP}=3.0 Hz, CH_3), 28.7 (CH_3), 28.6 (CH_3); ^{31}P NMR ($CDCl_3$, 162 MHz, 298K): δ 18.8 (s); ν_{max} (KBr): 2975, 2933, 2909, 2868, 1731, 1389, 1368, 1193, 1156, 1022, 951; ESI/MS *m/z* calcd for: $[C_{49}H_{89}N_3O_{14}P_2+Na]^+$: 1028.57; found: 1028.98.

*10. N,N-Bis[2-[[[2-(1,1-dimethylethoxy)-2-oxoethyl][[bis(1,1-dimethylethoxy)-phosphynyl]methyl]amino]ethyl]]-L-aspartic acid 1-(1,1-dimethylethyl) ester (**18**)*

5% Palladium on charcoal (0.75 g) was added to a solution of **17** (1.87 g; 1.86 mmol) in THF (80 mL) and the mixture was stirred under a hydrogen atmosphere at room temperature. After 1.5 h the catalyst was filtered and the solution was evaporated to give **18** (1.57 g; 92%) as a yellowish oil. R_f=0.14 (2-PrOH/Et_2O/petroleum ether, 5:15:75); ^{1}H NMR ($CDCl_3$, 400 MHz, 298K): δ 4.13 (1H, dd, J_1= 11.5 Hz, J_2= 4.2Hz, C*H*), 3.55 (2H, d, *J*=17.7 Hz, CH_2COOtBu), 3.50 (2H, d, *J*=17.7 Hz, CH_2COOtBu), 3.10-2.93 (4H, m, CH_2P), 2.90-2.76 (9H, m, NCH_2 and CH_2COOH), 2.65 (1H, dd, J_1= 15.8Hz, J_2= 4.1Hz), 1.49 (36H, d, *J*=2.0 Hz, tBu), 1.46 (9H, s, tBu), 1.45 (18H, s, tBu); ^{13}C NMR ($CDCl_3$, 100.6 MHz, 298K): δ 172.7 (CO), 171.8 (CO), 170.8 (CO), 83.0 (C), 82.2 (C), 81.3 (C), 61.4

(CH), 56.7 (d, J_{CP}=4.0 Hz, CH_2), 55.6 (d, J_{CP}=11.1 Hz, CH_2), 53.1 (d, J_{CP}=163.1 Hz, CH_2), 50.9 (CH_2), 35.8 (CH_2), 30.8 (CH_3), 28.7 (CH_3), 28.4 (CH_3); ^{31}P NMR ($CDCl_3$, 162 MHz, 298K): δ 19.0; ν_{max} (KBr): 3432 (br), 2976, 2934, 1733, 1456, 1392, 1369, 1275, 1221, 1153, 951; ESI/MS *m/z* calcd for: $[C_{42}H_{83}N_3O_{14}P_2+H]^+$ 916.54; found: 916.65.

References and notes

1. Gaynor, D.; Griffith, D. M. *Dalton Trans.* 2012, *41*, 13239-13257.
2. Braddock, M., Ed. *Biomedical Imaging. The Chemistry of Labels, Probes and Contrast Agents*, RSC Publishing, Cambridge, UK, 2012.
3. Alessio, E., Ed. *Bioinorganic Medicinal Chemistry*, Wiley-VCH, Weinheim, Germany, 2011.
4. Geraldes, C. F. G. C.; Laurent, S. *Contrast Media Mol. Imaging* 2009, *4*, 1-23.
5. Krause, W., Ed. *Contrast Agents I. Magnetic Resonance Imaging. Topics in Current Chemistry*, Springer Verlag, Berlin, Germany, 2002, Vol. 221.
6. Merbach, A. Tóth, É., Eds. *The Chemistry of Contrast Agents in Medical Magnetic Resonance Imaging*, John Wiley and Sons Ltd, Chichester, U.K., 2001.
7. Ramogida, C. F.; Orvig, C. *Chem. Commun.* 2013, *49*, 4720-4739.
8. Bhattacharyya, S.; Dixit, M. *Dalton Trans.* 2011, *40*, 6112-6128.
9. Wadas, T. J.; Wong, E. H.; Weisman, G. R.; Anderson, C. J. *Chem. Rev.* 2010, *110*, 2858-2902.
10. Liu, S. *Chem. Soc. Rev.* 2004, *33*, 445-461.
11. Cutler, C. S.; Hennkens, H. M.; Sisay, N.; Huclier-Markai, S.; Jurisson, S. S. *Chem. Rev.* 2013, *113*, 858-883.
12. Brechbiel, M. W. *Dalton Trans.* 2007, 4918-4928.

13. Anderegg, G.; Arnaud-Neu, F.; Delgado, R.; Felcman, J.; Popov, K. *Pure Appl. Chem.* 2005, *77*, 1445-1495.

14. Correira, J. D. G.; Paulo, A.; Raposinho, P. D.; Santos, I. *Dalton Trans.* 2011, *40*, 6144-6167.

15. S. Lee, J. Xie and X. Chen, *Chem. Rev.* 2010, *110*, 3087-3111.

16. Ferro-Flores, G.; Ramírez, F. de M.; Meléndez-Alafort, L.; Santos-Cuevas, C. L. *Mini Rev. Med. Chem.* 2010, *10*, 87-97.

17. Boswell, C. A.; Brechbiel, M. W. *Nucl. Med. Biol.* 2007, *34*, 757-778.

18. Milenic, D. E.; Brady, E. D.; Brechbiel, M. W. *Nat. Rev. Drug Discovery* 2004, *3*, 488-498.

19. Liu, S. *Adv. Drug Deliv. Rev.* 2008, *60*, 1347-1370.

20. Bartholomä, M. D. *Inorg. Chim. Acta* 2012, *389*, 36-51.

21. Liu, S.; Edwards, D. S. *Bioconjugate Chem.* 2001, *12*, 7-34.

22. Lattuada, L.; Barge, A.; Cravotto, G.; Giovenzana, G.B.; Tei, L. *Chem. Soc. Rev.* 2011, *40*, 3019-3049.

23. Anelli, P. L.; Fedeli, F.; Gazzotti, O.; Lattuada, L.; Lux G.; Rebasti, F. *Bioconjugate Chem.* 1999, *10*, 137-140.

24. Amedio J. C., Jr.; Van Wagenen, G., Jr.; Zavlin, G. *Synth. Commun.* 2000, *30*, 3755-3763.

25. Anelli, P. L.; Brocchetta, M.; Lattuada, L.; Manfredi, G.; Morosini, P.; Murru, M.; Palano, D.; Sipioni, M.; Visigalli M. *Org. Process Res. Dev.* 2009, *13*, 739-746.

26. Anelli, P. L.; Lattuada, L.; Lorusso, V.; Lux, G.; Morisetti, A.; Morosini, P.; Serleti, M.; Uggeri, U. *J. Med. Chem.* 2004, *47*, 3629-3641.

27. Lattuada, L.; Cappelletti, E.; De Miranda, M.; Umbelli, C. *Lett. Org. Chem.* 2009, *6,* 624-629.

28. Lattuada, L.; Dematтio, S.; Vincenzi, V.; Cabella, C.; Visigalli, M.; Aime, S.; GeninattiCrich, S.; Gianolio, E. *Bioorg. Med. Chem. Lett.* 2006, *16*, 4111-4114.

29. Aloj, L.; Caracò, C.; Panico, M.; Zannetti, A.; Del Vecchio, S.; Tesauro, D.; De Luca, S.; Arra, C.; Pedone, C.; Morelli, G.; Salvatore, M. *J. Nucl. Med.* 2004, *45*, 485-494.

30. Manzoni, L.; Belvisi, L.; Arosio, D.; Bartolomeo, M.P. ; Bianchi, A.; Brioschi, C.; Buonsanti, F.; Cabella, C.; Casagrande, C.; Civera, M.; De Matteo, M.; Fugazza, L.; Lattuada, L.; Maisano, F.; Miragoli, L.; Neira, C.; Pilkington-Miksa, M.; Scolastico, C. *ChemMedChem* 2012, *7*, 1084-1093.

31. Kim, J. H.; Lim, J. C.; Yun, K. C.; Choi, S. J.; Hong, Y. D. *J. Labelled Compd. Radiopharm.* 2012, *55*, 10-17.

32. Atkins, K. M.; Martínez, F. M.; Nazemi, A.; Scholl, T. J.; Gillies, E. R. *Can. J. Chem.* 2011, *89*, 47-56.

33. Lashley, M. R.; Niedzinski, E. J.; Rogers, J. M.; Denison, M. S.; Nantz, M. H. *Bioorg. Med. Chem.* 2002, *10*, 4075-4082.

34. Nair, S.A.; Kolodziej, A. F.; Bhole, G.; Greefield, M. T.; McMurry, T. J.; Caravan, P. *Angew. Chem. Int. Ed.* 2008, *47*, 4918-4921.

35. Lebduškova, P.; Hermann, P.; Helm, L.; Tóth, É.; Kotek, J.; Binnemans, K.; Rudovský, J.; Lukeš, I.; Merbach, A.E. *Dalton Trans.* 2007, 493-501

36. Aime, S.; Botta, S.; Frullano, L.; Geninatti Crich, S.; Giovenzana, G.; Pagliarin, R.; Palmisano, G.; Riccardi Sirtori, F.; Sisti, M., *J. Med. Chem.* 2000, *43*, 4017-4024.

37. Rudovský, J.; Hermann, P.; Botta, M.; Aime, S.; Lukeš, I. *Chem. Commun.* 2005, 2390-2392.

38. Aime, S.; Botta, M.; Cravotto, G.; Frullano, L.; Giovenzana, G.B.; Geninatti Crich, S.; Palmisano, G.; Sisti, M. *Helv. Chim. Acta*, 2005, *88*, 588-603.

39. Aime, S.; Cravotto, G.; Geninatti Crich, S.; Giovenzana, G.B.; Ferrari, M.; Palmisano, G.; Sisti, M. *Tetrahedron Lett.*, 2002, *43*, 783-786.

40. Wermuth, C. G. *The Practice of Medicinal Chemistry*, Academic Press, Oxford, 2011; pp. 303-310.

41. Lázár, I.; Hrncir, D.C.; Kim, W.-D.; Kiefer, G.E.; Sherry, A.D. *Inorg. Chem.* 1992, *31*, 4422-4424.

42. Aime, S.; Botta, M.; Geninatti Crich, S.; Giovenzana, G.; Pagliarin, R.; Sisti M.; Terreno, E. *Magn. Reson. Chem.* 1998, *36,* S200-S208.

43. Kan, A.T.; Oddo, J.E.; Tomson, M.B. *Langmuir* 1994, *10*, 1450-1455.

44. Kotek, J.; Lebdušková, P.; Hermann, P.; Vander Elst, L.; Muller, R. N.; Geraldes, C. F. G. C.; Maschmeyer, T.; Lukeš, I.; Peters, J. A. *Chem. Eur. J.* 2003, *9*, 5899-5915.

45. Kotek, J.; Kálmán, F. K.; Hermann, P.; Brücher, E.; Binnemans, K.; Lukeš, I. *Eur. J. Inorg. Chem.* 2006, 1976-1986.

46. Li, X.; Zhang, S.; Zhao, P.; Kovacs, Z.; Sherry, A.D. *Inorg. Chem.* 2001, *40*, 6572-6579.

47. Ouadi, A.; Bultel, K.; de France-Robert, A.; Loussouarn, A.; Morandeau, L.; Gestin, J-F. *Tetrahedron Lett.* 2004, *45*, 1395-1397.

48. Loussouarn, A.; Duflos, M.; Benoist, E.; Chatal, J.-F.; Le Baut, G.; Gestin, J.-F. *J. Chem. Soc., Perkin Trans. 1* 1998, 237-241.

49. Williams, M. A., Rapoport, H. *J. Org. Chem.* 1993, *58*, 1151-1158.

50. Quici, S.; Cavazzini, M.; Marzanni, G.; Accorsi, G.; Armaroli, N.; Ventura, B.; Barigelletti, F. *Inorg. Chem.* 2005, *44*, 529-537.

51. Couffignal, R.; Dardoize, F.; Goasdoue, C.; Goasdoue, N.; Laborit, H. M.; Topall, G. *Ann. Pharm. Fr.* 1990*, 48*, 321-325.

52. Cox, J. R.; Newton, M.G. *J. Org. Chem.*1969, *34*, 2600-2605.

53. Breipohl, G.; Will, D.W.; Peyman, A.; Uhlmann, E. *Tetrahedron* 1997, *53*, 14671-14686.

54. Taschner, E.; Chimiak, A.; Bator, B.; Sokolowska, T. *Liebigs Ann. Chem.* 1961, *646*, 134-136.

55. Dirscherl, G.; König, B. *Eur. J. Org. Chem.* 2008, 597-634.

56. Foley, D.; Pieri, M.; Pettecrew, R.; Price, R.; Miles, S.; Lam, H.K.; Bailey, P.; Meredith, D. *Org. Biomol. Chem.* 2009, *7*, 3652-36

Synthesis of phosphonic analogues of AAZTA and relaxometric evaluation of the corresponding Gd(III) complexes as potential MRI contrast agents

Claudia Guanci,[a] Roberta Pinalli,[b] Silvio Aime,[c] Eliana Gianolio,[c] Luciano Lattuada[b] and Giovanni B. Giovenzana[a]*

Submitted to *Tetrahedron Letters*, Dec 2014, code TETL-D-14-02963.

Abstract

AAZTA was developed in the last decade as an efficient chelating agent for lanthanides and other metal ions of diagnostic and therapeutic interest. Different derivatives of AAZTA were designed and synthesized in order to modulate the physico-chemical properties of the corresponding chelates or to conjugate them to carrier molecules for molecular imaging applications. In this work, mono- and diphosphonic analogues of AAZTA were synthesized and the effects of this isofunctional substitution on the properties of the corresponding Gd(III) complexes were preliminarily investigated by relaxometric techniques.

Magnetic Resonance Imaging (MRI) is a widely employed clinical diagnostic technique, in which paramagnetic Gd(III) chelates are frequently used to ensure a significant increase in the image contrast.[1-3] As the trivalent lanthanide ion exerts toxic effects, its stable complexation by a suitable polydentate ligand is mandatory to avoid undesired side-effects.[4] Acyclic or macrocyclic octadentate chelating

agents such as diethylenetriaminepentaacetic acid (DTPA) or 1,4,7,10-tetraazacyclododecane-1,4,7,10-tetraacetic acid (DOTA) are commonly employed to this purpose, along with a continuously increasing number of derivatives thereof.[5] The research in this field has brought to the identification of potentially alternative chelating agents, characterized by a satisfying stability in spite of a lower denticity. The reduction of ligand denticity aims at raising the contrast efficiency by increasing the number of coordinated water molecules ("*q*", hydration) of the metal centre. Examples of stable low-denticity chelating ligands for lanthanides may be found in the family of hydroxypyridinone-based ligands (HOPOs)[6] and in the large family of heptadentate systems represented by PCTAs,[7] TDITAs,[8] OBETA[9], CyPic3A[10] and AAZTA.[11]

The Gd(III)-AAZTA complex is endowed with high kinetic and thermodynamic inertness[11] and with significantly improved relaxometric properties with respect to the clinically employed MRI contrast agents (CAs), due to a favorable combination of higher hydration (q = 2) and a fast exchange of the coordinate water molecules.[12] Since its debut a decade ago, AAZTA has been inserted in a consistent number of derivatives. For example, lipophilic AAZTA chelates were used to form lipid-based aggregates reaching high relaxivity values,[13] while bifunctional derivatives were designed to embody remote free functional groups devoted to conjugation purposes.[14] Other examples are reported in which the AAZTA complexes are functionalized with suitable hydrophobic substrates in order to prompt their interaction with serum albumin[15] or with supramolecolar β-cyclodextrin containing systems.[16] Surprisingly, modification of the ligand coordination cage received limited attention. Apart from the fixed nitrogen arrangement represented by the 6-amino-1,4-diazepane backbone, examples of isofunctional substitutes of the carboxylic groups are scarce and limited to the inclusion of two azaxanthones heterocyclic residues.[17] Ermelindo *et al.* reported on AAZTA derivative in which two carboxylic groups are replaced by phosphinic moieties.[18] The active role of the donor group in the coordination of the metal ion calls for special attention in the

choice of the functional group. Gd(III)-chelates bearing different carboxylic group isosteres as phosphinic acid,[18-19] acylsulphonamide,[20] tetrazole[21] and pyridine[22] were studied in order to investigate the effect of this structural variation on the physico-chemical properties of the final complex.

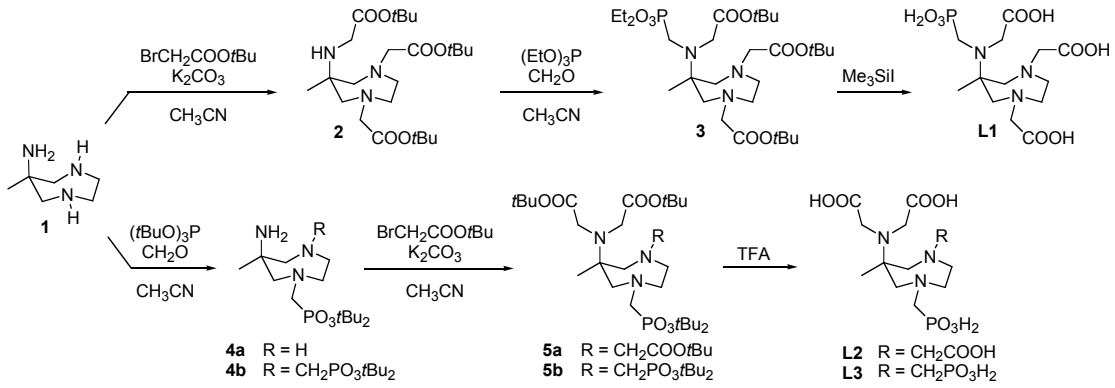

Scheme 1. Synthesis of ligands **L1-L3**.

Replacement of carboxylic with phosphonic groups is one of the classical isosteric substitution in medicinal chemistry.[23] The size and acidic properties of the phosphonic acid closely resemble the behavior of carboxylic acid. Its conjugate bases, *i.e.*: phosphonate and monohydrogen-phosphonate may participate in multiple coordination modes and display significant affinity with lanthanide(III) ions. Metal complexes embodying coordinating phosphonic groups are usually endowed with increased water solubility due to the presence of residual anionic charges and extended hydrogen bond networks. Phosphonic analogues of Gd(III)-based CAs often show improved relaxometric properties as a result of an increased solvation in the outer coordination sphere and of direct effects on the exchange of the coordinated water molecule(s).[24]

In this context, we were prompted to explore the possibility to substitute carboxylic with phosphonic groups on the ligand AAZTA and the consequences of this isofunctional replacement on the corresponding Gd(III) chelate. We report here the synthetic access to mono- and diphosphonic analogues of AAZTA (**L1**-**L3**, Scheme 1) and the preliminary relaxometric characterization of their Gd(III)-complexes, giving a defined picture of the effect of this substitution on their structure, dynamic and magnetic properties.

The preparation of the mixed carboxylic-phosphonic AAZTA analogues is depicted in Scheme 1. The synthetic access takes advantage of the different reactivity of the amine groups in the starting 6-amino-1,4-diazepane **1**.[12] The endocyclic secondary amines are more reactive towards alkylating agents and react first.[25] The exocyclic primary amine, plagued by the steric congestion represented by the tertiary carbon atom, needs more forcing conditions, to be exhaustively alkylated; its monoalkylation can be easily obtained operating in strictly stoichiometric conditions or with less reactive alkylating agents. Suitable combinations of the reaction with α-bromoesters or Kabachnik-Fields phosphonomethylation were then used to generate different arrangements of the carboxylic and phosphonic groups on the 6-amino-1,4-diazepane skeleton.

Reaction of the triamine **1** with 3 eq of *t*-butyl bromoacetate in acetonitrile in the presence of potassium carbonate leads to the trialkylated derivative **2**. This allows the installation of a single phosphonomethyl group (protected as ethyl ester) on the primary amine by reaction with paraformaldehyde and triethyl phosphite, giving the fully protected compound **3**. Complete removal of all esters was accomplished by treatment with iodotrimethylsilane followed by a protic workup, leading to the chelating agent **L1**, characterized by the presence of the methylenephosphonic group on the exocyclic nitrogen atom.

Installation of the phosphonomethyl residues on the endocyclic nitrogen atom(s) was accomplished by reacting triamine **1** with paraformaldehyde and 1 or 2 eq of tri-*t*-butyl phosphite, yielding the monosubstituted (**4a**) or the disubstituted (**4b**) derivative, respectively. Exhaustive alkylation of the remaining available positions was performed by reaction with *t*-butyl bromoacetate-K_2CO_3 in acetonitrile, generating the esters **5a** and **5b**. Final treatment with trifluoroacetic acid removed the *t*-butyl esters and completed the synthesis of the ligands **L2** and **L3**. Analytical characterization of **L1**-**L3** and the corresponding precursors are fully compatible with their chemical structures (Supplementary Material).

Relaxometric characterization of the Gd(III)-complexes of **L1**-**L3** were then undertaken in order to determine the effect of the isofunctional substitution on their physico-chemical properties. The chelates Gd-**L1**, Gd-**L2** and Gd-**L3** were prepared by combining equimolar solutions of the ligands and $GdCl_3$, then adjusting the pH to neutrality. The formation of the complexes was followed by ^{1}H-relaxometry and was observed to be complete within minutes. Relaxivity values of Gd-**L1-3** are reported in Table 1, compared with that of the parent chelate Gd-AAZTA.

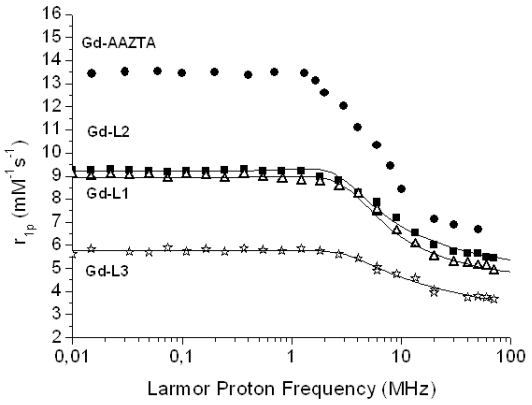

Figure 1. NMRD profiles of Gd-**L1-3** compared to the parent Gd-AAZTA

NMRD profiles were registered on aqueous solutions of Gd-**L1-3** (Fig. 1), together with ^{17}O-VT-NMR transverse relaxation data (Fig. S1, Supplementary

Material). Combined data analysis allowed to extract structural and dynamic parameters of the paramagnetic complexes, summarized in Table 1.

Table 1. Relaxometric parameters for Gd-**L1-3** and the parent Gd-AAZTA[a]

Complex	r_{1p} ($mM^{-1}s^{-1}$)	τ_M (ns)	τ_R (ps)	*q*
Gd-**L1**	5.5	190	97	1
Gd-**L2**	6.0	370	119	1
Gd-**L3**	4.1	1600	130	0.4
Gd-AAZTA[b]	7.1	90	74	2

[a] Measured at 20 MHz, 298K, pH 7. [b] Ref. 12

Observed r_{1p} values are lower than those of the parent Gd-AAZTA and indicative of a reduction in the hydration state of the metal in the three complexes. The progressive substitution of -COOH groups with $-PO_3H_2$ ones brings a parallel reduction in the number of coordinated water molecules, from 2 (Gd-AAZTA) to 1 in monophosphonic derivatives (**L1**, **L2**) and finally to a <1 value in the diphosphonic analogue **L3**, the latter value suggesting the presence of more than one species with $q = 0$ and $q = 1$ hydration states. Interestingly, the corresponding di-phosphinic system reported by Ermelindo *et al.*[18] shows a relaxivity of 6.1 $mM^{-1}s^{-1}$ that is strongly indicative of the presence of one coordinated water molecule. Ongoing from phosphinic to phosphonic coordinating moieties there is an improved ability of the ligand to wrap around the metal ion thus hampering the access of water molecule(s) to the inner coordination sphere. This finding

definitively parallels the behavior shown on passing from Gd-DOTA to Gd-DOTP. The relaxivity of the latter (4.7 $mM^{-1}s^{-1}$) was accounted in terms of a strong second sphere contribution arising from the ability of the charged phosphonic moieties to form H-bonding network of water molecules.[26] The close similarity of the relaxivities of Gd-DOTP and Gd-**L3** strongly supports the view that the latter complex too experiences a lower inner sphere hydration. The presence of H-bonded water molecules in the second coordination sphere appears to markedly affect the exchange lifetime (t_M) of the coordinated water molecule which passes from the value of 90 ns, in the parent Gd-AAZTA, to 190 ns, 370 ns and 1600 ns (for the fraction of Gd-**L3** which has one inner sphere water molecule) in Gd-**L1**, Gd-**L2** and Gd-**L3** respectively.

In conclusion, the synthetic approach to mixed phosphonic-carboxylic AAZTA analogues was demonstrated, leading to the preparation of three novel chelating agents. Relaxometric studies on the corresponding Gd(III) complexes showed an active participation of the phosphonic groups in the coordination of the paramagnetic lanthanide ion. The introduction of phosphonic groups progressively reduces the available space for directly coordinated water molecules and increases the second sphere contribution to relaxivity.

General experimental data:

Nuclear magnetic resonance spectra (^1H, ^{13}C, ^{31}P-NMR) were recorded at 9.4T on a Bruker Avance 400 spectrometer. Chemical shifts (δ) are quoted in parts per million (ppm) and referenced to the residual solvent peak. Coupling constants (*J*) are quoted in Hertz (Hz). Mass spectra (MS) were recorded on a ThermoFinnigan TSQ700 triple-quadrupole instrument equipped with an electrospray ionization source.

Experimental Section

Compound 2

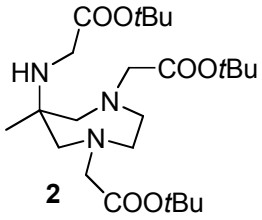

t-Butyl bromoacetate (2.30 mL, 15.5 mmol) diluted in 10 mL of acetonitrile, was added to a stirred solution of **1** (1.00 g, 7.7 mmol) and K_2CO_3 (2.10 g, 15.5 mmol) in acetonitrile (30 mL) and cooled to 0°C. After the addition, the reaction mixture was allowed to warm to room temperature and Na_2SO_4 (1.0 g) was added. The suspension was stirred at room temperature under N_2. After 4 h, 1.0 equivalent (1.10 mL, 7.7 mmol) of *t*-butyl bromoacetate was added and the reaction was allowed to stir at room temperature under N_2 for 24 h. The reaction was monitored by TLC ($CHCl_3$/MeOH 93:7, R_f = 0.2). The reaction mixture was then filtered and the solvent evaporated. The residue obtained was taken up with dichloromethane (50 mL) and washed with water (3x20 mL). The organic layer was dried on Na_2SO_4, filtered and concentrated under reduced pressure. The crude product was purified by column chromatography ($CHCl_3$/MeOH 93:7) to give compound **2** (1.60 g, 3.4 mmol) as a light yellow oil (yield: 45%). **^{1}H-NMR** ($CDCl_3$, 400MHz, 298K): δ 3.30 (s, 4H), 3.25 (s, 2H), 2.79 (m, 4H), 2.69 (d, 2H, *J*=13.8 Hz), 2.65 (d, 2H, *J*=13.8 Hz), 1.45 (s, 9H), 1.43 (s, 18H), 0.92 (s, 3H, CH_3). **^{13}C-NMR** ($CDCl_3$, 101 MHz, 298K): δ 172.2 (C), 171.3 (C), 81.2 2x(C), 65.0 (CH_2), 62.2 (CH_2), 57.5 (CH_2), 56.3 (C), 45.3 (CH_2), 28.6 (CH_3), 28.5 (CH_3), 23.0 (CH_3); **ESI-MS(+)** for $C_{24}H_{45}N_3O_6$ calcd: 471.3, found: 494.3 $[M+Na^+]^+$, 472.2 $[M+H^+]^+$, 438.2, 416.2, 382.1, 360.2, 326.1, 304.1.

Compound 3

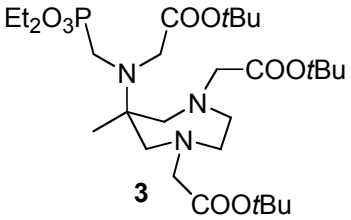

A suspension of paraformaldehyde (48 mg, 1.6 mmol) in acetonitrile (3.0 mL) was added dropwise in 30 min to a solution of **2** (0.5 g, 1.06 mmol) in acetonitrile (8 mL) at 80°C. The reaction mixture was stirred for further 30 min, then cooled to room temperature. A solution of $P(OEt)_3$ (0.27 g, 1.6

mmol) in acetonitrile (4 mL) was added dropwise over 20 min, then the mixture was stirred at room temperature. After 3 days additional 1.5 equivalent of paraformaldehyde (48 mg, 1.6 mmol) and 1.5 equivalent of $P(OEt)_3$ were added and the mixture allowed to stir for 4 days. The reaction was monitored by TLC (EtOAc/petroleum ether 2:1, $R_f = 0.6$). After evaporation of the solvent the residue was purified by column chromatography (EtOAc/petroleum ether 2:1) to give compound **3** (0.29 g, 0.47 mmol) as a light yellow oil (yield: 44%). **^{1}H-NMR** ($CDCl_3$, 400 MHz, 298K): δ 4.16 (m, 4H), 3.71-3.68 (d+s, 2H+2H), 3.32 (s, 4H), 3.10 (d, 2H, J = 14.1 Hz), 2.84-2.78 (m, 2H), 2.71-2.65 (m, 2H), 2.63 (d, 2H, J =14.1 Hz) , 1.47 (s, 18H), 1.46 (s, 9H), 1.33 (t, 6H, J = 7.1 Hz), 1.09 (s, 3H, CH_3); **^{13}C-NMR** ($CDCl_3$, 101 MHz, 298K): δ 173.1 (C), 171.2 (C), 81.1 (C), 80.7 (C), 65.8 (CH_2), 62.6 (CH_2), 62.4 (CH_2, d, J = 7.0 Hz), 62.0 (C, d, J = 7.0 Hz), 59.6 (CH_2), 53.1 (CH_2), 45.0 (CH_2, d, J = 9.2 Hz), 28.6 (CH_3), 28.5 (CH_3), 24.6 (CH_3), 16.9 (CH_3, d, J = 5.6 Hz); **^{31}P-NMR** ($CDCl_3$, 162 MHz, 298K): δ 27.7; **ESI-MS** for $C_{29}H_{56}N_3O_9P_1$ calcd: 621.4, found: 644.3 [M+Na^+], 622.6 [M+H^+], 588.4, 532.3, 413.4, 341.3, 285.4, 229.5.

Compound L1

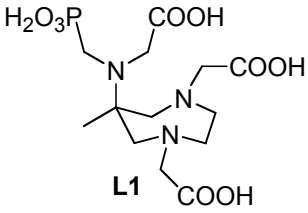

L1

Iodotrimethylsilane (0.93 g, 4.6 mmol) was added to a solution of **3** (0.29 g, 0.46 mmol) in dry dichloromethane (10 mL). The solution was stirred at room temperature for 20 h. The mixture was then extracted with water (2x10 mL) and the aqueous phases were collected and concentrated under reduced pressure. The crude product was purified by cation exchange resin column to afford compound **L1** (0.11 g, 0.27 mmol) as a white solid (yield: 60%). **^{1}H-NMR** (D_2O, 400 MHz, 298K): δ 3.76-3.68 (m, 2H), 3.58 (s, 2H), 3.53 (s, 4H), 3.47-3.28 (m, 6H), 2.91 (d, 2H, J = 11.2 Hz), 1.08 (s, 3H, CH_3). **^{13}C-NMR** (D_2O, 101 MHz, 298K) δ 178.3 (C), 173.1 (C), 62.6 (CH_2, d, J = 8.2 Hz), 60.5 (CH_2), 60.0 (CH_2), 56.4 (CH_2), 51.6 (CH_2), 50.0 (CH_2, d, J = 145.0 Hz), 16.8 (CH_3); **^{31}P-NMR** (D_2O,

162 MHz, 298K): δ 16.6; **ESI-MS(-)** for $C_{13}H_{24}N_3O_9P_1$ calcd: 397.1, found: 418.2 $[M+Na^+]^-$, 396.2 $[M-H^+]^-$, 284.3.

Compound 4a

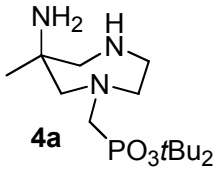

A solution of paraformaldehyde (0.12 g, 4.0 mmol) in DMF (5.0 mL) was added dropwise in 30 min to a solution of **1** (1.0 g, 7.7 mmol) in CH_3CN (15 mL) at 80°C. The reaction mixture was stirred for further 30 min and then cooled to room temperature. A solution of tri-*t*-butylphosphite (0.97 g, 3.9 mmol) in acetonitrile (5 mL) was added dropwise over 20 min, then the mixture was stirred at room temperature for 10 days. The reaction was monitored by TLC ($CHCl_3$/MeOH/NH_3 = 70:15:2, R_f = 0.5). After evaporation of the solvent, the residue was purified by two sequential chromatographic columns ($CHCl_3$/MeOH/NH_3 = 70:15:2, R_f = 0.5) to yield **4a** as a light yellow oil (yield: 33%). **^{1}H NMR** ($CDCl_3$, 400 MHz, 298K): δ 2.97-2.71 (m, 6H), 2.62-2.53 (m, 4H), 2.38 (bs, 3H), 1.473 (s, 9H), 1.468 (s, 9H), 0.96 (s, 3H). **^{13}C NMR** ($CDCl_3$, 101 MHz, 298K): δ 80.3 (C), 70.4 (d, CH_2, J = 8.0 Hz), 62.9 (CH_2), 60.2 (d, CH_2, J = 7.3 Hz), 59.8 (d, CH_2, J = 163.4 Hz), 56.6 (C), 51.3 (CH_2), 30.9 2x(CH_3), 26.2 (CH_3). **^{31}P-NMR** ($CDCl_3$, 162 MHz, 298K): δ 18.6. **ESI-MS(+)** for $C_{15}H_{34}N_3O_3P_1$ calcd: 335.2, found: 358.1 $[M+Na^+]$, 336.1 $[M+H^+]$, 280.1, 223.9.

Compound 5a

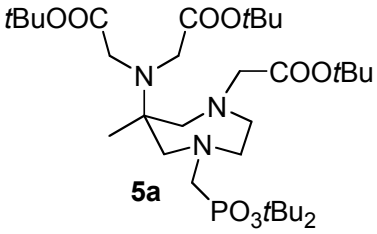

t-Butyl bromoacetate (0.73 mL, 5.0 mmol) was added to a stirred solution of **4a** (0.42 g, 1.25 mmol) and K_2CO_3 (0.69 g, 5.0 mmol) in acetonitrile (10 mL) cooled to 0°C. After the addition, the reaction mixture was allowed to warm to room temperature and Na_2SO_4 (0.30 g) was added. The suspension was refluxed under N_2 for 2 h and stirred at room temperature for 2 days. The suspension was filtered and the solvent

evaporated. The crude product was purified by flash chromatography (petroleum ether/AcOEt 8:2, then 7:3) to give **5a** (0.61 g, 0.9 mmol) as a light yellow oil (yield: 72%). TLC: Petroleum Ether/EtOAc = 7:3, R_f = 0.2; **^{1}H NMR** (400 MHz, $CDCl_3$, 298K): δ 3.66 (s, 4H), 3.26 (s, 2H), 3.03 (d, 1H, J = 13.9 Hz), 3.02 (d, 1H, J = 13.9 Hz), 2.96-2.63 (m, 6H), 2.64 (d, 1H, J = 14.1 Hz), 2.56 (d, 1H, J = 13.9 Hz), 1.50 (s, 9H), 1.49 (s, 9H), 1.43 (s, 27H), 1.11 (s, 3H). **^{13}C NMR** (101 MHz, $CDCl_3$, 298K): δ 173.1 (C), 171.3 (C), 81.1 (C), 80.6 (C), 69.8 (CH_2, d, J = 13.5 Hz), 66.6 (CH_2), 62.7 (CH_2), 61.2 (C), 60.5-60.2 2x(CH_2), 59.8 (CH_2, d, J = 161.4 Hz), 52.3 (CH_2), 31.0 2x(CH_3), 28.6 (CH_3), 28.5 (CH_3), 24.7 (CH_3). **^{31}P-NMR** ($CDCl_3$, 162 MHz, 298K): δ 18.6. **ESI-MS(+)** for $C_{33}H_{64}N_3O_9P_1$ calcd: 677.4, found: 700.5 $[M+Na^+]^+$, 678.5 $[M+H^+]$, 644.4, 564.4.

Compound L2

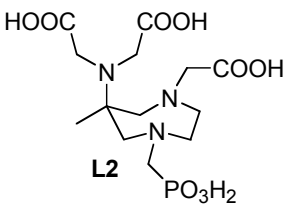

L2

A solution of compound **5a** (0.17 g, 0.25 mmol) in trifluoroacetic acid (10 mL) was stirred at room temperature for 40 h. The mixture was then evaporated, the residue taken up with dichloromethane (3x10mL) and the solution evaporated under reduced pressure. The crude oil was precipitated with diethyl ether and filtered to afford compound **L2** as a white solid in quantitative yield. **^{1}H-NMR** (D_2O, 400MHz, 298K): δ 4.11-3.45 (m, 8H), 3.88 (s, 2H), 3.64 (s, 4H), 3.33 (d, 2H, J = 14.7 Hz), 1.08 (s, 3H, CH_3); **^{13}C-NMR** (D_2O, 101 MHz, 298K): δ 176. 6 (C), 170.2 (C), 61.2 (CH_2), 60.2 (C), 58.5 (CH_2), 55.2 (CH_2, d, J = 136.9 Hz), 52.8 (CH_2), 52.7 (CH_2), 51.2 (CH_2) 18.4 (CH_3); **^{31}P-NMR** (D_2O, 162 MHz, 298K): δ 8.8; **ESI-MS(+)** for $C_{13}H_{24}N_3O_9P_1$ calcd: 397.1, found: 420.3 $[M+Na^+]$, 398.3 $[M+H^+]$.

Compound 4b

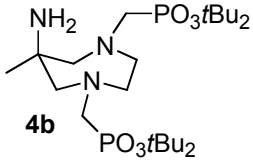

A suspension of paraformaldehyde (0.46 g, 15.5 mmol) in acetonitrile (5.0 mL) was added dropwise in 30 min to a solution of **1** (1.0 g, 7.7 mmol) in acetonitrile (15 mL) at 80°C. The reaction mixture was stirred for further 30 min and then cooled to room temperature. A solution of tri-*t*-butylphosphite (3.87 g, 15.5 mmol) in acetonitrile (10 mL) was added dropwise in 20 min, then the mixture was stirred at room temperature. After one week, 1 equivalent of tri-*t*-butylphosphite (1.9 g, 7.7 mmol) was added to the solution and the mixture was stirred at room temperature for an additional week. The reaction was monitored by TLC ($CHCl_3$/MeOH/25% aq. NH_3 90:10:0.5, R_f= 0.2). After evaporation of the solvent, the residue was purified by column chromatography ($CHCl_3$/MeOH/25% aq. NH_3 9:1:0.05) to give compound **4b** (1.8 g, 3.3 mmol) as a light yellow oil (yield: 43%). **^{1}H-NMR** ($CDCl_3$, 400 MHz, 298K): δ 3.05-2.67 (m, 12H), 1.48 (s, 18H), 1.47 (s, 18H), 1.38 (s, 3H); **^{13}C-NMR** ($CDCl_3$, MHz, 298K): δ 83.4 (C), 65.5 (CH_2, d, J = 7.9 Hz), 58.6 (CH_2, d, J = 161.3 Hz), 57.62 (CH_2, d, J = 5.5 Hz), 56.8 (C), 31.0-30.9 2x(CH_3), 21.2 (CH_3); **^{31}P-NMR** ($CDCl_3$, 162 MHz, 298K) δ 18.9; **ESI-MS(+)** for $C_{24}H_{53}N_3O_6P_2$ calcd: 541.3, found: 564.0 $[M+Na^+]^+$, 542.1 $[M+H^+]^+$, 486.1, 430.1, 374.0, 318.0, 236.1.

Compound 5b

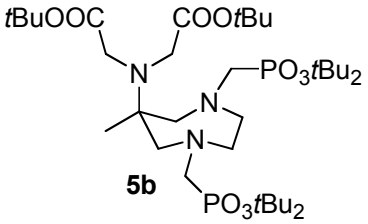

t-Butyl bromoacetate (0.49 mL, 3.3 mmol), diluted in acetonitrile (5.0 mL), was added to a stirred solution of **4b** (0.60 g, 1.11 mmol) and K_2CO_3 (0.46 g, 3.3 mmol) in acetonitrile (10 mL) cooled to 0°C. After the addition, the reaction mixture was allowed to warm to room temperature and Na_2SO_4 (0.30 g) was added. The suspension was refluxed under N_2 for 7 h, then cooled to room temperature, filtered and evaporated. The crude product was taken up with dichloromethane (10 mL) and washed with water (3 x 10 mL). The organic layer was dried on Na_2SO_4, filtered and concentrated under reduced pressure. The

obtained crude product was purified by flash chromatography (petroleum ether/AcOEt 3:7) to give **5b** (0.23 g, 0.3 mmol) as a light yellow oil (yield: 27%). TLC: Petroleum Ether/EtOAc = 3:7, R_f = 0.1; **^{1}H-NMR** ($CDCl_3$, 400 MHz, 298K): δ 3.66 (s, 4H), 3.15-2.63 (m, 12H), 1.51 (s, 18H), 1.49 (s, 18H), 1.45 (s, 18H), 1.16 (s, 3H); **^{13}C-NMR** ($CDCl_3$, MHz, 298K); 173.0 (C), 83.0 (C), 80.8 (C), 63.2 (CH_2, d, J = 5.5 Hz), 61.4-57.4 ($3CH_2$+C), 30.9 2x(CH_3), 28.5 (CH_3), 21.2 (CH_3); **^{31}P-NMR** ($CDCl_3$, 162 MHz, 298K): δ 18.1; **ESI-MS** for $C_{36}H_{73}N_3O_{10}P_2$ calcd: 769.48, found: 792.5 $[M+Na^+]^+$, 770.5 $[M+H^+]^+$, 656.6.

Compound L3

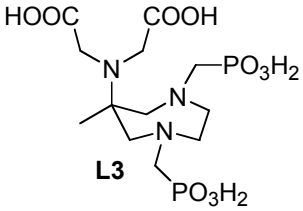

L3

A solution of compound **5b** (0.23 g, 0.30 mmol) in a mixture of trifluoroacetic acid (10 mL) and dichloromethane (10 mL) was stirred at room temperature for 4 h. The mixture was then evaporated, the residue taken up with dichloromethane (3x10 mL) and the residue dissolved in TFA (10 mL). The solution was stirred at room temperature for 12 h. Dichloromethane (3x10 mL) was then added and the solution evaporated under reduced pressure. The residue was treated with diethyl ether, then **L3** was isolated by filtration as a white solid (yield: 62%). **^{1}H-NMR** (D_2O, 400 MHz, 298K): δ 3.20 (s, 4H), 2.96 (m, 2H), 2.88 (d, 2H, J = 14.2 Hz), 2.77 (m, 2H), 2.69 (d, 2H, J = 14.2 Hz), 2.60 (d, 4H, J = 10.2 Hz), 0.92 (s, 3H); **^{13}C-NMR** (D_2O, 101 MHz, 298K): δ 181.8 (C), 66.4 (d, CH_2, J = 6.5 Hz), 61.1 (C), 59.2 (d, CH_2, J = 134.0 Hz), 58.5 (CH_2), 55.0 (CH_2), 20.9 (CH_3); **^{31}P-NMR** (D_2O, MHz, 298K) δ 16.8; **ESI-MS** for $C_{12}H_{25}N_3O_{10}P_2$ calcd: 433.10, found: $[M-H^+]^-$ 432.2.

Figure S1. *Temperature dependence of the water ^{17}O NMR transverse relaxation rates for Gd-**L1-3** and the parent Gd-AAZTA.*

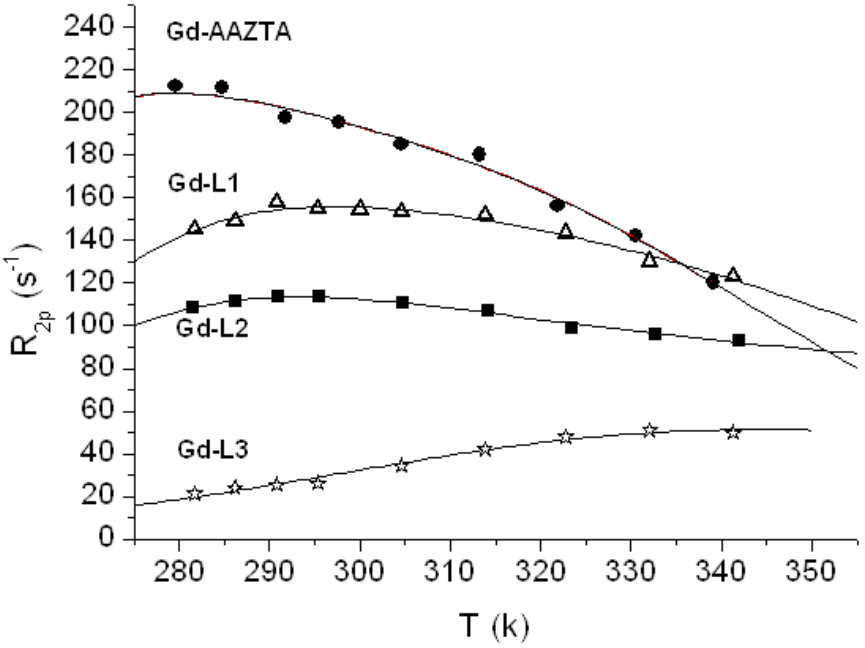

Acknowledgments

MIUR (Grant PRIN 2012SK7ASN), AIRC Investigator Grant IG 14565, CIRCMSB and Compagnia di San Paolo are gratefully acknowledged.

References and notes

1. Geraldes, C. F. G. C.; Laurent, S. *Contrast Media Mol. Imaging* **2009**, *4*, 1-23.

2. *Contrast Agents I. Magnetic Resonance Imaging. Topics in Current Chemistry*; Krause, W., Ed.; Springer:Berlin, Germany, 2002; Vol.221.

3. *The Chemistry of Contrast Agents in Medical Magnetic Resonance Imaging*; Merbach, A., Tóth, É., Eds.; John Wiley and Sons Ltd: Chichester; UK, 2001.

4. Kribben, A.; Witzke, O.; Hillen, U.; Barkhausen, J.; Daul, A. E.; Erbel, R. *J. Am. Coll. Radiol.* **2009**, *53*, 1621-1628; (b) Kuo, P. H.; Abu-Alfa, A.; Bucala, R.; Griffith, J.; Carlson, K.; Girardi, M.; Weinreb, J.; Cowper, S. *Appl. Radiol.* **2009**, *38*, 22-33; (c) Morcos, S. K.; Haylor, J. *World J. Radiol.* **2010**, *2*, 427-433.

5. Stasiuk, G.J.; Long, N.J. *Chem. Commun.* **2013**, *49*, 2732-2746.

6. Datta, A.; Raymond, K. N. *Acc. Chem. Res.* **2009**, *42*, 938-947.

7. Aime, S.; Botta, M.; Geninatti Crich, S.; Giovenzana, G. B.; Jommi, G.; Pagliarin, R.; Sisti, M. *Inorg. Chem.* **1997**, *36*, 2992-3000.

8. Baranyai, Z.; Tei, L.; Giovenzana, G. B.; Kálmán, F.K.; Botta, M. *Inorg. Chem.* **2012**, 51, 2597-2607.

9. Baranyai, Z.; Botta, M.; Fekete, M.; Giovenzana, G. B.; Negri, R.; Tei, L. *Chem. Eur. J.* **2012**, 18, 7680-7685. b) Negri, R.; Baranyai, Z.; Tei, L.; Giovenzana, G. B.; Platas-Iglesias, C.; Bényei, A.; Bodnár, J.; Vágner, A.; Botta, M. *Inorg. Chem.* **2014**, *53*, 12499-12511.

10. Gale, E. M.; Kenton, N.; Caravan. P. *Chem. Commun.* **2013**, *49*, 8060-8062.

11. Baranyai, Z.; Uggeri, F.; Giovenzana, G. B.; Bényei, A.; Brücher, E.; Aime, S. *Chem. Eur. J.*, **2009**, *15*, 1696-1705.

12. Aime, S.; Calabi, L.; Cavallotti, C.; Gianolio, E.; Giovenzana, G.B.; Losi, P.; Maiocchi, A.; Palmisano, G.; Sisti, M. *Inorg. Chem.*, **2004**, *43*, 7588-7590.

13. Aime, S.; Gianolio, E.; Giovenzana, G.B.; Longo, D.; Longo, I.; Menegotto, I. *Chem. Eur. J.* **2007**, *13*, 5785-5797. b) Briley-Saebo, K.C.; Geninatti, S.; Barazza, A.; Cormode, D.; Mulder, W. J. M., Chen, W.; Giovenzana, G. B.; Aime, S.; Fayad, Z. A. *J. Phys. Chem. B* **2009**, *113(18)*, 6283-6289.

14. Lattuada, L.; Barge, A.; Cravotto, G.; Giovenzana, G.B.; Tei, L. *Chem. Soc. Rev.* **2011***, 40,* 3019-3049. b) Mamedov, I.; Engelmann, J.; Eschenko, O.; Beyerlein, M.; Logothetis, N. K. *Chem. Commun.* **2012**, *48*, 2755-2757. b) Minazzi, P.; Lattuada, L.; Menegotto, I.G.; Giovenzana, G. B. *Org. Biomol. Chem.*, **2014**, *12*, 6915-6921.

15. Gianolio, E.; Cabella, C.; Colombo Serra, S.; Valbusa, G.; Arena, F.; Maiocchi, A.; Miragoli, L.; Tedoldi, F.; Uggeri, F.; Visigalli, M.; Bardini, P.; Aime, S. *J. Biol. Inorg. Chem.* **2014**, *19*, 719-726.

16. Martinelli, J.; Thangavel, K.; Tei, L.; Botta, M. *Chem. Eur. J.* **2014**, *20*, 10944-10952.

17. Imperio, D.; Giovenzana, G.B.; Law, G.-L. Parker, D.; Walton, J.W. *Dalton Trans.* **2010**, *39*, 9897-9903.

18. Ermelindo A.; Gambino, G.; Tei, L. *Tetrahedron Lett.* **2013**, *54*, 6378-6380.

19. Kotková, Z.; Pereira, G. A.; Djanashvili, K.; Kotek, J.; Rudovský, J.; Hermann, P.; Vander Elst, L.; Muller, R. N.; Geraldes, C. F. G. C.; Lukeš, I.; Peters, J. A. *Eur. J. Inorg. Chem.* **2009**, 119-136.

20. Aime, S.; Botta, M.; Cravotto, G.; Frullano, L.; Giovenzana, G.B.; Geninatti Crich, S.; Palmisano, G.; Sisti, M. *Helv. Chim. Acta* **2005**, *88*, 588-603.

21. Aime, S.; Cravotto, G.; Geninatti Crich, S.; Giovenzana, G.B.; Ferrari, M.; Palmisano, G.; Sisti, M. *Tetrahedron Lett.* **2002**, *43*, 783-786.

22. Cheng, T.-H.; Wang, Y.-M.; Lee, W.-T.; Liu, G.-C. *Polyhedron* **2000**, *19*, 2027-2037.

23. Wermuth, C. G. *The Practice of Medicinal Chemistry*; Academic: Oxford, UK, **2011**; pp. 303-310.

24. Aime, S.; Botta, M.; Frullano, L.; Geninatti Crich, S.; Giovenzana, G.B.; Pagliarin, R.; Palmisano, G.; Sirtori, F.R.; Sisti, M. *J. Med. Chem.* **2000**, *43(21)*, 4017-4024.

25. Elemento, E.; Parker, D.; Aime, S.; Gianolio, E.; Lattuada, L. *Org. Biomol. Chem.* **2009**, *7*, 1120-1131. b) Artali, R.; Bombieri, G.; Giovenzana, G.B.; Galli, M.; Lattuada, L.; Meneghetti, F. *Inorg. Chim. Acta* **2013**, 407, 306-312.

26. Aime, S.; Botta, M.; Terreno, E.; Anelli, P. L.; Uggeri, F. *Magn. Reson. Med.* **1993**, *30*, 583-591.

AMPED: a new platform for picolinate based luminescent lanthanide chelates

Claudia Guanci, Giovanni Giovenzana, Luciano Lattuada, Carlos Platas-Iglesias, and Loïc J. Charbonnière*

Unpublished

Abstract. The synthesis of a new nonacoordinating ligand based on a AMPED (6-amino-6-methylperhydro-1,4-diazepine) scaffold functionalized by three picolinate (6-carboxy-2-methyl-pyridine) arms is described. Coordination of lanthanide(III) cations (Ln = Eu and Tb) was monitored by spectrophotometric titration, UV-Vis absorption and steady-state emission spectroscopy, showing the formation of [LnL] complexes in aqueous solutions. The corresponding Eu and Tb complexes were isolated and characterized, and their spectroscopic properties (luminescence quantum yields, excited state lifetimes) were determined in buffered water (TRIS/HCl, pH 7.4) and compared to existing data of the literature. DFT modeling of the complexes showed the picolinate arms to be perfectly wrapped around the Ln^{3+} cations, affording an excellent shielding of the metal as confirmed by the determination of the hydration number of q = 0 for both complexes. High resolution emission spectrum was used to determine the radiative lifetime of Eu in the complex (t_{rad} = 3.05 ms) and the metal centred luminescence quantum yield (0.20). The modest 0.11 overall luminescence quantum yield of the complex is a consequence of a medium energy transfer efficiency (0.50) and a low metal centred luminescence efficiency attributed in part to the presence of numerous NH and CH bonds in close proximity to the metal centre.

Introduction

Luminescent lanthanide (Ln) complexes have found a particular niche in spectroscopic applications combining elemental spectral signatures, long luminescence lifetimes, large Stokes' shifts,[1,2] and sensing[3] or upconversion properties.[4] Particular efforts have been devoted to the design of highly luminescent lanthanide tags[5] for their use in time-resolved luminescence analytical applications and microscopy.[6] Such complexes are basically constituted of three main components: i) a pre-organizing scaffold aiming at providing kinetically and thermodynamically stable Ln complexes; ii) antenna units which collect the exciting photons and transfer the corresponding energy to the Ln excited states; and iii) an activated pending arm for the covalent grafting of the Ln label to the (bio)material of interest. Although the pioneering efforts have been mainly devoted to macropolycyclic scaffolds to ensure the stability of the complexes,[7] pre-organizing scaffolds based on macrocyclic moieties[8] or on strong electrostatic interactions[9] also proved to be stable enough for bioanalytical applications and far less demanding in terms of synthetic efforts. Among the numerous examples dealing with macrocyclic structures, scaffolds based on tetraazacycloalkanes (in particular cyclen[10] but also cyclam[11]) and triazacycloalkanes (mainly triazacyclononane or TACN)[12] were deeply investigated.

More recently, the synthesis of 6-amino-6-methylperhydro-1,4-diazepine (AMPED) was reported[13] and it soon appeared to be an interesting scaffold for the preparation of chelating agents, employed for the formation of stable Ln complexes,[14] with a particular emphasis on Gd based relaxation agents.[15] The structure of AMPED proposes two possible entries into the introduction of an activated function for biolabeling, *i.e.*: the alkyl chain on the quaternary carbon atom[16] and possibly the regioselective sequential alkylation on the nitrogen atoms taking advantage of the differential reactivity of primary and secondary amines.[17] Considering these different parameters, the question of the use of AMPED as a scaffold for luminescent Ln complexes became obvious, providing that an adequate

antenna was used. As an archetypal one, the picolinate arm appeared as an evidence as it has been introduced on a plethora of scaffolds including podant types,[18] linear polyamines,[19] and cyclic polyamines[15a,20], but also because the *para* position of the central pyridyl ring can easily be modified by inclusion of unsaturated groups to extend the electronic delocalisation and to improve the antenna effect.[21]

In this contribution, we describe the synthesis of an AMPED based nonadentate ligand LH_3 for the complexation of Ln cations. Eu(III) and Tb(III) complexes were prepared and characterized together with their spectroscopic properties.

Results and discussion

Scheme 1 presents the synthetic protocol for the obtention of ligand LH_3. AMPED was prepared according to literature procedure[12] by a two steps procedure involving a nitro-Mannich-type reaction with nitroethane, paraformaldehyde and dibenzylethylenediamine diacetate followed by reductive hydrogenation-debenzylation with H_2, Pd/C. The picolinate precursor **1** was prepared according to a literature three step procedure[22] from dipicolinic acid, esterified into its dimethyl ester before partial reduction of one of the ester functions and chlorination with $SOCl_2$. Alkylation of AMPED with five equivalents of **1** was carried out in acetonitrile in the presence of potassium carbonate as a base with a modest 20% yield. Despite all our efforts, including a large excess of **1**, it was not possible to isolate the tetraalkylated compound corresponding to the bisalkylation of the primary amine of AMPED. Nevertheless, compound **2** was particularly interesting as the remaining secondary amine group could represent a suitable site for the introduction of an activating function for biolabeling. Finally, basic hydrolysis of the ester functions followed by acidification of the medium afforded ligand **L**H_3 in a decent 77% yield.

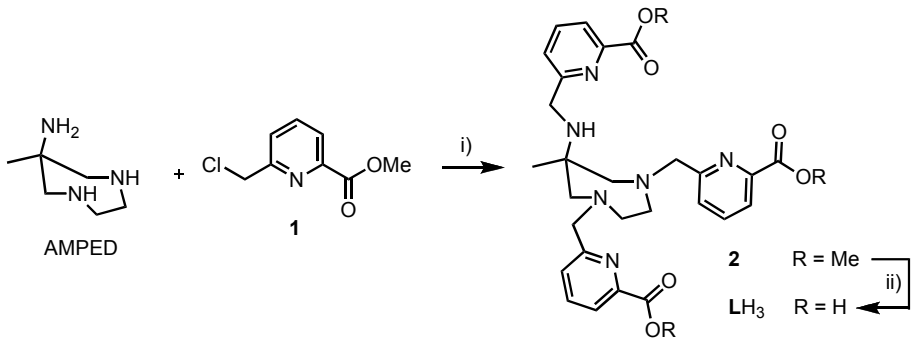

Scheme 1. Synthesis of **L**H_3.
i) K_2CO_3, CH_3CN, r.t. 72h; 20%. ii) NaOH, H_2O, r.t. 14h, then HCl; 77%.

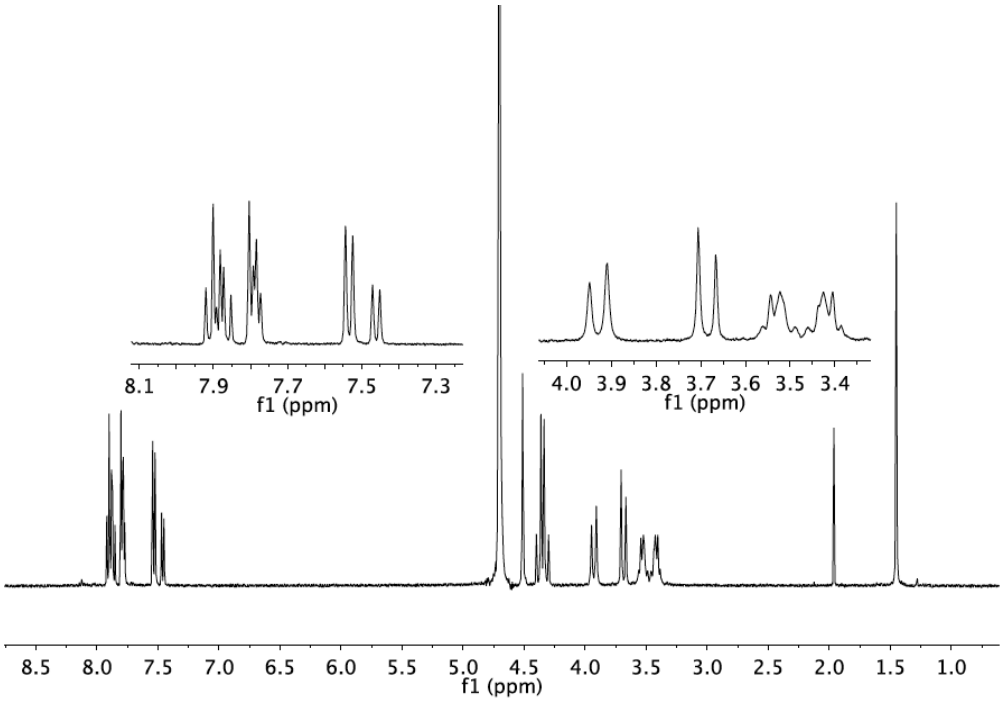

Figure 1. ^{1}H-NMR of LH_3 (D_2O, 400 MHz, 298K)

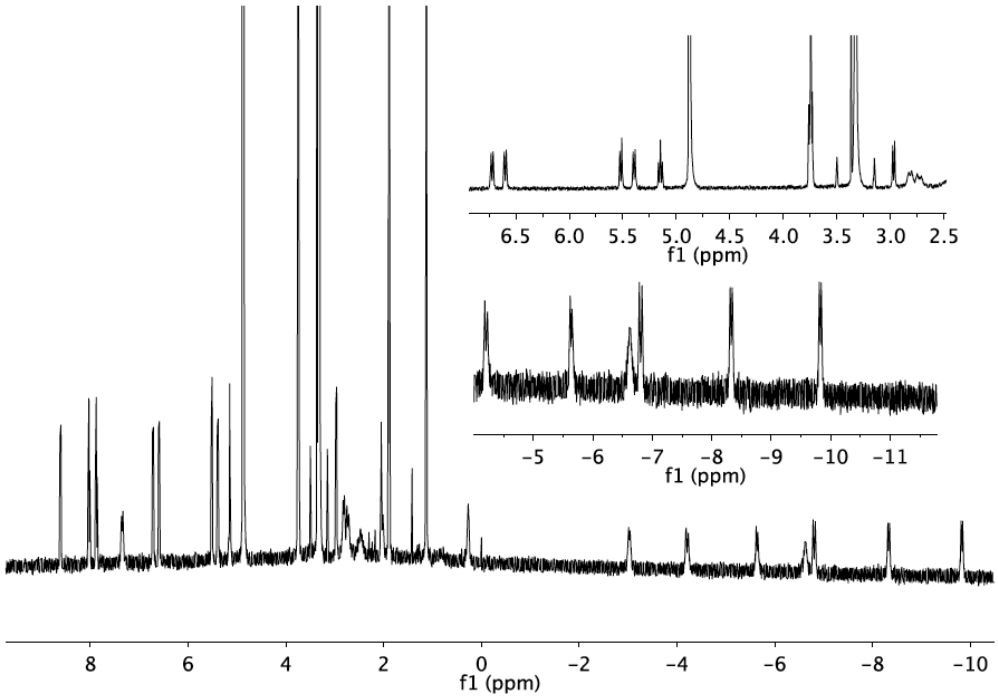

Figure 2: ^{1}H-NMR of Eu-L (D_2O, 400 MHz, 298K)

The complexation of Eu and Tb was monitored by titration experiments in which the absorption and emission spectra of buffered solutions of the ligand in TRIS/HCl (0.01 M, pH = 7.4) were monitored as a function of increasing aliquots of the chloride salts of Ln. Figure 3 displays the evolution of the emission spectra during the titration with Tb. Upon addition of Tb, the excitation through the ligand pp* absorption bands at 265 nm resulted in the observation of thin emission bands at 490, 543, 583 and 621 nm, with weaker signals at 653, 670 and 681 nm. These emission bands are typical of the $^{5}D_4 \rightarrow {}^{7}F_J$ transitions (J = 6 to 0 respectively) centred on Tb.[1] The titration showed the intensity of these bands to linearly

increase up to one equivalent, after which the emission intensity did not change anymore. This evolution points to the formation of a single new species with a one Tb to one ligand composition. The same behavior was observed for Eu. On the basis of this composition, the [LnL] complexes were prepared by mixing equimolar concentrations of ligands and complexes in water at pH 4.5 and heating for 4 hours at 80°C. The complexes were isolated by precipitation with THF from the water solutions. The electrospray mass spectrometry of the complexes displayed the expected pattern corresponding to the [LnL] complexes, with the expected isotopic distribution corresponding to the ^{151}Eu and ^{153}Eu isotopes.

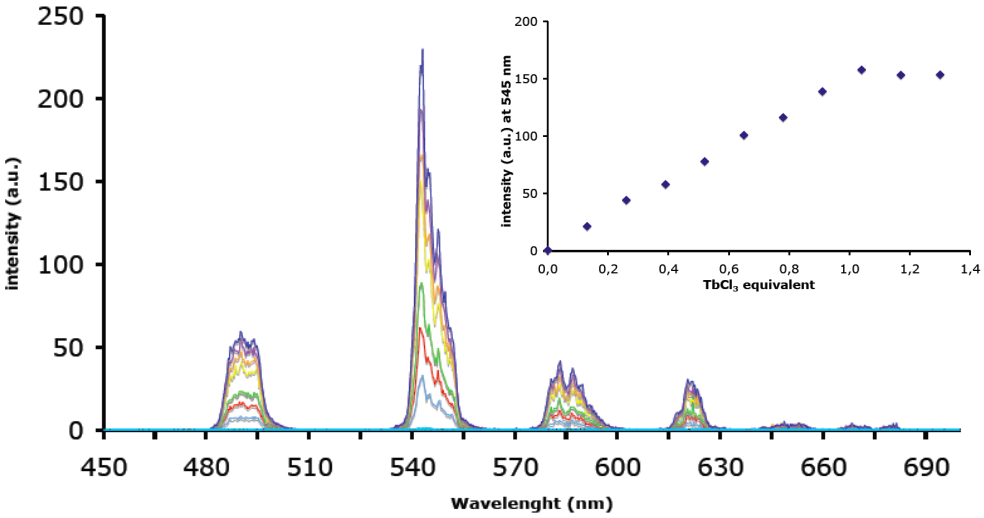

Figure 3. Evolution of the emission spectra of a solution of L upon addition of $TbCl_3.6H_2O$ (TRIS/HCl, 0.01 M, pH = 7.4). Inset: Evolution of the emitted intensity at 545 nm.

The UV-Vis absorption spectra and steady-state emission spectra of the complexes are presented in Figure 4, while Table 1 summarizes the main spectroscopic properties of the complexes in water.

Table 1. Absorption maximum (l_{max}), metal centred excited state lifetime in water (t_{H_2O}) and heavy water (t_{D_2O}), overall luminescence quantum yield (f_{H_2O}) and hydration number (q) for the [LnL] complexes (Ln = Eu and Tb).

	λ_{max} (nm) / ε ($M^{-1}.cm^{-1}$)	t_{H_2O} (ms)	t_{D_2O} (ms)	Φ_{H_2O}	q[a]
[EuL]	273 (15900)	0.61	0.73	0.11[b]	0
[TbL]	273 (15600)	1.83	2.00	0.21[c]	0

[a] calculated according to ref [23] (see text). [b] using $[Ru(bipy)_3]Cl_2$ in non-degassed water as reference ($f = 0.04$)[24]. [c] using R6G in water as reference ($f = 0.76$)[25].

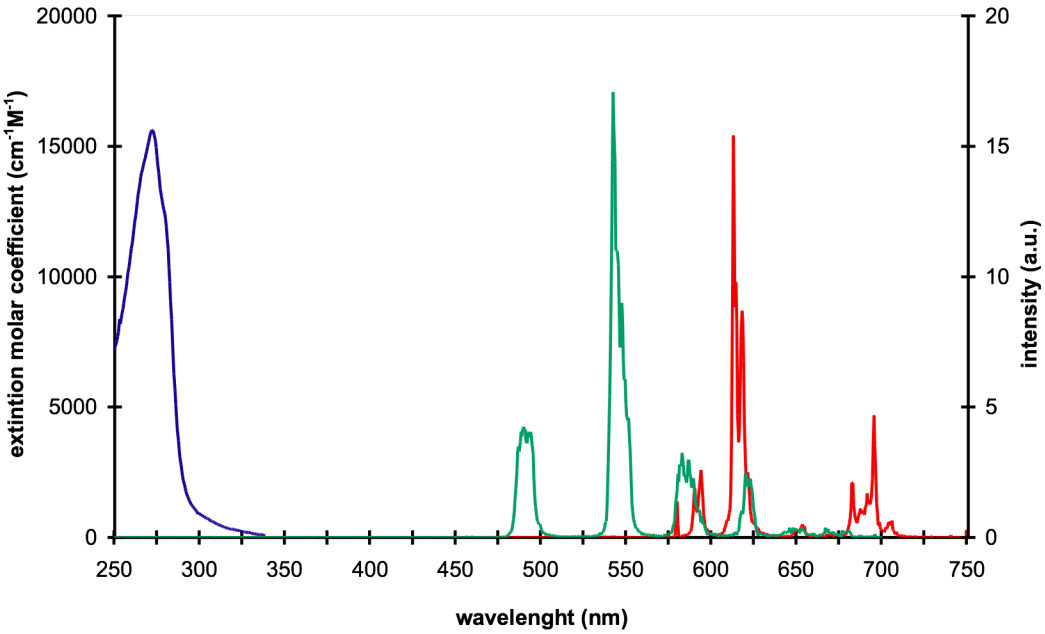

Figure 4. UV-Vis absorption spectrum of [TbL] (blue) and emission spectra of [EuL] (red) and [TbL] (green) in water.

The absorption spectra of the complexes are both dominated by an intense absorption band with maximum at 273 nm, attributed to π→π* transitions centered on the picolinate moieties. Upon excitation into this transition both complexes

displayed the typical emission bands arising from the $^5D_0 \rightarrow {}^7F_J$ (J = 0 to 4) for Eu and $^5D_4 \rightarrow {}^7F_J$ (J 0 to 6) for Tb. The excited state lifetimes of the complexes were recorded in water and deuterated water allowing for the determination of the hydration number, *i.e.* the number of water molecules in the first coordination sphere of the Ln cation, according to Horrocks methodology[26] using refined coefficients determined by Parker *et al.*[19] For both Eu and Tb, the analysis showed the coordination sphere to be fully saturated by the nine coordination sites of the ligand, leaving no free space for the coordination of water molecules, thereby affording an excellent protection of the luminescent cations towards non radiative deactivation. The luminescence quantum yield of the Eu complex (ϕ = 0.11) is in excellent agreement with that obtained for other nonacoordinated ligands containing three picolinate arms, such as the derivative of TACN derivative (ϕ = 0.09),[27] or its phosphinate based analogue (ϕ = 0.07-0.09).[28]

DFT calculations. Following the methodology reported in recent computational studies,[29] the [EuL] complex was characterized by means of DFT calculations using the TPSSh functional and the large-core relativistic ECP of Dolg *et al*., which includes 52 electrons in the core for Eu^{3+}. The ligand coordinates to the Eu^{3+} ion using a N_6O_3 donor set composed of the three amine nitrogen atoms, the three nitrogen atoms of the pyridyl rings and three oxygen atoms of the carboxylate groups (Figure 5). The latter donor atoms provide the strongest interaction with the metal ion (Eu-O distances in the range 2.38-2.41 Å), followed by the nitrogen atoms of the pyridyl moieties (2.59-2.62 Å). The calculated distances between the Eu^{3+} ion and the amine nitrogen atoms of the ligand (2.66-2.83 Å) are only slightly longer than those observed in the solid state for the Gd^{3+} complex of AAZTA (2.60-2.78 Å), while following the sequence Ln-N1 < Ln-N3 < Ln-N2.[30]

The N3-CH_2-CH_2-N dihedral angle (-33.2°) is close to those observed in the Eu^{3+}complex of the related AAZTA-CH_2CH_2OH ligand (-28.2°),[31] the Ga^{3+} complexes with hexadentate ligands L^1-L^4 [32] (Scheme 1) and the Cu complex with

AAZTA, resulting in twist-chair conformations of the 1,4-diazepine seven-membered ring. This torsion angle is somewhat smaller in the Gd^{3+} complex of AAZTA-C_2H_4COOBn (-20.8°)[33] and Cu(H_2AZZATA) (-23.7°),[34] approaching an eclipsed conformation in the Gd^{3+} complex of AAZTA (-2.9°),[22] which is characteristic of the chair conformation.

The assignment of a coordination polyhedron to describe the metal coordination environment in [EuL] is not straightforward. Among the different coordination polyhedra most frequently observed for nine-coordinate metal complexes are the monocapped square antiprism, the tricapped trigonal prism and the muffin.[35] These polyhedral provide shape measures S(A) = 3.41, 2.57 and 3.05, respectively (the shape measure S(A) = 0 for a structure fully coincident in shape with the reference polyhedron, while the maximum allowed value of S(A) is 100).[36] Thus, the best description of the metal coordination environment in [EuL] is given by a distorted monocapped square antiprism.

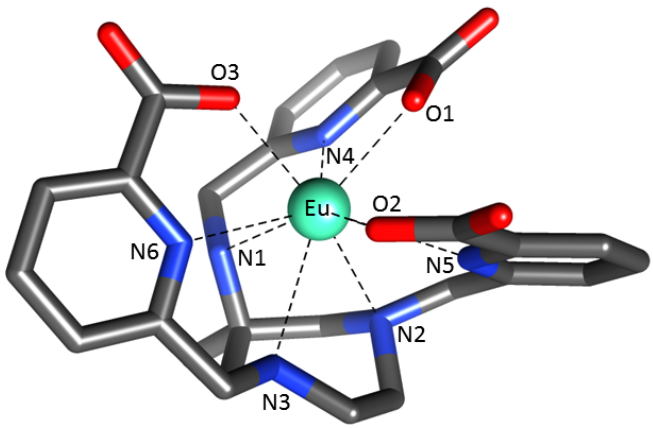

Figure 5. Structure of the [EuL] complex optimized in aqueous solution at the TPSSh/LCRECP/6-31G(d,p) level. Bond distances of the metal coordination environment: Eu-O1, 2.409 Å; Eu-O2, 2.382 Å; Eu-O3, 2.390 Å; Eu-N1, 2.658 Å; Eu-N2, 2.827 Å; Eu-N3, 2.722 Å; Eu-N4, 2.590 Å; Eu-N5, 2.620 Å; Eu-N1, 2.613 Å.

Experimental section.

Synthesis. All chemicals were purchased from Sigma-Aldrich and were used without purification unless otherwise stated. AMPED was prepared according to ref. 12, while compound **1** was prepared following the procedure reported in ref. 21.

AAZ(Pic)$_3$ trimethylester. To a suspension of AMPED (200.0 mg, 1.55 mmol) in CH_3CN (15 mL), powdered dry K_2CO_3 (1.284 g, 9.29 mmol) and methyl 6-chloromethylpicolinate (1.437 g, 7.75 mmol) were sequentially added. The reaction was stirred at room temperature for 4 days. The reaction was monitored by DP TLC DCM/MeOH/NH_3 90:9:1. The mixture was filtered to remove the salts and evaporated at reduced pressure. The residue was dissolved in DCM (20 mL), washed with brine (10 mL), dried on Na_2SO_4 filtered and evaporated under *vacuum*. The crude product was purified by flash chromatography column (DCM/MeOH/NH_3 98:1:1→ 96:3:1) leading to 177.8 mg of pure product as a pale yellow solid (yield: 20%) . ^{1}H-NMR ($CDCl_3$, 298K, 400 MHz): δ 7.93 (d, 3H, J = 7.6Hz), 7.84 (d, 2H, J = 7.8Hz), 7.73 (t, 3H, J = 7.7Hz), 7.52 (m, 1H), 3.94 (s, 9H), 3.92 (s, 4H), 3.73 (s, 2H), 2.83 (d, 2H, J = 13.3Hz), 2.75-2.55 (m, 6H), 2.30 (bs, 1H), 0.92 (s, 3H). ^{13}C-NMR ($CDCl_3$, 298K, 100.1 MHz): δ 165.80 (C), 165.74 (C) 160.81 (C), 147.13 (C), 147.12 (2C), 137.35 (CH), 137.16 (CH), 126.49 (CH), 125.40 (CH), 123.63 (CH), 123.22(CH), 66.48 (CH_2), 66.03 (CH_2), 58.42 (CH_2), 56.53 (C), 52.83 (CH_3), 52.71 (CH_3), 47.49 (CH_2), 22.89 (CH_3). MS (m/z, for $[C_{30}H_{37}N_6O_6]^+$): calcd 577.2696, found 577.2718. EA calcd for $[C_{30}H_{36}N_6O_6 \cdot H_2O]$ (%) C 60.59, N 14.13, H 6.44, found (%) C 60.86, N 14.45, H 6.19.

AAZ(Pic)$_3$. AAZ(Pic)$_3$-trimethylester (60 mg, 0.104 mmol, MW = 576.27 g/mol) was dissolved in NaOH 1M solution (1.1 mL). The reaction was stirred overnight at room temperature. The consumption of starting material was monitored by DP-

TLC DCM/MeOH/NH3 80:19:1, while RP-TLC ACN (0.1% TFA)/H_2O (0.1% TFA) was used to monitor the product. After concentration under vacuum, the residue was dissolved in water and acidified untill pH = 2, finally dried at reduced pressure. The crude was purified by RP-FPLC ACN(0.1% TFA)/H_2O(0.1% TFA) 0:100 →100:0 affording to 67.7 mg of pure product as white solid (yield: 54.8%). ^{1}H-NMR (D_2O, 298K, 400 MHz):, 7.90 (t, 2H, *J* = 7.8Hz), 7.87 (t, 1H, *J* = 7.9Hz), 7.79 (d, 2H, *J* = 7.8Hz), 7.78 (d, 2H, *J* = 7.7Hz), 7.53 (d, 2H, *J* = 7.8Hz), 7.46 (d, 1H, *J* = 7.8), 4.51 (s, 2H), 4.37 (d, 2H, *J* =14.9 Hz), 4.32 (d, 2H, *J* =14.9 Hz), 3.93 (d, 2H, *J* = 15.6Hz), 3.69 (d, 2H, *J* = 15.7Hz), 3.56-3.49 (m, 2H), 3.46-3.38 (m, 2H), 1.45 (s, 3H). ^{13}C-NMR (D_2O, 298K, 101 MHz): 166.91 (C), 166.28 (C), 153.32 (C), 151.62 (C), 146.24 (C), 145.87 (C), 140.52 (CH), 140.02 (CH), 128.24 (CH), 126.36 (CH), 125.42 (CH), 125.28(CH), 61.75 (CH_2), 59.86 (CH_2), 52.71 (CH_2), 43.82 (C), 18.12 (CH_3). MS (m/z, for $[C_{27}H_{31}N_6O_6]^+$): calcd 535.2321, found 535.2321.

Eu-AAZ(Pic)$_3$: AAZ(Pic)$_3$ (20,0 mg, pure 45.4%, 0.017 mmol, MW = 534.64 g/mol) was dissolved in ultrapure water (1mL) and $EuCl_3$*$6H_2O$ (7.0 mg, 0.019 mmol, 1.1 eq, MW = 366.41 g/mol) was added. The pH was adjusted to 4.50 with NaOH 0.1M and solution was stirred at 80°C for 4h. The reaction was monitored by RP-TLC ACN(0.1% TFA)/H2O(0.1% TFA) 5:5 observing a fluorescent red spot at 254 nm. After 4h at 80°C the mixture was cooled at room temperature and pH adjusted to 7 with NaOH 0.1M. The solution was concentrated and the complex was finally purified by precipitation with THF affording to 8.1 mg of Eu-AAZ(Pic)$_3$ as a white solid (yield 69.6%). **^{1}H-NMR** (D_2O, 298K, 400 MHz): 8.61 (d, *J* = 8Hz), 8.03 (t, *J* = 8Hz), 7.88 (t, *J* = 8Hz), 7.35 (d, *J* = 16Hz), 6.72 (d, *J* = 8Hz), 6.60 (d, *J* = 8Hz), 5.52 (d, *J* = 8Hz), 5.40 (d, *J* = 4Hz), 5.15 (t, *J* = 8Hz) 3.75 (m), 3.50 (m), 3.15 (m), 2.97 (d, J = 8Hz), 2.81 (d, *J* = 12Hz), 2.73 (d, *J* = 16Hz), 2.48 (bs), 2,05 (s), 2.03 (d, *J* = 16Hz), 1.89 (m), 1.42 (s), 1.13 (s) 0.27 (bs), -3.03 (bs), -4.20 (d, *J* = 12Hz), -5.63 (d, *J* = 16Hz), -6.64 (bs), -6.81(d, *J* = 16Hz) -

8.32(d, *J* = 16Hz), -9.82(d, *J* = 12Hz). **MS** (m/z, for $[C_{27}H_{27}EuN_6NaO_6]^+$): calcd 707.1097, found 707.0283.

Tb-AAZ(Pic)$_3$: AAZ(Pic)$_3$ (20 mg, pure 45.4%, 0.017 mmol, MW = 534.64 g/mol) was dissolved in ultrapure water (1mL) and $TbCl_3$*$6H_2O$ (7.1 mg ,0.019 mmol, 1.1 eq, 373.38 g/mol) was added. The pH was adjusted to 4.50 with NaOH 0.1M and solution was stirred at 80°C for 4h. The reaction was monitored by RP-TLC ACN(0.1% TFA)/H2O(0.1% TFA) 5:5 observing a fluorescent red spot at 254 nm. After 4h at 80°C the mixture was cooled at room temperature and pH adjusted to 7 with NaOH 0.1M. The solution was concentrated and the complex was finally purified by precipitation with THF affording to 7.1 mg of Tb-AAZ(Pic)$_3$ as white solid (60.5%). **MS** (m/z, for $[C_{27}H_{27}TbN_6NaO_6]^+$): calcd 713.1128, found 713.0242.

Spectroscopy. UV-Vis absorption spectra were recorded on a Specord 205 (Analytik Jena) or a Perkin Elmer lambda 950 spectrometer. Steady-state luminescence emission and excitation spectra were recorded on a Horiba Jobin Yvon Fluorolog 3 spectrometer working with a continuous 450 W Xe lamp. Detection was performed with a Hamamatsu R928 photomultiplier. All spectra were corrected for the instrumental response. When necessary, a 399 nm cut off filter was used to eliminate the second order artifacts. Phosphorescence decays were measured on the same instrument working in the phosphorescence mode, with 50 μs delay time and a 100 ms integration window or working in the Time Correlated Single Photon Counting (TCSPC) Lifetime Spectroscopy mode, both using a Xenon flash lamp as the excitation source. Monoexponential decay profiles were fitted with the FAST program from Edinburgh Instruments or with the Data station software from Jobin Yvon. Luminescence quantum yields were measured according to conventional procedures, with optically diluted solutions (optical density < 0.05), using rhodamine 6G in water (ϕ = 76.0%)[37] as reference for Tb and $[Ru(bipy)_3]Cl_2$ in water (ϕ = 4.0%)[38] for Eu. Estimated errors are ± 15%.

DFT calculations. Full geometry optimizations of the [EuL] system were performed in aqueous solution employing DFT within the hybrid meta-GGA approximation with the TPSSh exchange-correlation functional,[39] and the Gaussian 09 package (Revision B.01).[40] In these calculations we used the large-core relativistic effective core potential (LCRECP) of Dolg *et al.* and the related [5s4p3d]-GTO valence basis set for Eu,[41] while C, H, N and O atoms were described with the standard 6-31G(d,p) basis set for. In the LCRECP approach, the $46+4f^6$ electrons of Eu^{3+} are included in the core, leaving the outermost 11 electrons to be treated explicitly. Thus, LCRECP calculations were conducted on a pseudo-singlet state configuration. No symmetry constraints have been imposed during the optimizations. The default values for the integration grid (75 radial shells and 302 angular points) and the SCF energy convergence criteria (10^{-8}) were used in all calculations. The stationary points found on the potential energy surfaces as a result of the geometry optimizations have been tested to represent energy minima rather than saddle points via frequency analysis. Time-dependent density functional theory (TDDFT)[42] was used for the calculation of the 40 lowest energy singlet-singlet electronic transitions and the lowest-lying singlet-triplet transition of [Eu(amped)] in aqueous solution. Solvent effects (water) were evaluated by using the integral equation formalism variant of the polarizable continuum model (IEFPCM),[43] as implemented in Gaussian 09.

Conclusion

The AMPED backbone was selected as an alternative scaffold for the preparation of an original nonacoordinating ligand (AAZ-Pic_3) by functionalization with three picolinic residues. Eu(III) and Tb(III) complexes of this innovative chelating agent were prepared and a detailed investigation of their photophysical properties is reported, along with a DFT study of the corresponding molecular structures. Efficient coordination is evidenced either by luminescence measurements (q=0) or by modeling, where the wrapping of the novel chelating agent on the lanthanides

trivalent ion with all nine donor groups in a distorted monocapped square antiprism geometry can be appreciated. The luminescence properties of Eu- and Tb-complexes parallel those observed for similar nonacoordinate systems, with an overall quantum yield of 0.11 and 0.21, respectively.

On the base of these results, AAZ-Pic_3 represents an original starting point for the development of innovative and efficient luminescent probes for OI applications.

Acknowledgements. C. P.-I. thanks Centro de Supercomputación de Galicia (CESGA) for providing the computer facilities.

References

1. a) M.C. Heffern, L.M. Matosziuk and T.J. Meade (2014) *Chem. Rev.* **114**, 4496. S.V. b) Eliseeva and J.-C.G. Bünzli (2010) *Chem. Soc. Rev.* **39**, 189. c) A. de Bettencourt-Dias, P.S. Barber, S. Viswanathan (2014) *Coord. Chem. Rev.***165**, 273-274.

2. a) S.J. Butler and D. Parker (2013) *Chem. Soc. Rev.* **42**, 1652. b) T. Liu, A. Nonat, M. Beyler, M. Regueiro-Figueroa, K. Nchimi Nono, O. Jeannin, F. Camerel, F. Debaene, S. Cianférani-Sanglier, R. Tripier, C. Platas-Iglesias and L.J. Charbonnière (2014) *Angew. Chem. Int. Ed.* **53**, 7259.

3. a) F. Auzel (2004) *Chem. Rev.* **104**, 139. b) L. Aboshyan-Sorgho, C. Besnard, P. Pattison, K.R. Kittilstved, A. Aebischer, J.-C.G. Bünzli, A. Hauser and C. Piguet (2011) *Angew. Chem. Int. Ed.* **50**, 4108.

4. a) J. Xu, T.M. Corneillie, E.G. Moore, G.-L. Law, N.G. Butlin and K.N. Raymond (2011) *J. Am. Chem. Soc.* **133**, 19900. b) S.J. Butler, L. Lamarque, R. Pal and D. Parker (2014) *Chem. Sci*, **5**, 1750. c) M. Starck, P. Kadjane, E. Bois, B. Darbouret, A. Incamps, R. Ziessel and L.J. Charbonnière *Chem. Eur. J.* 2011, **17**, 9164.

5. a) A. Grichine, A. Haefele, S. Pascal, A. Duperray, R. Michel, C. Andraud and O. Maury (2014) *Chem. Sci*., **5**, 3475. b) M. Delbianco, V. Sadovnikova, E. Bourrier, G. Mathis, L. Lamarque, J.M. Zwier and D. Parker (2014) *Angew. Chem. Int. Ed.*, **53**, 10718. c) D. Geißler, S. Linden, K. Liermann, K.D. Wegner, L.J. Charbonnière and N. Hildebrandt (2014) *Inorg. Chem*., **53**, 1824.

6. a) B. Alpha, J.-M. Lehn and G. Mathis, *Angew. Chem., Int. Ed.* 1987, **26**, 266. b) S.P. Vila-Nova, G.A.L. Pereira, R.Q. Albuquerque, G. Mathis, H. Bazin, H. Autiero, G.F. de Sa and S. Alves Jr. (2004) *J. Lumin.* **109**, 173.

7. a) J.W. Walton, A. Bourdolle, S.J. Butler, M. Soulie, M. Delbianco, B.K. McMahon, R. Pal, H. Puschmann, b) J.M. Zwier, L. Lamarque, O. Maury, C. Andraud and D. Parker (2013) *Chem. Commun.*, **49**, 1600. b) D.J. Bornhop, J.M.M. Griffin, T.S. Goebel, M.R. Sudduth, B. Bell and M. Motamedi (2003) *Appl. Spectrosc.* **57**, 1216. c) S. Deslandes, C. Galaup, R. Poole, B. Mestre-Voegtlé, S. Soldevila, N. Leygue, H. Bazin, L. Lamarque and C. Picard, *Org. Biomol. Chem.* 201, **10**, 8509.

8. a) S. Abada, A. Lecointre, M. Elhabiri, D. Esteban-Gomez, C. Platas-Iglesias, G. Tallec, M Mazzanti and L.J. Charbonnière, *Chem. Commun.*, 2012, **48**, 4085. b) K. Nchimi Nono, A. Lecointre, M. Regueiro-Figueroa, C. Platas-Iglesias and L.J. Charbonnière (2011) *Inorg. Chem.*, **50**, 1689.

9. See for examples: a) R. Carr, L. Di Bari, S. Lo Piano, D. Parker, R.D. Peacock and J. M. Sanderson *Dalton Trans.* 2012, **41**, 13154. b) A.M. Prokhorov, V.N. Kozhevnikov, D.S. Kopchuk, H. Bernard, N. Le Bris, R.Tripier, H. Handel, B. Koenig, D.N. Kozhevnikov, *Tetrahedron* 2011, **67**, 597. c) S. Quici, C. Scalera, M. Cavazzini, G. Accorsi, M. Bolognesi, L. Armelao, G. Bottaro, *Chem. Mater.* 2009, **21**, 2941. d) A.M. Nonat, C. Allain, S. Faulkner and T. Gunnlaugsson *Inorg. Chem.* 2010, **49**, 8449. e) M.P. Placidi, L.S. Natrajan, D. Sykes, A.M. Kenwright and S. Faulkner, *Helv. Chim. Acta* 2009, **92**, 2427.

10. L.J. Charbonnière, N. Weibel, R.F. Ziessel *J. Org. Chem.* 2002, **67**, 3933.

11. See for examples: a) M. Giraud, E.S. Andreiadis, A.S. Fisyuk, R. Demadrille, J. Pécaut, D. Imbert, M. Mazzanti, *Inorg. Chem.* 2008, **47**, 3952. b) N.H. Evans, R. Carr, M. Delbianco, R. Pal, D.S. Yufit and D.

Parker *Dalton Trans.* 2013, **42**, 1510. c) M. Soulié,F. Latzko, E. Bourrier, V. Placide, S.J. Butler, R. Pal, J.W. Walton, P.L. Baldeck, B. Le Guennic, C. Andraud, J.M. Zwier, L. Lamarque, D. Parker and O. Maury, *Chem. Eur. J.* 2014, **20**, 8636.

12. S. Aime, L. Calabi, C. Cavallotti, E. Gianolio, G.B. Giovenzana, P. Losi, A. Maiocchi, G. Palmisano and M. Sisti *Inorg. Chem.* 2004, **43**, 7588.

13. Z. Baranyai, F. Uggeri, G.B. Giovenzana, A. Bényei, E. Brücher, S. Aime, *Chem. Eur. J.*, 2009, **15**, 1696.

14. a) E. Gianolio, G.B. Giovenzana, D. Longo, I. Longo, I. Menegotto, S. Aime *Chem. Eur. J.* 2007, **13**, 5785. b) K.C. Briley-Saebo, S. Geninatti Crich, D.P. Cormode, A. Barazza, W.J.M. Mulder, W. Chen. G.B. Giovenzana, E.A. Fisher, S. Aime, Z.A. Fayad *J. Phys. Chem. B* 2009, **113**, 6283. c) E. Gianolio, C. Cabella, S. Colombo Serra, G. Valbusa, F. Arena, A. Maiocchi, L. Miragoli, F. Tedoldi, F. Uggeri, M. Visigalli, P. Bardini, S. Aime *J. Biol. Inorg. Chem.* 2014, **19**, 715.

15. a) P. Minazzi, L. Lattuada, I.G. Menegotto, G.B. Giovenzana *Org. Biol. Inorg. Chem.* 2014, **12**, 6915. b) I. Mamedov, J. Engelmann, O. Eschenko, M. Beyerlein, N. Logothetis *Chem. Commun.* 2012, **48**, 2755. c) G. Gugliotta, M. Botta, G.B. Giovenzana and L. Tei *Bioorg. Med. Chem. Lett.* 2009, **19**, 3442.

16. a) E. Elemento, D. Parker, S. Aime, E. Gianolio, L. Lattuada, *Org. Biomol. Chem.* 2009, **7**, 1120. b) R. Artali, G. Bombieri, G.B. Giovenzana, M. Galli, L. Lattuada, F. Meneghetti, *Inorg. Chim. Acta* 2013, **407**, 306.

17. a) C. Gateau, M. Mazzanti, J. Pécaut, F.A. Dunand and L. Helm *Dalton Trans.* 2003, 2428. a) N. Weibel, L.J. Charbonnière and R.F. Ziessel *Tetrahedron Lett.* 2006, 47, 1793. b) L.J. Charbonnière, N. Weibel, P. Retailleau and R.F. Ziessel *Chem. Eur. J.* 2007, **13**, 346. c) L.J. Charbonnière, S. Mameri, P. Kadjane, C. Platas-Iglesias and R.F. Ziessel *Inorg. Chem.* 2008, **47**, 3748.

18. a) N. Chatterton, Y. Bretonnière, J. Pécaut and M. Mazzanti *Angew. Chem. Int. Ed.* 2005, **44**, 7595. b) C. Marchal, Y. Filinchuk, D. Imbert, J;-C.G. Bünzli, M. Mazzanti, *Inorg.Chem.* 2007, **46**, 6242. c) E. Balogh, M. Mato-

Iglesias, C. Platas-Iglesias, E. Toth, K. Djanashvili, J.A. Peters, A. de Blas and T. Rodrıguez-Blas *Inorg. Chem.* 2006, **45**, 8719.

19. a) M. Roger, L.M.P. Lima, M. Frindel, C. Platas-Iglesias, J.-F. Gestin, R. Delgado, V. Patinec and R. Tripier, *Inorg. Chem.* 2013, **52**, 5246. b) M. Regueiro-Figueroa, B. Bensenane, D. Esteban-Gomez, L.J. Charbonnière, G. Tircso, A. de Blas, T. Rodriguez-Blas and C. Platas-Iglesias *Inorg. Chem.,* 2011, **50**, 4125. c) A. Rodríguez-Rodríguez, D. Esteban-Gómez, A. de Blas, T. Rodríguez-Blas, M. Fekete, M. Botta, R. Tripier and C. Platas-Iglesias *Inorg. Chem.* 2012, **51**, 2509.

20. a) A. D'Aléo, A. Picot, P.L. Baldeck, C. Andraud and O. Maury, *Inorg. Chem.* 2008, **47**, 10269. b) Q. Wang, K. Nchimi Nono, M. Syrjänpää, L.J. Charbonnière, J. Hovinen and H. Härmä, *Inorg. Chem.* 2013, **52**, 8461.

21. M. Mato-Iglesias, A. Roca-Sabio, Z. Pálinkás, D. Esteban-Gómez, C. Platas-Iglesias, É. Tóth, A. de Blas, T. Rodríguez-Blas *Inorg. Chem.* 2008, **47**, 7840.

22. A. Beeby, I.M. Clarkson, R.S. Dickins, S. Faulkner, D. Parker, L. Royle, A.S. de Sousa, J.A.G. Williams and M. Woods *J. Chem. Soc. Perkin Trans 2*, **1999**, 493.

23. J. Olmsted. *J. Phys. Chem.* 1979, ***83***, 2581.

24. H. Ishida, S. Tobita, Y. Hasegawa, R. Katoh, N. Noaki *Coord. Chem. Rev.* 2010, **254**, 2449.

25. W. D.W. Horrocks Jr and D. Sudnick, *J. Am. Chem. Soc.* 1979, **101**, 334.

26. G. Nocton, A. Nonat, C. Gateau and M. Mazzanti, *Helv. Chim. Acta*, 2009, **92**, 2257.

27. J. W. Walton, R. Carr, N. H. Evans, A. M. Funk, A. M. Kenwright, D. Parker, D. S. Yufit, M. Botta, S. De Pinto, K.-L. Wong, Inorg. Chem. 2012, **51(15)**, 8042-8056

28. M. Regueiro-Figueroa, D. Esteban-Gómez, A. de Blas, T. Rodríguez-Blas, C. Platas-Iglesias, *Chem. Eur. J.* 2014, **20**, 3974-3981.

29. S. Aime, G. Bombieri, C. Cavallotti, G. B. Giovenzana, D. Imperio, N. Marchini, *Inorg. Chim. Acta* 2008, **361**, 1534-1541.

30. R. S. Sengar, A. Nigam, S. J. Geib, E. C. Wiener, *Polyhedron* 2009, **28**, 1525-1531.

31. D. Parker, B. P. Waldron, D. S. Yufit, *Dalton Trans.,* 2013, **42**, 8001-8008.

32. R. Artali, G. Bombieri, G. B. Giovenzana, M. Galli, L. Lattuada, F. Meneghetti, *Inorg. Chim.Acta* 2013, **407**, 306-312.

33. Z. Baranyai, F. Uggeri, A. Maiocchi, G. B. Giovenzana, C. Cavallotti, A. Takács, I. Tóth, I. Bányai, A. Bényei, E. Brucher, S. Aime, *Eur. J. Inorg. Chem.* 2013, 147-162.

34. [35]A. Ruíz-Martínez, D. Casanova, S. Alvarez, *Chem. Eur. J.* 2008, **14**, 1291-1303.

35. M.Llunell, D. Casanova, J. Cirera, P. Alemany, S. Alvarez, S. SHAPE. Program for the stereochemical analysis of molecular fragments by means of continuous shape measures and associated toolds.Version 2.1.

36. J. Olmsted, *J. Phys. Chem.* 1979, **83**, 2581.

37. H. Ishida, S. Tobita, Y. Hasegawa, R. Katoh and N. Noaki *Coord. Chem. Rev.* 2010, **254**, 2449.

38. J. M. Tao, J. P. Perdew, V. N. Staroverov, G. E. Scuseria, *Phys. Rev. Lett.* 2003, **91**, 146401/1-146401/4.

39. Gaussian 09, Revision **B.01**, M. J. Frisch, G. W. Trucks, H. B. Schlegel, G. E. Scuseria, M. A. Robb, J. R. Cheeseman, G. Scalmani, V. Barone, B. Mennucci, G. A. Petersson, H. Nakatsuji, M. Caricato, X. Li, H. P. Hratchian, A. F. Izmaylov, J. Bloino, G. Zheng, J. L. Sonnenberg, M. Hada, M. Ehara, K. Toyota, R. Fukuda, J. Hasegawa, M. Ishida, T. Nakajima, Y. Honda, O. Kitao, H. Nakai, T. Vreven, J. A. Montgomery, Jr., J. E. Peralta, F. Ogliaro, M. Bearpark, J. J. Heyd, E. Brothers, K. N. Kudin, V. N. Staroverov, R. Kobayashi, J. Normand, K. Raghavachari, A. Rendell, J. C. Burant, S. S. Iyengar, J. Tomasi, M. Cossi, N. Rega, J. M. Millam, M. Klene, J. E. Knox, J. B. Cross, V. Bakken, C. Adamo, J. Jaramillo, R.

Gomperts, R. E. Stratmann, O. Yazyev, A. J. Austin, R. Cammi, C. Pomelli, J. W. Ochterski, R. L. Martin, K. Morokuma, V. G. Zakrzewski, G. A. Voth, P. Salvador, J. J. Dannenberg, S. Dapprich, A. D. Daniels, Ö. Farkas, J. B. Foresman, J. V. Ortiz, J. Cioslowski, and D. J. Fox, Gaussian, Inc., Wallingford CT, 2009.

40. M. Dolg, H. Stoll, A. Savin, H. Preuss, *Theor. Chim.Acta* 1989, **75**, 173-194.

41. a) R. E. Stratmann, G. E. Scuseria, M. J. Frisch, *J. Chem. Phys.* 1998, **109**, 8218–8224; b) R. Bauernschmitt, R. Ahlrichs, *Chem. Phys. Lett.* 1996, **256**, 454–464. (c) M. E. Casida, C. Jamorski, K. C. Casida, D. R. Salahub, *J. Chem. Phys.*1998, **108**, 4439–4449.

42. . Tomasi, B. Mennucci, R. Cammi. *Chem. Rev.* 2005, **105**, 2999–3093.

Conclusions

Lanthanide(III) ions are widely employed in diagnostic imaging applications, due to their wide array of physical properties. Paramagnetic Gd(III) complexes are routinely employed in clinical Magnetic Resonance Imaging (MRI), with novel applications being explored for Eu(III) and Yb(III) chelates. The unique luminescence properties of Eu(III), Tb(III), are unsurpassed in the development of fluorescent probes for time-gated optical bioassays and other Optical Imaging (OI) applications. Moreover, several radioactive isotopes in the Ln(III) family are used or being studied for radiodiagnostic techniques (PET, SPECT) or radiotherapy.

In this context, the research activity of the PhD project was focused on the design and the preparation of chelating agents for lanthanide (Ln(III)) ions and the preliminary evalutation of the corresponding Ln(III) complexes as potential probes for diagnostic imaging applications.

During the PhD period, different topics of this wide area of research were examined. The research was focused in particular on Ln(III) complexes to be used in MRI and OI, leading to the completion of three different subprojects, respectively.

A first section of this PhD was devoted to the design and development of phosphonic analogues of chelating agents. Chelating agents for Ln(III) usually rely on polyaminopolycarboxylic structures. Phosphonic acids represent classical isosteric replacement of the carboxylic acid groups, and some phosphonic derivatives of selected chelating agents were recently described in the literature and reported to impart improved properties to the corresponding chelates.

During this PhD, three different and unprecedented derivatives of the ligand AAZTA were synthesized, embodying different arrangements of one or two

phosphonic acid residues. The relaxometric properties of the corresponding Gd(III) complexes, relevant for MRI applications, were determined.

Additional work was performed in order to prepare bifunctional derivatives of mono and diphosphonic analogues of the well known DTPA ligand. These analogues have been shown to form Gd-chelates endowed with improved relaxometric properties. In our work, remote functional groups were installed on the DTPA-phosphonic analogues, paving the way to the preparation of conjugated paramagnetic probes.

Finally, the core triamine of the above cited ligand AAZTA (*i.e.*: AMPED, 6-amino-6-methyl-1,4-perhydrodiazepine) was chosen for the development of a novel nonadentate chelating agent, to be employed for the formation of coordinatively saturated Ln(III) complexes for Optical Imaging applications. The AMPED triamine was decorated with three chelating picolinic acid residue, leading the the novel ligand AAZ$(Pic)_3$. The latter was employed for the preparation of the corresponding Eu(III) and Tb(III) complexes, showing a compact distorted square antiprismatic coordination cage. The luminescence properties of these complexes were similar or in some instances better than those of similar nonacoordinated systems.

The results of the activity of the PhD will be summarized in three different articles, one of them published in 2014, a second one recently submitted and a third one in preparation.

List of publications

- **Synthesis of bifunctional chelating agents based on mono and diphosphonic derivatives of diethylenetriaminepentaacetic acid**
  Giovanni B. Giovenzana, Claudia Guanci, Silvia Demattio, Luciano Lattuada, Veronica Vincenzi

  Published: Tetrahedron 2014 Vol. 70, Issue 32, pages 4809-4813

- **Synthesis of phosphonic analogues of AAZTA and relaxometric evaluation of the corresponding Gd(III) complexes as potential MRI contrast agents**
  Claudia Guanci, Roberta Pinalli, Silvio Aime, Eliana Gianolio, Luciano Lattuada and Giovanni B. Giovenzana

  Submitted: Tetrahedron Letters, Dec 2014, code TETL-D-14-02963

- **AMPED: a new plateforme for picolinate based luminescent lanthanide cations**
  Claudia Guanci, Giovanni Giovenzana, Carlos Platas-Iglesias and Loïc J. Charbonnière

  Unpublished

Acknowledgements

I started this experience of PhD with interest and curiosity in November 2011 in that little and sometimes too confused Organic Chemistry Lab. During this period I improved my knowledge and practice as organic chemist, perhaps I tried.

So, the time for the acknowledgements is arrived: for the important opportunity my best greetings to Luciano and Giovanni, who, for the first time, I would mention with their name (instead of the surname) to enhance the intensity of my gratitude: Luciano for the ideas, the projects and the interest with which he supported my activity, while Giovanni for the limitless cultural baggage that he has donated to me un till today, but also for his fine tiptoe manner to take personally his students.
A special greetings to Loic and his Lab, who offer to me the possibility to explore the surprising manner to do research at the CNR of Strasbourg, expecially to Parastoo with who I spent many night to compare our not so different cultures.

However, the most important revelation of this PhD is Arianna, to who I want dedicate this delivery: for the wonderful moments lived together, the intollerance shared, the essential mutual supports during the difficulties faced.

At all, Thank you!
Claudia